A WATER MODEL STUDY OF BOTTOM-BLOWN OXYGEN STEELMAKING PROCESS

By

N. BHARATHA BALLAL

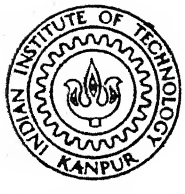

DEPARTMENT OF METALLURGICAL ENGINEERING

INDIAN INSTITUTE OF TECHNOLOGY, KANPUR

JANUARY, 1979

A WATER MODEL STUDY OF BOTTOM-BLOWN OXYGEN STEELMAKING PROCESS

A Thesis Submitted
in Partial Fulfilment of the Requirements
for the Degree of
DOCTOR OF PHILOSOPHY

By
N. BHARATHA BALLAL

to the
DEPARTMENT OF METALLURGICAL ENGINEERING
INDIAN INSTITUTE OF TECHNOLOGY, KANPUR
JANUARY, 1979

ME- 1979-D-BAL-WAT

CERTIFICATE

Certified that this work on "A Water Model Study of Bottom-Blown Oxygen Steelmaking Processes" has been carried out under my supervision and that it has not been submitted elsewhere for a degree.

A. Ghosh
Professor
Department of Metallurgical Engineering
Indian Institute of Technology
Kanpur.

ACKNOWLEDGEMENTS

I owe a great debt of gratitute to Professor A. Ghosh for his able guidance and constant encouragement during the course of this work.

I am grateful to Professors K.K. Sircar and A.K. Gupta for the discussion I had with them during the initi stages of this work. It is a pleasure to acknowledge the sincere efforts of Mr. A. Sharma throughout the course of the work. I am thankful to Mr. V.P. Gupta for his cooperation during the fabrication of the apparatus. Colleagues in the laboratory deserve my warmest thanks for their cooperation and help. I would also wish to thank Mr. R.N. Srivastava for the painstaking efforts in typing the manuscript.

Special mention should be made of all my friends, among members of the faculty, graduate and undergraduate students, for making my stay at Kanpur a pleasant and worthwhile experience.

The grant for this work from Steel Authority of India Ltd., Ranchi is gratefully acknowledged.

N.B. BALLAL

CONTENTS

LIST OF TABLES

LIST OF FIGURES

LIST OF SYMBOLS

A	constant in Eq. A1.5, Appendix I, dimensionless
a, b	parameters of the Eq. 3.9, dimensionless
C	coefficient of discharge, dimensionless
C_b	concentration of oxygen in the bulk of the electrolyte in equilibrium with air, mole/cc
C_b^o	concentration of oxygen in water in equilibrium with air, mole/cc
C_i	concentration at the electrode surface, mole/cc
$C^*_{CO_2}$	normalised concentration of $CO_2 = \dfrac{\text{pct. } CO_2}{(\dot{Q}_{CO_2}/\dot{Q}_{air})}$, dimensionless
c	constant of proportionality in Eq. 3.10, dimensionless
D	diffusion coefficient of oxygen in the electrolyte, cm^2/sec
D_1	inside pipe diameter of orifice meter, cm
D_2	orifice diameter, cm
d_b	diameter of the simulating vessel, cm
d_e	diameter of the electrode, cm
d_j	diameter of the inner pipe in the tuyere, cm
F	Faraday constant, coulombs
g	acceleration due to gravity, cm/sec^2
h	height of the water bath, cm
h_w	differential pressure across the orifice, cm of water
i	electrode current, ampere

i_d	instantaneous value of limiting current, ampere
$\bar{i}_d$	time-averaged value of limiting current, ampere
i'_d	fluctuating component of limiting current, ampere
K	flow coefficient for the orifice meter, dimensionless
K'	constant in Eq. A2.6, dimensionless
K_∞	flow coefficient for infinite Reynolds number, dimensionless
k	instantaneous value of the mass transfer coefficient, cm/sec
$\bar{k}$	time-averaged value of mass transfer coefficient, cm/sec
k'	fluctuating component of mass transfer coefficient, cm/sec
L	characteristic length, cm
L_e	effective length of the electrode in the direction of the mean flow, cm
l	distance to which the inner pipe of the tuyere is projecting into the vessel, cm
N_A	mass transfer rate for component A, moles/cm^2 sec
N_{Eu}	Euler number, dimensionless
N_{Fr}	Froude number, dimensionless
$N_{Fr'}$	modified Froude number, dimensionless
N^j_{Re}	Reynolds number for the gas flow in the inner pipe of the tuyere, dimensionless
N^l_{Re}	Reynolds number for the flow of the liquid, dimensionless
N^o_{Re}	Reynolds number for the flow through the orifice, dimensionless
N^s_{Re}	Reynolds number for the gas flow in the annular space of the tuyere, dimensionless

N_{Wb}	Weber number, dimensionless
n	number of electrons involved in the electrochemical reaction, dimensionless
P_1	pressure at the upstream pressure tap, cm of mercury
P_2	pressure at the tuyere exit, cm of mercury
$\dot{Q}_{air}$	flow rate of air, liters/min
$\dot{Q}_{CO_2}$	flow rate of carbon dioxide, liters/min
$\dot{Q}_j$	flow rate of gas through the inner pipe of the tuyere, liters/min
$\dot{Q}_s$	flow rate of gas through the annular space of the tuyere, liters/min
R	universal gas constant, cal/°K mole
r	radial distance from the vessel axis, cm
s	instantaneous value of the velocity gradient at the wall, cm^{-1}
$\bar{s}$	time-averaged value of velocity gradient at the wall, sec^{-1}
s'	fluctuating component of velocity gradient at the wall, sec^{-1}
T	temperature, °K
t	time, sec
t_s	width of the annulus in the tuyere, cm
t^*	time constant of the concentration boundary layer defined in Eq. 2.12, sec
V	voltage, volts
v_j^o	velocity of the jet gas at the tuyere exit, cm/sec
v_s^o	velocity of the shrouding gas at the tuyere exit, cm/sec

v_1	velocity of the liquid, cm/sec
W	mass flow rate of air through the orifice meter, gm/cc
x	parameter in Eq. 3.7, dimensionless
Y_1	expansion factor, dimensionless
z	vertical distance downstream from the tuyere exit, cm
β	the diameter ratio in the orifice meter = D_2/D_1, dimensionless
Γ	gamma function
ρ_1	density of air at upstream pressure tap conditions, gm/cc
ρ_2	density of air at the tuyere exit, gm/cc
ρ_j^o	density of the gas through the inner pipe at the tuyere exit, gm/cc
ρ_l	density of the liquid, gm/cc
ρ_s^o	density of the shrouding gas at the tuyere exit, gm/cc
μ_j	viscosity of the gas through the inner pipeof the tuyere, poise
μ_l	viscosity of the liquid, poise
μ_s	viscosity of the shrouding gas, poise
μ_{air}	viscosity of air, poise
σ	surface tension of the liquid, dyne/cm
τ	instantaneous value of the wall shear stress, dyne/cm^2
$\bar{\tau}$	time-averaged value of the wall shear stress, dyne/cm^2
τ'	fluctuating component of the wall shear stress, dyne/cm^2

A WATER MODEL STUDY OF BOTTOM-BLOWN OXYGEN STEELMAKING PROCESSES

A Thesis Submitted
in Partial Fulfilment of the Requirements
for the Degree of
DOCTOR OF PHILOSOPHY
by
N. BHARATHA BALLAL
to the
Department of Metallurgical Engineering
Indian Institute of Technology, Kanpur
January 1979

SYNOPSIS

Investigations of a water model of bottom-blown oxygen steelmaking processes like OBM/Q-BOP were undertaken to understand certain aspects of the dynamics of these processes. The study was restricted to the bottom part of the model and emphasis was on understanding and predicting the influence of some process parameters on the bottom refractory wear.

Dimensional analysis was made to design the simulating vessel and to identify the important dimensionless groups. The experimental investigation consisted of two parts:

a) Experiments with single tuyere

b) Experiments with multiple tuyeres.

In the first part, experiments were conducted with a single tuyere located centrally in the bottom of a cylindrical

vessel made of perspex. The tuyere consisted of two concentric pipes through which two gases could be blown into the vessel. The gas blown through the inner pipe simulated oxygen of the bottom-blown process, and the gas introduced through the annulus surrounding the inner pipe simulated the shrouding gas. The inner pipe diameter (d_j) was 0.65 cm and the annulus thickness was 0.075 cm. The inner jet pipe could be moved up and down so that experiments could be done with the inner jet pipe protruding into the vessel.

The study with single tuyere was divided into two sub-sections:

i) Study of mixing of gases in two concentric jets submerged in water.

ii) Measurement of mass transfer coefficients and shear stresses at the bottom due to the flow of liquid.

In the first sub-section measurements were made to obtain concentration profiles at various heights downstream from the tuyere exit to determine the degree of mixing of two concentric jets of dissimilar gases submerged in water. Air was employed to simulate oxygen and carbon dioxide to simulate the shrouding gas. Gas samples were taken along the cross-section of the jet at heights of 1 cm, 3 cm and 5 cm above the tuyere. Gases were analysed using a gas-chromatograph. Three flow rates of air were employed, viz., 50, 100 and 150

liters per minute. Flow rates of carbon dioxide were 5 pct, 10 pct and 15 pct of these flow rates.

It was found that the shrouding gas is not very effective in physically shielding the liquid from the inner jet stream even very close to the tuyere. The concentration profiles at a distance of 1 cm downstream from the tuyere exit were independent of the flow rates of air ($\dot{Q}_{air}$) at a fixed ratio of flow rates of carbon dioxide and air ($\dot{Q}_{CO_2}/\dot{Q}_{air}$). The maxima in these profiles occurred just above the annulus, which seems to indicate that the carbon dioxide jet did not get significantly deflected by the presence of the air jet. The maximum in the normalized concentration $C^*_{CO_2}$ defined as:

$$C^*_{CO_2} = \frac{\text{pct. } CO_2}{(\dot{Q}_{CO_2}/\dot{Q}_{air})}$$

varied linearly with the ratio $\dot{Q}_{CO_2}/\dot{Q}_{air}$. It was, moreover, observed that the mixing process was complete within a distance of 7 to 10 d_j in the range of flow rates studied.

Since the fluid flow pattern near the bottom should have an appreciable effect on the chemical and the mechanical aspects of bottom wear, the wall shear stress and the mass transfer coefficients along the bottom of the vessel were measured using the electrochemical technique in the second section of the single tuyere experiments.

Electrodes mounted flush on the wall served as the cathodes in the diffusion-limited electrochemical transfer of oxygen dissolved in water to the electrode in the presence of a large amount of an indifferent electrolyte. Electronic circuits were designed and fabricated to measure the average electrode current and the rms value of the fluctuations in the current. In these experiments air simulated both oxygen and the shrouding gas of the prototype. Measurements were made at air flow rates of 50, 100, 150, and 200 liters/minute. Three bath heights (h) viz. 40, 30 and 20 cms were employed and the percentage of air in the annulus was 0, 5 and 10 of the total air flow. Tuyere protrusions into the bath (l) were 0, d_j and $2d_j$.

As the mass transfer coefficient in related to the wall shear stress, the results of the experiments have been discussed only with respect to the latter. These discussions can easily be extended to mass transfer coefficients also.

The shear stress decreased drastically with increasing distance from the tuyere. At points very close to the tuyere, the shear stress decreased with decreasing flow rate of air but the trend reversed at points further removed.

It was found that the rms values of the fluctuations τ' in shear stress were directly proportional to the average shear stress ($\overline{\tau}$) according to the following correlation:

$$\sqrt{\overline{\tau'^2}} = 0.40\,\overline{\tau}$$

All other correlations, therefore, have been attempted only for the average shear stress.

Percentage air in the annulus and the length of tuyere protrusion (l) into the bath had significant effects only at the electrode very close to the tuyere. At other electrodes along the bottom and along the sidewalls the shear stress was not affected by these parameters to any perceptible extent.

Correlations have been attempted for variation of $\overline{\tau}$ at the electrode closest to the tuyere. The Euler number (N_{Eu}) may be defined as:

$$N_{Eu} = \frac{\overline{\tau}}{v_j^{o2}\,\rho_j^{o}}$$

where v_j^o is the average velocity of the jet in the inner pipe at the exit and ρ_j^o is the jet gas density. N_{Eu} varied with the modified Froude number ($N_{Fr'}$) in the following fashion:

$$N_{Eu} = a(N_{Fr'})^b$$

where

$$N_{Fr'} = \frac{v_j^{o2}}{gh}\left(\frac{\rho_j^o}{\rho_l - \rho_j^o}\right)$$

a, b = parameters dependent on process variables

g = acceleration due to gravity

h = bath height

ρ_l = liquid density.

One important observation was that the parameters a and b in the above equation were independent of the percentage of air in the annulus. As the velocity of gas flowing through the annulus was small compared to that through the inner tube, this observation seems to indicate that the momentum put into the system largely determines the flow of the liquid.

Visual observations of the liquid flow were made with slit lighting. Dust particles and polystyrene beads were used as tracers. Some photographs were also taken. The general flow pattern is a torus-shaped vortex with the liquid moving up in the axial region and coming down in the peripheral region. The flow was found to be fluctuating with large amplitudes due to the fluctuations at the gas/liquid interface. There was some secondary recirculation at the corner where the sidewall meets the bottom. The behaviour of the jet was also studied with still and movie photography.

In the second part of the work, experiments were done with 3, 6 and 12 tuyeres of 0.325 cm i.d. with blowing rates varying between 150 and 340 liters per minute. Tuyeres

were placed in symmetric and asymmetric fashions. The general behaviour observed with these systems were similar to those encountered in measurements with single tuyeres. In axially symmetric tuyere arrangements, the flow rate dependence reversed at points away from the axis of the vessel. Moreover, the rms value of the fluctuations was directly proportional to the average shear stress, though the proportionality constants were different from that in experiments with single tuyeres.

In symmetrically placed tuyeres, the shear stress level all over the bottom came down as the number of tuyeres increased from one to twelve at a fixed flow rate of air. In asymmetric arrangements, the shear stress levels were higher as compared to those obtained with symmetric configurations. Significant reduction in shear stress with projection of tuyeres into the bath was observed only in asymmetric tuyere configurations.

Significance of these findings to wear of bottom refractory in bottom-blown oxygen steelmaking converters has been discussed.

CHAPTER 1

INTRODUCTION

1.1. BOTTOM-BLOWN OXYGEN STEELMAKING PROCESSES

1.1.1. Development of the Processes

Steelmaking reactions are heterogeneous in nature and occur at the interfaces between, primarily, a gas and a liquid or a liquid and a liquid. These reactions, therefore, involve mass transfer to and from the interfaces apart from the interfacial chemical reactions. At steelmaking temperatures, the latter are very fast, and so, most of the reactions are limited by the rate of the mass transfer processes to and from the interfaces. Degree of mixing in each of the three phases, i.e., metal, slag and gas, is therefore of great importance in determining the rate of refining. Agitation of the bath would enhance the rate of mass transfer of the reactants and the products. Moreover, a process that would increase the interfacial area itself between these phases would increase the refining rate enormously. Such faster refining rates would enable a better utilisation of capital, increasing the productivity of a plant. The process is also expected to lead to thermal economy because lesser is the time of refining, lesser is the heat loss.

Hence it was in this context that the refining of molten iron by bottom-blowing of air as envisaged by Sir Henry Bessemer in the nineteenth century was a revolutionary steelmaking process. It speeded up the process enormously as the gas and the metal were brought into intimate contact and vigorous stirring of the metal bath and the slag was achieved. Use of basic refractories, as in the Thomas Converters, enabled one to treat even high phosphorus hot metal.

The bottom blowing of air, however, could not allow use of large amounts of scrap. Nitrogen in air carried away a large amount of heat. Moreover, requirements of low nitrogen and phosphorous in steel could not be met by these processes. The solution for these problems was the use of tonnage oxygen in place of air. As a matter of fact, Sir Henry Bessemer himself had contemplated blowing pure oxygen through the bottom of a converter.

The refractory wear around the tuyeres, however, were excessive upon blowing of pure oxygen through the bottom. Even in the basic Bessemer process, bottom wear is a problem. Besides increasing the cost due to increased consumption of lining, the bottom had to be changed often, bringing down the productivity of the converters. Hence in the nineteen fifties the top-blown Basic Oxygen Process (BOP) was invented. Since then top-blown processes have grown rapidly in the steelmaking scene and hold a pre-eminent position at

present. Such expansion of the BOP is basically due to its favourable capital investment and operating costs compared to the open-hearth process of steelmaking.

In continental Europe, the hot metal is high in phosphorus. The common LD process is unable to refine it unless double-slagging is adopted making it more expensive. Therefore, the Basic Bessemer process, which is capable of refining high phosphorus iron, has been in existence along with other steelmaking processes, in spite of the disadvantages mentioned already.

Moreover, conversion of an existing open-hearth shop into an LD shop is quite costly. Few facilities of an OH shop can be utilized in an LD shop. In addition to this, such a conversion would disturb the scrap economics of an integrated steel plant, because the Basic Oxygen Process can absorb only a limited amount of scrap in its charge (about 30 pct. maximum).

Due to all these considerations, efforts have been going on for a long time to solve the problem of bottom refractory wear when oxygen is blown through the bottom. Model studies were carried out, for example, with water-cooled copper plates as bottoms through which oxygen could be blown.[1] However, such studies were fruitless till Savard and Lee of L'Aire Liquide, Canada came up with the novel idea of

shrouding the oxygen jet with a hydrocarbon which cracks endothermically on emerging from the tuyeres.[2] This idea was later adapted by Maximilian shutte mbH (MAXHÜTTE) of Germany for use in their bottom-blown steelmaking process which is known as the OBM (Oxygen Baden-Blassen Maxhütte) process. They used gaseous hydrocarbons as the shrouding medium. Later CRM of Belgium and US Steel Corporation of the U.S.A. collaborated with Maxhütte in developing the process further.[2-4] It is known as the OBM process of steelmaking in Europe and as Q-BOP in the U.S.A. A similar process has been independently developed by Creusot Loire of France who employed liquid hydrocarbon like fuel oil as the shrouding fluid.[5] The world production of steel by these Bottom-Blown Oxygen Processes (BBOP) was 13.5 million tonnes in 1976.[6]

One of the basic advantages of the BBOP over the LD process is the lower capital cost involved. Absence of top lance system leads to a lower height of the building. There is about 65 pct. increase in useful volume of the converter.[7] The furnace is within the crane command. Therefore, the furnace can be removed from the blowing bay and relined at a separate relining stand.[8] The tap-to-tap time for the BBOP (45 mins.) is also smaller compared to the LD process (55 mins.).[9] Moreover, this process holds great attraction where existing open-hearth or Thomas Converter shops have to be converted into one of the oxygen converter

shops. Superstructure already existing can be utilised whereas the LD shop would necessitate a completely new construction. Lesser fume generation in the bottom-blown processes is also an advantage from environmental point of view.

1.1.2. Description of the Process and Comparison with the LD Process of Steelmaking

The BBOP processes use 5 to 20 tuyeres in the removable bottom, the number of tuyeres being dependent on the converter size. These tuyeres consist of two concentric pipes. Through the inner pipe oxygen and generally also lime powder are introduced. This jet is shrouded by a hydrocarbon introduced through the annular space between the two pipes. Tuyeres are distributed either symmetrically or asymmetrically in the bottom such that a most favourable blowing behaviour is achieved. Both trunnions supporting the converter are hollow, one of which carries the gas that is introduced through the inner pipe and the other carries the shrouding fluid. A schematic sketch of a BBOP converter is given in Figure 1.1.[10]

Figures 1.2 and 1.3 show the progress of refining in the BOP and the OBM steelmaking respectively.[11] It can be observed that the curves for carbon, silicon and phosphorous have similar shapes. However, there is a marked difference in the behaviour of manganese. In the OBM process

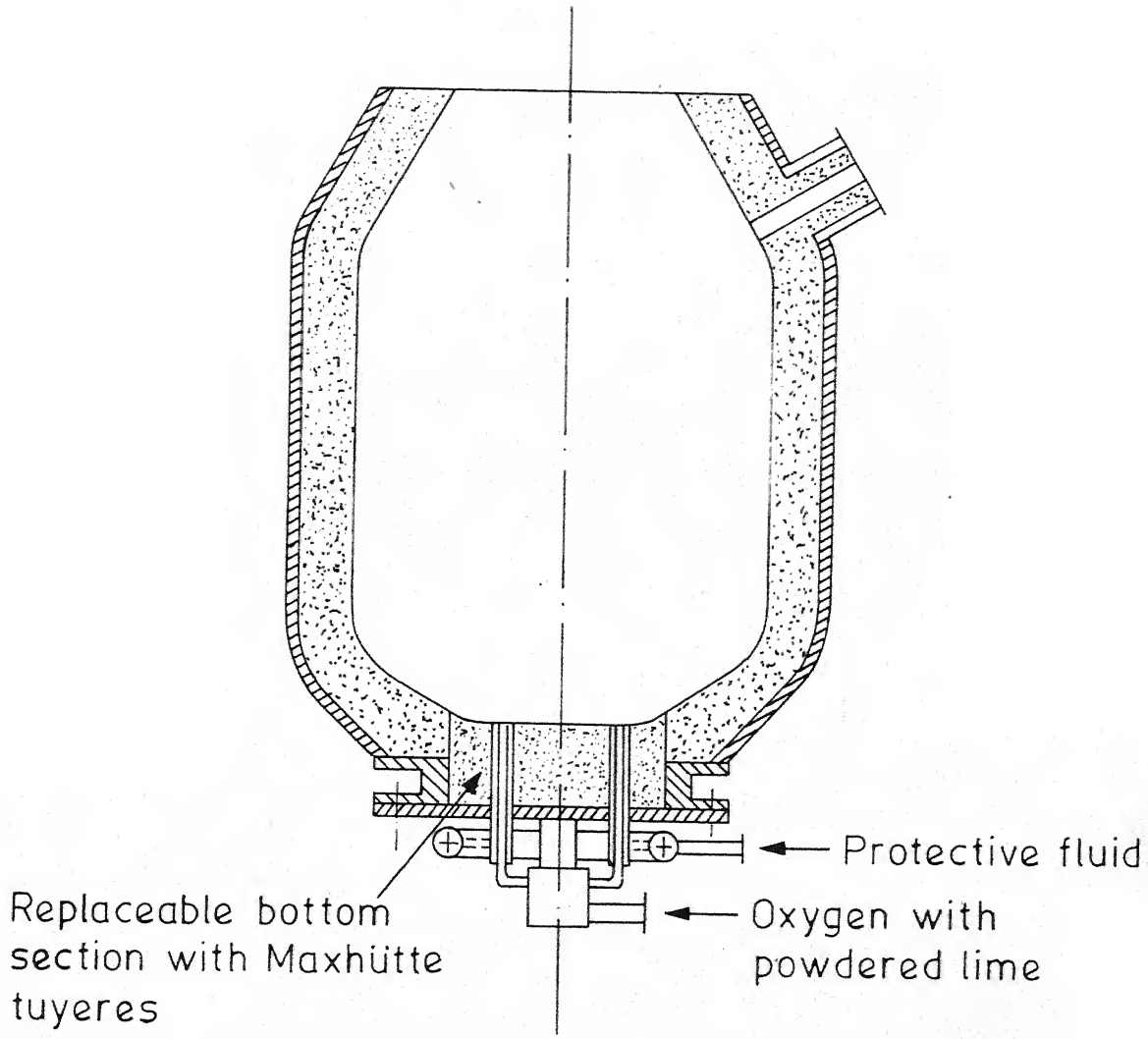

Fig. 1.1 Schematic diagram of a BBOP converter[10]

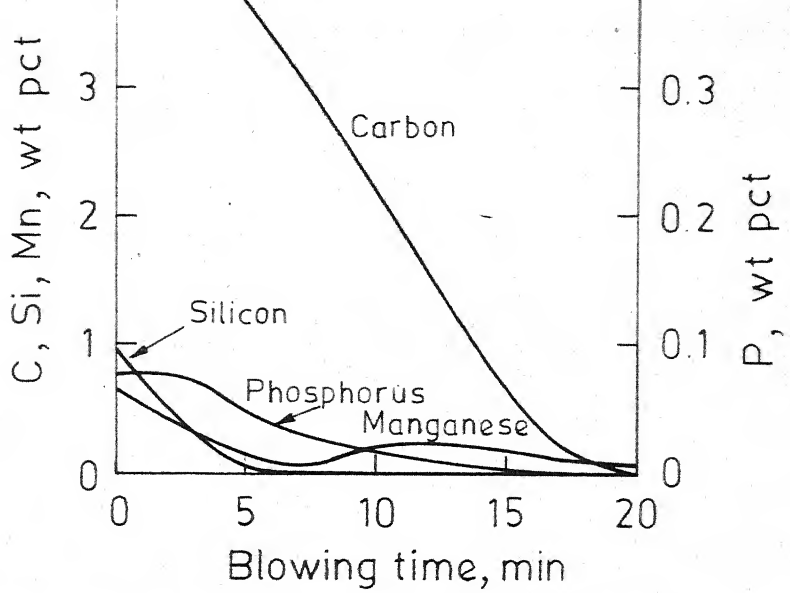

Fig. 1.2 Oxidation of carbon, phosphorus, silicon and manganese during blowing (5100 Nm^3/hr) of 40-ton BOP heat[11].

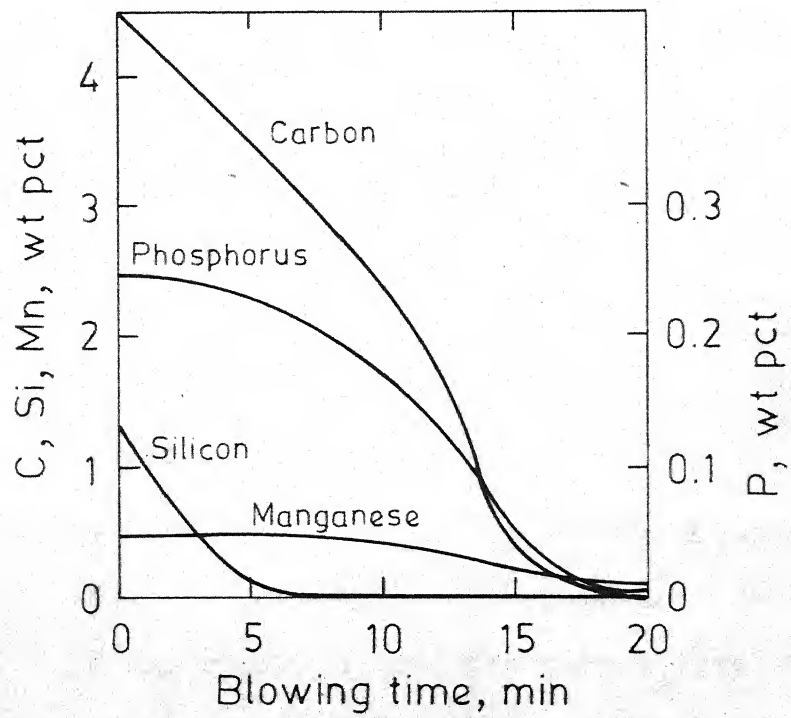

Fig. 1.3 Oxidation of carbon, phosphorus, silicon and manganese during blowing (5100 Nm^3/hr) of 40-ton Q-BOP heat[11].

where lime is also blown with oxygen, there is almost no oxidation of manganese until almost all silicon is removed. This is in striking contrast to the behaviour in the top-blown processes, where manganese and silicon are oxidised together. As a matter of fact, manganese recovery in the OBM process is claimed to be higher than in the BOP resulting in significant savings in ladle additions.[2,11,12]

Another important fact observed with the bottom-blown practices is the iron oxide content of the slag.[2,10,12,13] Figure 1.4 shows the typical variation of FeO content of the slag with the progress of the blow for the BOP and the OBM processes. It may be noted that the iron oxide content of the slag remains at about 5% during 90% of the total refining period. Even at the end of the blow, the FeO content is still quite low as compared to the top-blown processes. Such low iron oxide in slag and the resultant lower oxygen in steel result in considerable saving in deoxidants, ladle additions and ladle refractories. Moreover, lower iron oxide in slag would mean higher yield of steel.

Fruehan and Martonik[14] studied the decarburization reaction and came to the conclusion that there is a change in the mechanism of the reaction when the carbon level falls below 0.3%. At higher carbon levels, the diffusion in the gaseous phase may be rate controlling. At lower carbon contents, however, liquid-phase mass transfer becomes

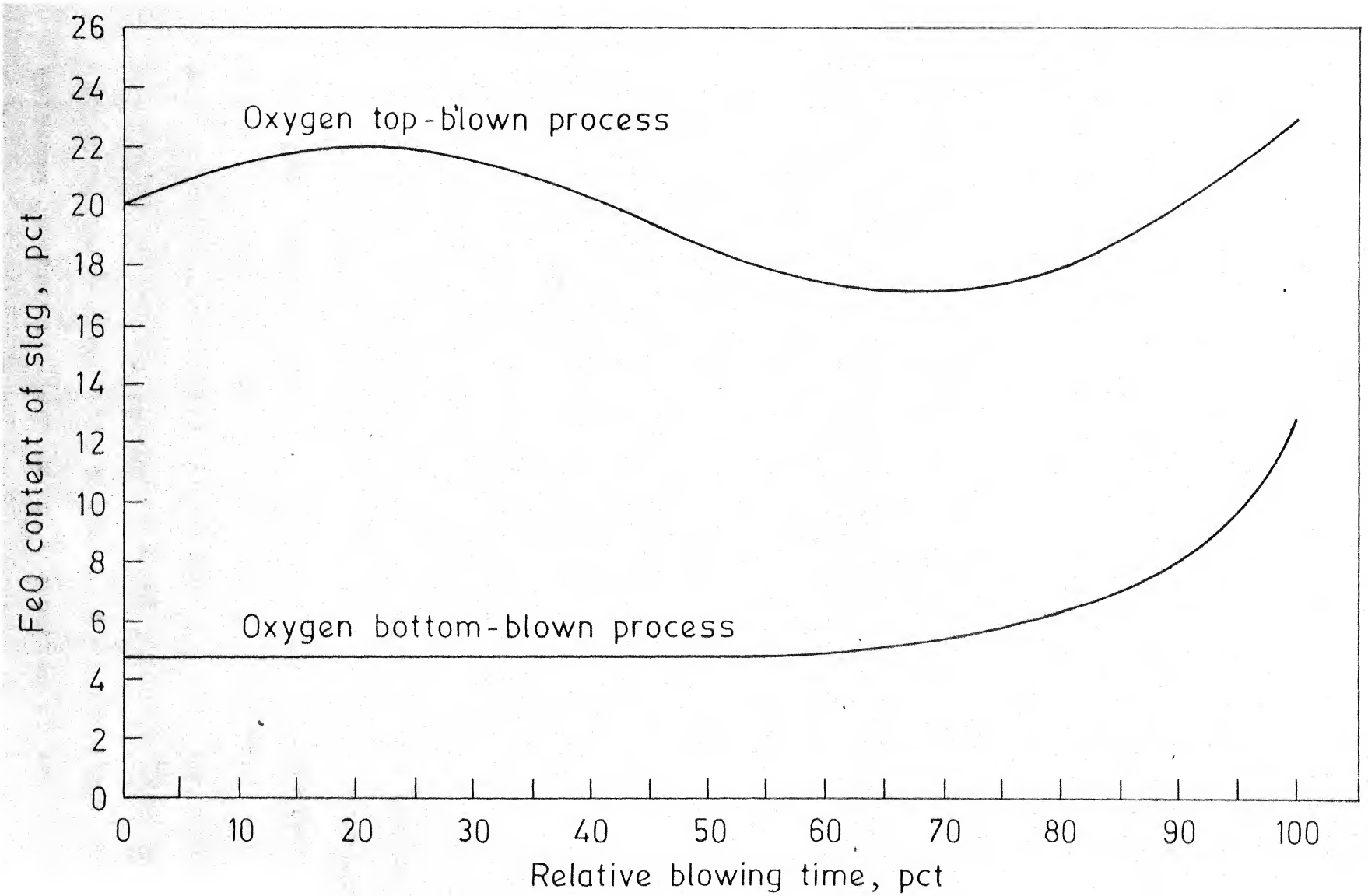

Fig. 1.4 FeO content of slag in oxygen top-blown and oxygen bottom-blown converters[10].

important and the rate decreases with decreasing carbon content. Anyhow, in bottom-blown processes lower carbon contents can be achieved without excessive oxidation of the bath. With a slag containing 17 pct. iron oxide, the final carbon content is about 0.03 to 0.04 pct.[10] This is of importance in the production of electrical sheets. Moreover, such low carbon levels permit the use of cheap carbon-containing ferro-alloys.

Fume generation in a BBOP is much lower than in the top-blown processes and is comparable to that in the Basic Bessemer process, resulting into an increased yield. Moreover, Fruehan[15] has proposed that the copious fumes that are evolved during the final stages of the blow in low carbon steel heats can be reduced if oxygen jet is diluted with argon. This modified practice would also decrease the final oxygen content of the bath and increase the manganese recovery.

One of the important advantages of the bottom-blown processes over top-blown processes is the decreased slopping. Quiet blows were obtained with high-phosphorus irons even with the use of lumpy lime.[7] Slopping was encountered when refining low-phosphorus pig iron using lumpy lime. However, introduction of powdered lime along with oxygen mitigated this problem. Less slopping allows a greater utilisation of the converter volume,

increasing production for a given size of the converter. Moreover, BBOP tolerates greater amount of silicon in hot metal than the top-blown processes because of decreased slopping in the former process. At Gary Works of US Steel, hot metal containing 2 pct. silicon has been treated successfully. In BOP, on the other hand, silicon in hot metal is usually kept below 1.2 pct.[9] In addition to these, blowing lime powder with oxygen brings down lime consumption enormously. The Q-BOP converters of Gary Works of US Steel averages 68 kg of lime per ton of steel compared to about 84 kg per ton in BOP's.[8,10]

Dephosphorisation when using lumpy lime is as successful in the BBOP as in the BOP with high-phosphorus iron.[8] With bottom blowing of lime with oxygen dephosphorisation has been claimed to be better than in the top-blown processes.[8,11,13] Desulphurisation is also claimed to be better.[2-4,7,10,12]

Problems of hydrogen and nitrogen are not severe and can be easily controlled,[10] where very low hydrogen levels are needed as in unkilled steel grades, a short blow of nitrogen at the end of the normal blow would reduce hydrogen to the desirable level. Moreover, argon degassing can be effected in the vessel itself eliminating the necessity of a separate degassing facility.[12,15]

Percentage of scrap in the charge can be more than that in the BOP due to better availability of heat as a result of smaller blowing time etc. Scrap percentage can be still more increased by preheating the scrap charge in the converter by burning the hydrocarbon.[10] Moreover, due to better mixing in the vessel, larger pieces of scrap can be charged.[10] Where scrap availability is less, it has been claimed that iron ore can be used easily.[9]

To summarise there are many advantages of the new bottom-blown oxygen steelmaking processes over the top-blown ones. It appears that the former are certainly going to gain more and more popularity in future.

1.1.3. Mechanisms of Reactions and the Dynamics of the Bottom-Blown Processes

Reported information about the reaction mechanisms in the bottom-blown steelmaking processes is scanty. Goto and Eketrop[16] made a preliminary analysis to show how bottom-blowing is an attractive proposition where metal/slag/gas reactions are involved. They speculate that pure oxygen is consumed very rapidly just above the tuyeres, producing iron oxide droplets. These oxide droplets then react with other elements in the bath. However, based on the behaviour of manganese during the blow and the fact that phosphorus in steel falls below the equilibrium value calculated from final metal and slag analyses, Turkdogan[11,13] has proposed

the model of 'gas diffusion-limited enhanced vapourisation' of the elements. This was substantiated in controlled experiments by Kor and Turkdogan[17] where it was found that metal alloys, as well as pure metals, are subjected to enhanced vapourisation in reactive atmospheres. In the proposed reaction scheme the following stages are envisaged:

(i) Vapourisation of elements or their oxides enhanced by the oxidation of vapours in the oxidising atmosphere of the submerged jet stream.

(ii) The reaction of bulk-metal or slag with the particles of the products of the gas-phase reactions.

(iii) The slag-metal-gas reaction in the emulsified slag layer.

Fruehan[15] analysed the possibilities of degassing by argon in the bottom-blown processes. He also proposed that the rate of the decarburisation reaction is limited by liquid-phase mass transfer in the final stages. In the initial stages when carbon content is high, it may be limited by gaseous diffusion.

Silberman[18] studied the mechanism of bubble formation in the air-water system and showed that when nozzle Reynolds number exceeds 10^4, the sizes of the bubbles found sufficiently downstream from the nozzle exit were independent of the nozzle size and are proportional to $N_{Re}^{-0.05}$ where N_{Re} is the nozzle Reynold's number.

Themelis et al[19] studied side-blown air-jets in water and found that the boundary of the jet fluctuates. They also found that the average jet cone angle was between 19° and 22°. However, Oryall and Brimacombe[20] measured the jet cone angle for air-jets in mercury and found that the initial expansion angle is about 150°. Liquid density seems to have a strong influence on the initial jet expansion. The latter investigators also observed the pulsating nature of submerged jets. Penetration of side-blown jets of air in water have also been studied.[19-21] Themelis et al[19] derived an equation to predict the trajectory of a gas jet injected horizontally into a liquid. Etienne[22] conducted a water-model study of the bottom-blown process at room temperature to examine bath motions and slopping as a function of tuyere configuration. He found that there was a minimum number of tuyeres for every configuration to achieve a quiet blow. The number was related to bath depth, Jet Froude Number and tuyere distribution. Symmetrical placing of the tuyeres in a central strip caused the bath to oscillate vigorously causing excessive splashing. Smaller bath heights favoured fewer splashes.

Szekely and coworkers[23-26] measured and predicted flow pattern, velocity and turbulence energy in a water model system in which argon was introduced from the bottom. Their mathematical model was successful in predicting the

general flow pattern in the system. However, one of the boundary conditions in the model is the velocity along a cylindrical cone surrounding the jet, which has to be measured experimentally.

From the above discussion, it is clear that the bottom-blown steelmaking processes are not completely understood; more studies have to be done before a coherent picture of the process emerges.

1.1.4. Refractory Wear

One of the basic problems of the bottom-blown oxygen steelmaking is refractory wear. Bottom wears out faster than the rest of the body, and the bottom refractory has to be replaced at least once during a campaign.[10,12,27] This problem is particularly important in India, because the refractory performance of Indian LDs compare unfavourably with those of the World's leading steel producers[27] (Table 1.1).

Table 1.1

LD Refractory Performance in Various Steel Plants of the World

Rourkela, India	170
Bokaro, India	160
Sidmon, Belgium	600
Italsidar, Italy	1400

The mechanism of refractory wear, however, is not clear. It could be of three types: chemical attack of the refractory by slag/metal (corrosion), mechanical wear of the refractory (erosion), and softening of the refractory at high temperatures and consequent spalling during thermal shock.[27] The relative importance of these three is not known. However, someof the basic features of refractory wear are enumerated below:[28,29]

a) Iron oxide in the slag or in the brick decreases the life of the refractory enormously.

b) Life of the refractory decreases with increasing silicon content in the metal.

c) Residual carbon in the tar-bonded or pitch-impregnated bricks increases the resistance of the bricks to slag attack by many folds.

d) Increasing the bulk density of the material decreases its wear.

e) In porous refractories, slag penetrates into the pores.

The first two features mentioned above suggest the chemical nature of the problem. Iron oxide and silica react with CaO and MgO of the basic refractory. Residual carbon probably helps in pore blockage and reduction of iron oxide to iron which is less corrosive.[30]

The importance of erosion, however, is not very clear. Grains of refractory have been found in molten glass

in a refractory tank.[30] This is probably due to a combined corrosion-erosion action where the bonding material between the grains is corroded and the projected grains are eroded away.

Bottom wear in BBOP may be due to any or all of the following factors:

a) Higher temperatures near the tuyeres cause decreased strength of the refractory and increased erosion.

b) Passing of nitrogen or air when vessel is empty results in thermal shocks and consequent spalling.

c) Formation of small slag globules rich in iron oxide and silica at the gas-metal interface and their consequent reaction with the refractory.

d) Physical action of erosion due to high flow rates and velocity fluctuations in the metal. This effect is expected to be more near the tuyeres because the jet as it emerges is fluctuating and breaks up into small bubbles within three or four jet diameters downstreams into smaller bubbles causing shear stress and velocity fluctuations.

e) Penetration of steel into the pores dissolving the residual carbon which causes augmentation of attack by slag particles.

f) Entrapment of slag particles into metal which react with the refractory.

Nilles and Boudin,[7] in their experiments with a 21 T OBM converter using natural gas or propane gas as the shrouding fluid observed that bottom wear was very regular all over the bottom with asymmetrically placed tuyeres. This leads one to believe that the shrouding with these gases is quite effective. Apart from this, information that would throw light on bottom refractory wear in bottom-blown processes is lacking.

1.2. OBJECTIVES OF THE PRESENT INVESTIGATION

Discussions in Section 1.1 show that the BBOP is an attractive alternative to the top-blown processes of steelmaking not only in new steel plants but also in the existing plants where open-hearth shops are to be converted into a pneumatic steelmaking shop. Some iron and steel plants in the U.S.A. are even replacing the BOP converters with Q-BOP converters.[2,10] In India, Steel Authority of India Ltd. are exploring the possibility of using this process in their steel plants.[27]

In this context it is necessary that the process be understood properly, so that modifications necessary to suit the Indian conditions can be effected better. The problem of refractory wear, which is expected to be severe in India as mentioned earlier, has to be studied in greater detail to evaluate the process prospects.

Refractory wear of the bottom during oxygen bottom-blowing was brought down in the BBOP by the use of shrouding fluid around the oxygen jet. Various shrouding fluids like propane, natural gas, coke-oven gas, liquid hydrocarbons like fuel oil have been used or proposed.[9] Aeron and Ramachandran[9] did a preliminary analysis to find out the possibility of the use of coke-oven gas and liquid petroleum gas as shrouding fluid. It was made with the assumption that the mechanism by which the shrouding gas protects the fluid is by cooling the tuyere zone on cracking. However, the details of how the shielding fluid protects the tuyeres is not known. There can be two mechanisms by which such protection takes place:

a) The surrounding jet physically shields the oxygen jet, taking the zone of metal/oxygen reactions away from the tuyeres.

b) Cooling of the tuyeres zone by endothermic cracking of the hydrocarbon.

Fluid flow at the bottom of the converter should play an important role in bottom wear. High degree of turbulence enhances the mass transfer of the reactants and the products from the refractory surface if chemical attack is the mechanism of wear. Highly turbulent flow with large eddies can also help in increasing iron penetration into the refractory which, as was stated earlier, may weaken the refractory. Small recirculations near the jet can cause a

build up of highly oxidising slag particles which would attack the refractory lining. The fluctuating nature of the flow causes fluctuations in shear stress at the bottom which may result in the mechanical erosion of the refractory. Moreover, the temperature near the tuyere is expected to be affected by the fluid flow patterns.

Besides the importance of fluid flow on bottom refractory wear, fluid flow and mixing in the converter as such influence the dynamics of the process significantly. Therefore it was decided to do some investigations on this aspect with emphasis on understanding of the bottom refractory wear.

1.3. PLAN OF INVESTIGATION

Investigations on mixing and fluid flow in many high temperature metallurgical processes have been carried out employing room-temperature models. Such models are built by glass or perspex. Some room-temperature liquid would simulate molten metal. If the liquid is water, then the technique may also be termed as water modelling.

Advantages of such models are:

a) The fluid flow can be visualised,

b) Variables can be controlled and measurements made with precision.

Of course, these model studies have their own limitations and their results should not be extrapolated to predict behaviour of prototypes blindly. One has to exercise his judgement.

It was decided that a water model study of the BBOP would be worthwhile in order to ascertain the mixing and fluid flow pattern since very little information is available in the literature. However, the emphasis in such an investigation would be to try to collect some relevant data in connection with bottom refractory wear.

It was decided to carry out the water model study along the following specific directions:

a) Study of the mixing of two coaxial jets placed centrally at the bottom of a perspex vessel, to specifically find out whether the shrouding gas physically shields the inner jet.

b) Studies involving flow measurements at the bottom in order to unearth the pattern of flow as well as to determine the effect of various process parameters. The investigation was again to be divided into:

   i) studies with a single tuyere placed axially in a cylindrical (or rectangular) vessel, and

   ii) studies with multiple tuyeres.

In the model, it was planned to use water to simulate molten metal and air to simulate oxygen. Carbon

dioxide would simulate the shrouding gas in jet mixing studies. In shear stress measurements, however, air would simulate the shrouding gas also.

With these broad objectives in mind, the following plan was chalked out:

1. To design and fabricate a laboratory-size perspex model of the bottom-blown converter for experiments with single tuyere and multiple tuyeres.
2. To design and fabricate the following auxiliary set-ups:
   a) an arrangement to supply gases to tuyeres at controlled flow rates and to measure the same.
   b) an optical set-up for flow visualization.
3. To conduct experiments with single coaxial tuyere and determine mixing of the jet gas and the shrouding gas downstream from the tuyere nozzle by sampling and analysis of carbon dioxide by gas-chromatograph.
4. To conduct trials and perfect the technique of measurement of wall shear stress and/or velocity of water near the wall.
5. To make measurements of wall shear stress and/or velocity of water near the walls when blowing with single tuyere as well as multiple tuyeres.
6. To visualise the flow pattern in the model and if possible, to conduct photography.

7. To study the effects of flow of air in the inner pipe and in the annular space between the two pipes of the tuyere, height of the water bath and the projection of the inner jet pipe into the bath as appropriate for individual sets of measurement in experiments with single tuyere.
8. To study the effects of the number of tuyeres, their arrangement in the bottom and the projection into the bath in experiments with multiple tuyeres.
9. To correlate and interpret the results.

CHAPTER 2

EXPERIMENTAL EQUIPMENT AND PROCEDURE

In the present investigation, a room temperature model study of the bottom-blown oxygen steelmaking processes was carried out using water to simulate hot metal. Experiments were conducted in a cylindrical perspex (polyacrylic) vessel with a detachable bottom. The general layout of the apparatus is described in Section 2.1. In gas mixing studies, air simulated oxygen and carbon dioxide simulated the shrouding gas. The experiments were conducted by measuring the concentrations of air and carbon dioxide at various points across the jet at various distances downstream from the tuyere. The details of these experiments are presented in Section 2.2. Several attempts made to measure flow velocities were unsuccessful. Brief descriptions of these techniques are given in Section 2.3. Finally it was decided that useful information could be obtained by measuring the mass transfer coefficient and the shear stress at the wall by the electrochemical technique which is reviewed and described in the above section. In the experiments using the above technique, air simulated both oxygen and the shrouding gas. The descriptions of the equipments and the experimental procedure for these experiments are presented in Section 2.4. Visual

observations of flow as well as movie photography were undertaken to a limited extent. These are described in Section 2.5.

2.1. GENERAL LAYOUT OF THE APPARATUS

The general layout of the apparatus is shown schematically in Figure 2.1. It consists of a simulating vessel and two gas flow lines, one connected to the inner tube of the tuyere in the bottom of the vessel and the other connected to the annular space between the two pipes in the tuyere. The air flow-line consisted of an air-compressor, a flow regulating valve, a chamber in which temperature measurement could be done and an crifice meter to measure the air flow rate. The shrouding gas flow-line, which supplied gas to the annular space in the tuyere consisted of a carbon dioxide cylinder, a flow regulating valve, a chamber for temperature measurement and a rotameter for measuring the flow rate. At very small flow rates of the shrouding gas, a capillary flow meter replaced the rotameter. There was a provision for routing part of the air into the shrouding gas flow-line for experiments in which mass transfer coefficients/ shear stresses were measured.

2.1.1. Dimensional Analysis:

A dimensional analysis was carried out with a view to design the simulating vessel and the tuyeres. Following is

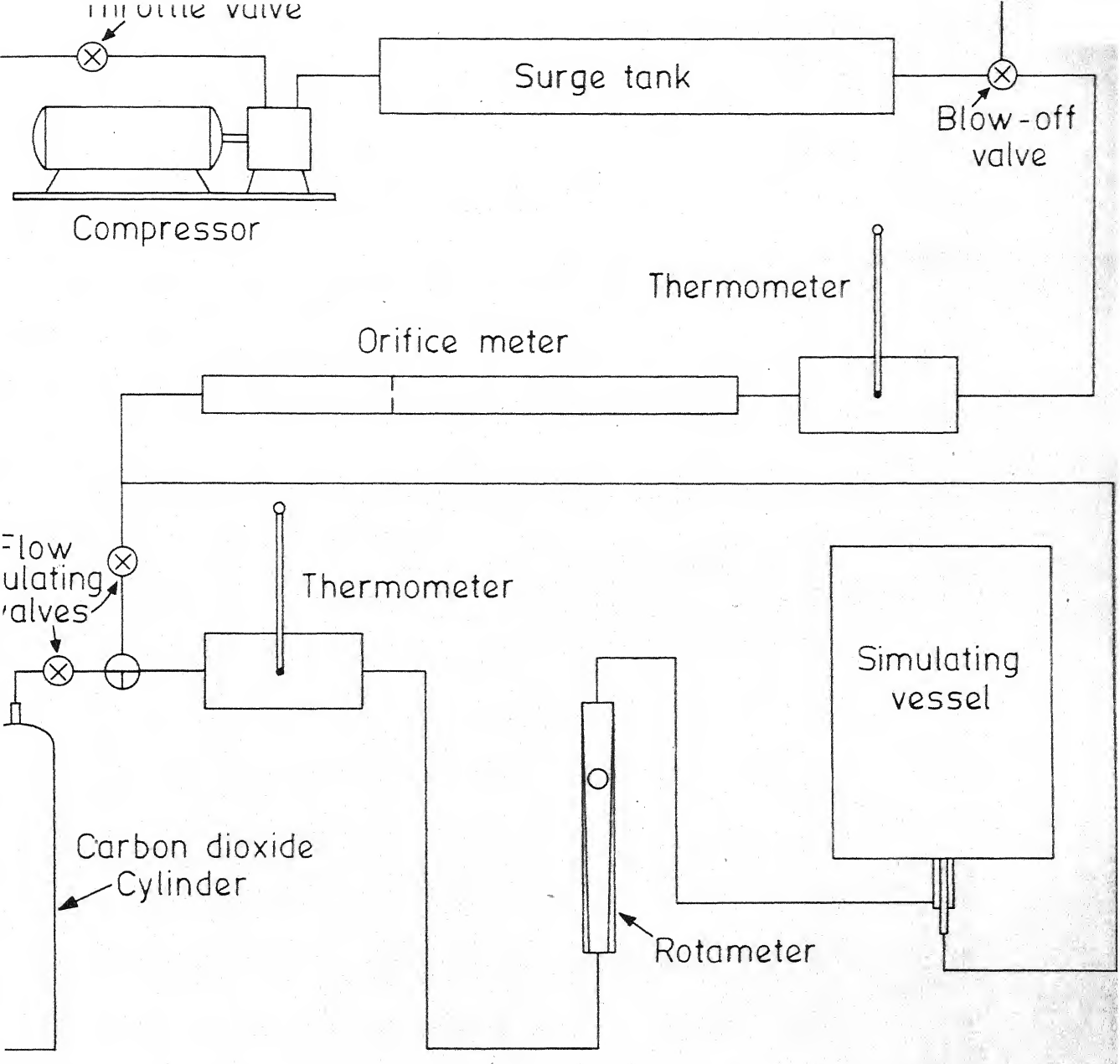

Fig. 2.1 Schematic diagram of the layout of the apparatus.

a list of process variables in a bottom blown converter which may have a bearing on the liquid flow in the converter. All of the following variables, however, may not be important. For the sake of brevity, gas flowing in the inner pipe of the tuyere will be termed as the jet gas and the gas flowing in the annular space between the two pipes as the shrouding gas.

Variable	Symbol
Velocity of the jet gas at the tuyere exit	v_j^o
Velocity of the shrouding gas at the tuyere exit	v_s^o
Diameter of the inner pipe	d_j
Thickness of the annular space between the two pipes	t_s
Distance to which the inner pipe is projecting into the liquid	l
Density of the jet gas at the tuyere exit	ρ_j^o
Density of the shrouding gas at the tuyere exit	ρ_s^o
Density of the liquid	ρ_l
Height of the liquid bath	h
Viscosity of the jet gas	μ_j
Viscosity of the shrouding gas	μ_s
Viscosity of the liquid	μ_l
Surface tension of the liquid	σ

If $v_l(x, y, z)$ is the velocity of the liquid at a point (x, y, z), then by Rayleigh's method of indices, one obtains after some rearrangement:

$$v_l(x, y, z) = f\left[\frac{v_s^o}{v_j^o}, \frac{t_s}{d_j}, \frac{l}{d_j}, \frac{h}{d_j}, \frac{\rho_j^o}{\rho_l - \rho_j^o}, \frac{\rho_s^o}{\rho_l - \rho_j^o}, N_{Fr}, N_{Re}^j, N_{Re}^s, N_{Re}^l, N_{Wb}, \frac{x}{d_j}, \frac{y}{d_j}, \frac{z}{d_j}\right] \qquad 2.1$$

where

i) N_{Fr} is the Froude number, $\frac{v_j^{o2}}{g d_j}$,

ii) N_{Re}^j, N_{Re}^s and N_{Re}^l are the Reynolds numbers for the jet gas flow, the shrouding gas flow and the liquid flow in the vessel respectively, and defined as $N_{Re}^j = v_j^o \, d_j \, \rho_j^o / \mu_j$ and so on, and

iii) N_{Wb} is the Weber number, $\sigma / (\rho_j^o \, d_j \, v_j^{o2})$.

For the type of flow one encounters in bottom blowing where buoyancy effects are important, it is meaningful to use the modified Froude number $N_{Fr'}$ rather than N_{Fr}[31], where the former is defined as

$$N_{Fr'} = \frac{v_j^{o2}}{g d_j} \frac{\rho_j^o}{\rho_l - \rho_j^o} \qquad 2.2$$

Amongst the dimensionless variables in eq. 2.1, Reynolds number, which is a ratio of inertial forces to viscous forces, is not definable for the liquid flow in this system and has been ignored. However, it is to be noted that the kinematic viscosity of molten steel and water are comparable and hence the viscous effects are also expected to be comparable. At very high N^{j}_{Re}, the bubble size in the jet has been found to be a very weak function of N^{j}_{Re} [18]. Moreover, as the turbulence in the jet is large, agitation overrides the viscous effects; gravity and inertia are the leading forces and the effect of Reynolds number becomes insignificant.[22] Hence N^{j}_{Re} and N^{s}_{Re} have not been considered when selecting the vessel size. In determining the flow of the liquid in the vessel, surface tension may not play an important role, while momentum of the jet should be of overriding importance. Theofanus et al[32], for example, found that the effect of surface tension on mass transfer from a jet to the surrounding fluid is quite small. However, in the jet behaviour itself, like mixing of the two jets, it may have some importance. In the present investigation, however, Weber number has not been simulated because simultaneous simulation of the Weber number and the modified Froude number would require flow rates of air beyond the capacity of the laboratory model. It was therefore decided that a convenient tuyere size would be chosen, and flow rates of air selected to simulate modified Froude number of the prototype.

Data of a typical blow in a 25 T converter at Maxhütte (Table 2.1) converting high-phosphorous iron was taken for the purpose of simulation.[33] Design data for a larger converter could not be obtained. Based on these, the dimensions of the simulating vessel and the tuyeres were decided upon, keeping experimental limitations in mind.

Table 2.1

Data for a 25 T OBM Converter at Maxhütte A.G., Germany[33]

Tuyere:	
Number of tuyeres	20
Inner pipe i.d.	12 mm
Inner pipe o.d.	14 mm
Thickness of the annulus	2 mm
Blowing:	
Total flow rate of oxygen at full blow	5000 Nm^3/hr
Total flow rate of propane (shrouding gas)	170 Nm^3/hr
Average velocity of oxygen at the tuyere exit	4.9×10^4 cm/sec
Dimensionless groups for the oxygen jet:	
N^j_{Re}	3.9×10^5
$N^j_{Fr'}$	330
N^j_{Wb}	3.5×10^3

The air compressor available to us could deliver air at a flow rate of only about 350 liters/min. Therefore, it was decided to choose the diameter of the inner tube in the tuyere to be 0.65 cm for single tuyere measurements. For this size, the flow rate of air from the compressor was sufficient, with enough margin, to simulate the modified Froude number of the prototype.

The dimensions of the Maxhütte converter, referred to in Table 2.1, were not available. On the other hand, the bath height in a 30 T OLP converter at IRSID, France is about 83 cm and the diameter is about 2.6 meters.[34] Based on these, the height of water in the vessel for the experiments were kept at 40 cm. (except for those sets where bath height was a variable). The diameter of the vessel was kept at about 50 cm, as vessels of larger size were difficult to handle in the laboratory.

In multi-tuyere experiments, the diameter of the tuyeres was chosen to be 0.325 cm, which allowed simulation of $N^{j}_{Fr'}$ when twelve tuyeres were used.

2.1.2. Simulating Vessel

The simulating vessel used in these investigations is shown in Figure 2.2. It consisted of a tank of 51 cm x 51 cm square cross-section and 67 cm. height made of 1 cm thick optically clear perspex sheet. The sides of this

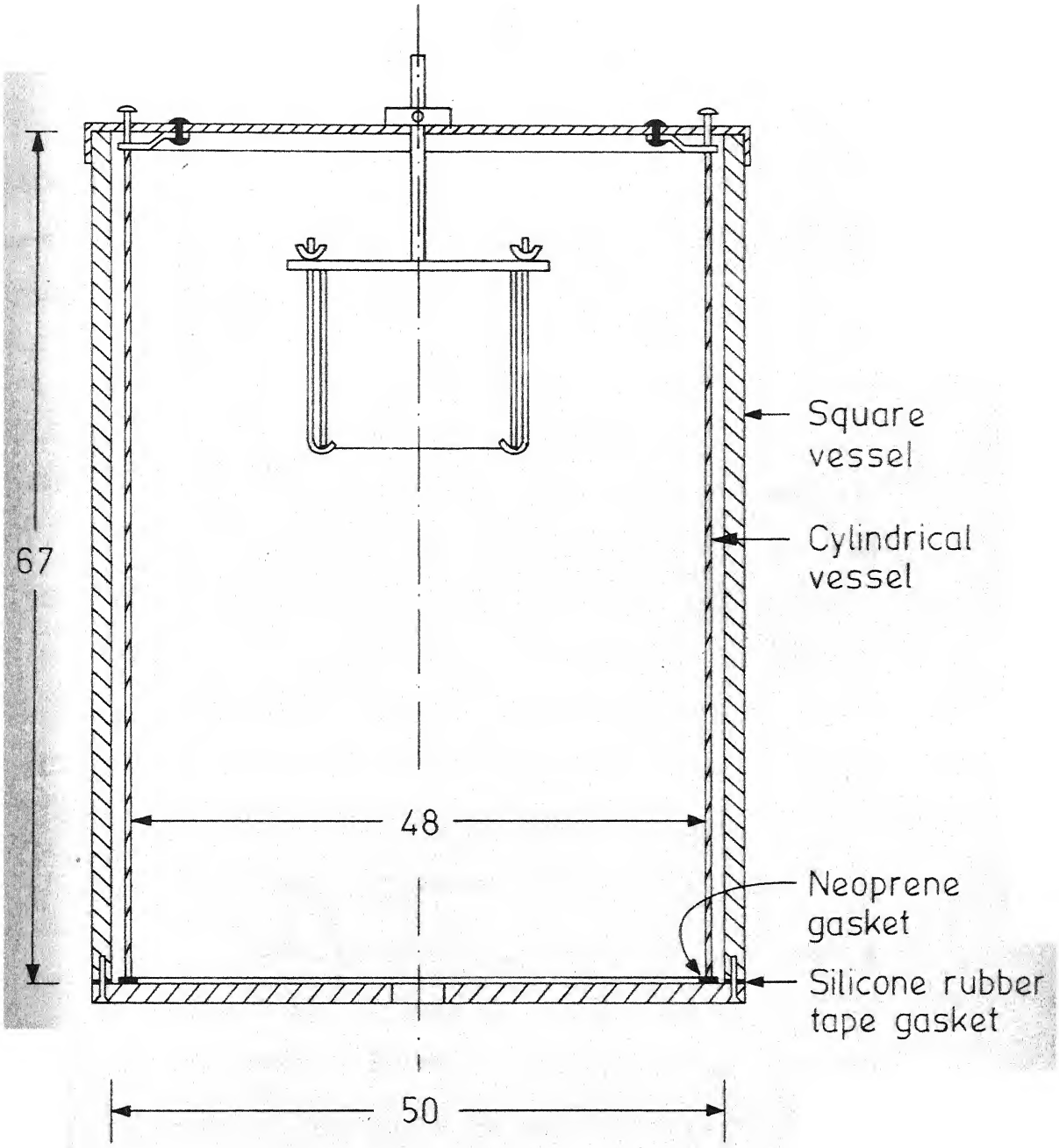

All dimensions are in cm

Fig. 2.2 Simulating vessel

vessel were joined using chloroform and supported by a frame of aluminium angles. The bottom was detachable and was fixed to the side walls with screws, with a silicone tape gasket in between.

A vessel of square cross-section with flat walls allows photography and visualization of flow without optical distortions. However, it was found that such a shape of the vessel resulted in appreciable corner effects in the fluid flow pattern. Therefore, later on a cylinder of perspex open at both ends of 48 cm i.d. and 65 cm height was placed inside the square vessel and the intervening space was also kept filled with water so as to avoid optical distortions. The lower end of the cylinder was sealed against the bottom by a neoprene gasket and pressure from the top.

With a single tuyere placed axially, the bath was found to oscillate quite vigorously. This kind of behaviour has also been reported by Etienne[22] in his water model studies. Small oscillations in the bath due to surface waves make the gas jet oscillate too. This causes the spout above the jet to move, which in turn results in higher bath oscillations. In such a manner, the oscillation amplitude builds up. As these oscillations made handling of the apparatus quite difficult, a spout breaker was provided to reduce this oscillating and at the same time interfere with

the flow to the minimum extent. The spout breaker was a short 15 cm dia. glass cylinder open at both ends kept vertically about 2.5 cm above the quiescent bath surface. This stopped the movement of the spout bringing down the amplitude of the oscillations.

The bottom of the vessel used in single tuyere experiments had a central threaded hole into which the tuyere could be fitted. In experiments with multiple tuyeres, this bottom was replaced by the one shown in Figure 2.3. This consisted of 35 threaded holes into which the tuyeres could be fitted. The holes were distributed such that various configurations of tuyeres could be achieved. The holes not in use were plugged with perspex stoppers and neoprene gaskets.

2.1.3. Tuyeres

Concentric tuyeres were employed in experiments with single tuyeres. In experiments with multiple tuyeres, the tuyeres were simple tubes.

Figure 2.4 shows the concentric tuyere assembly. It consisted of an inner pipe of constant cross-section through which air was to be blown. This pipe was placed coaxially in an outer pipe which was threaded onto the bottom of the simulating vessel. The inner pipe was sealed to the outer pipe using an O-ring and a knurled knob so that the projection of the inner pipe into the vessel could be

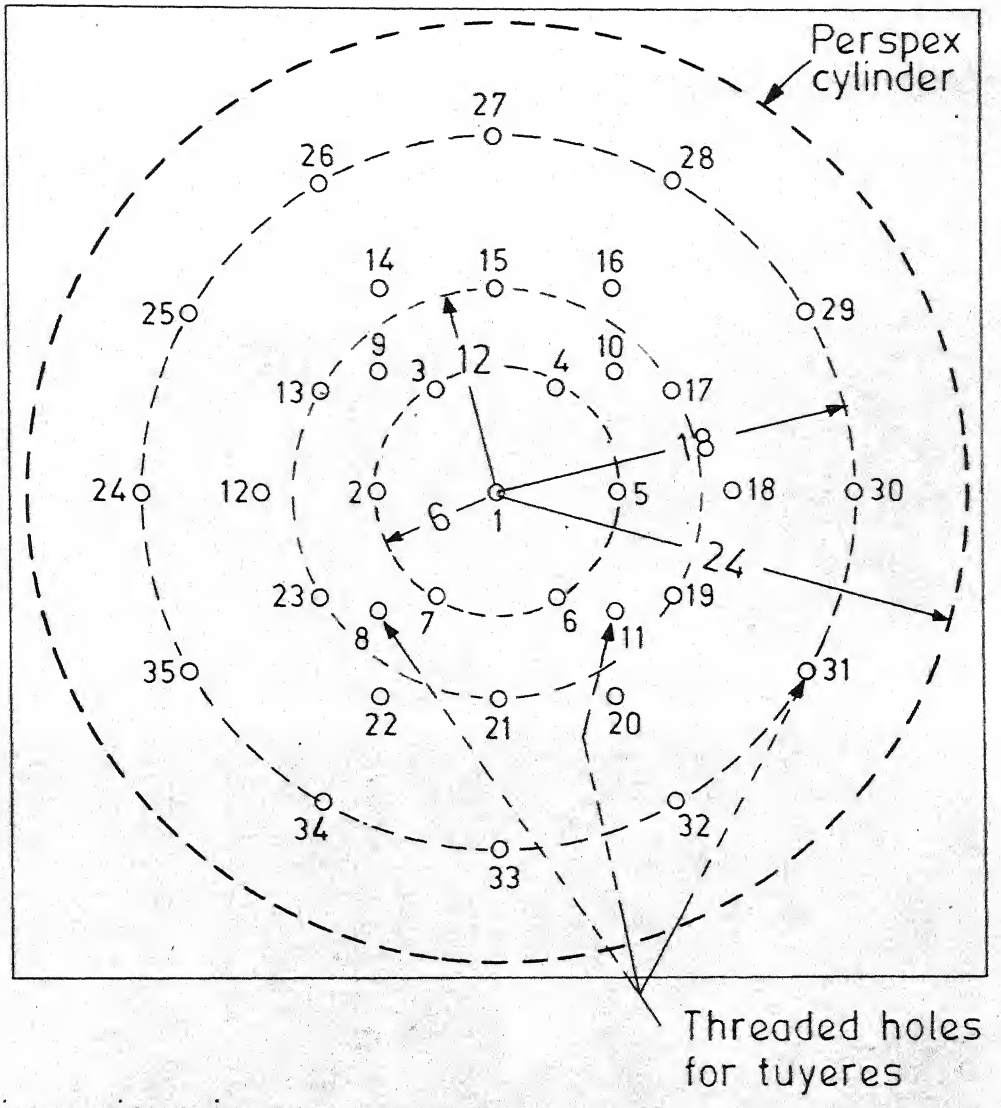

Dimensions in cm

Fig. 2.3 Bottom for experiments with multiple tuyeres.

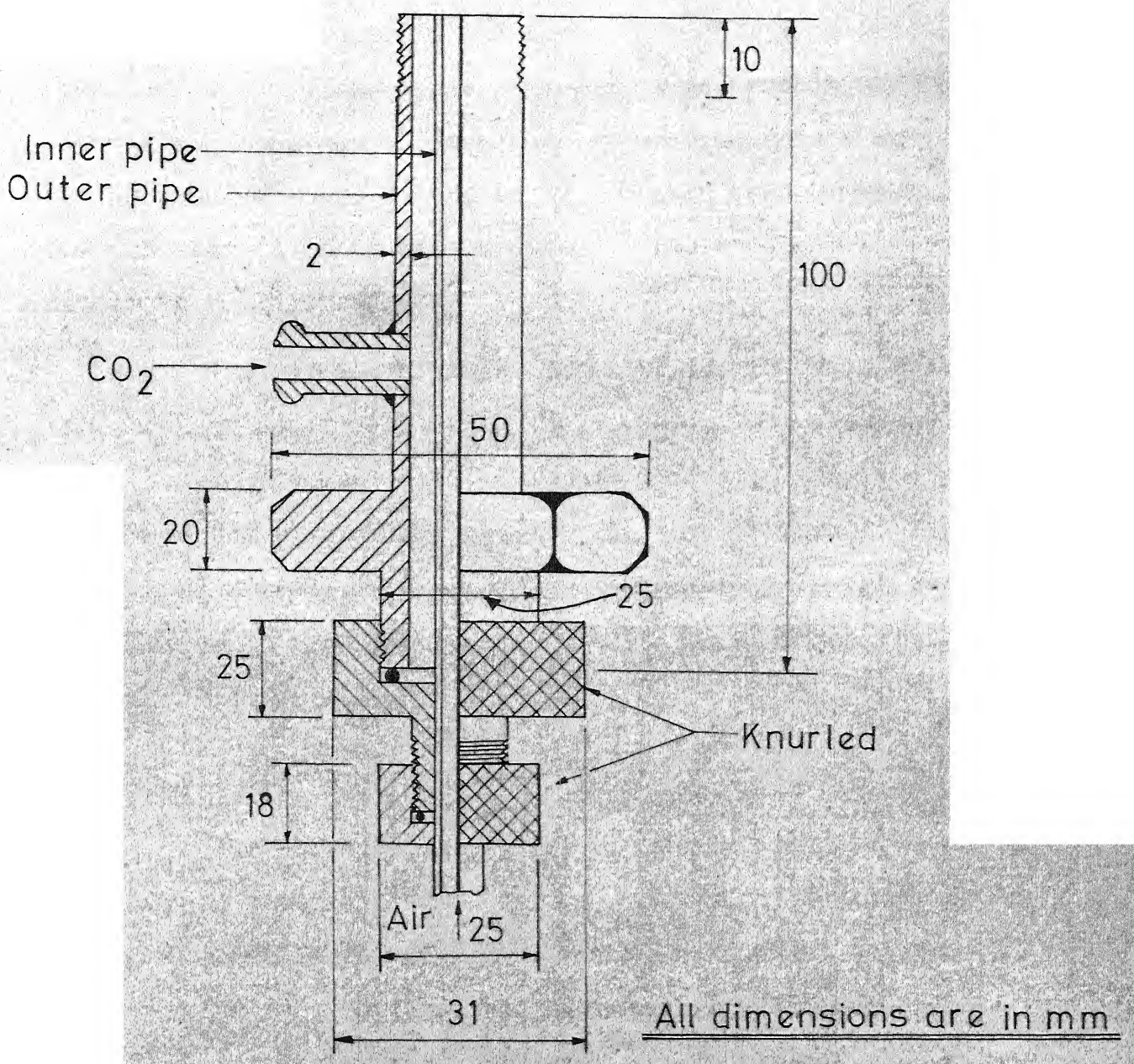

Fig. 2.4 Tuyere used in single tuyere experiments.

adjusted at will. The shrouding gas was introduced into the annular space between the two pipes through a side-tube soldered to the outer pipe. The design was such that various combinations of diameters of the inner tube and widths of the annulus could be obtained. In this work however only one combination of sizes was employed the dimensions of which are shown in Figure 2.4.

The tuyeres employed in multi-tuyere experiments are shown in Figure 2.5. They were simple tubes, threaded on the outer side so that they could be fitted into the bottom of the simulating vessel. The tuyere shown in Figure 2.5a, when fitted, was flush with the bottom; the one shown in Figure 2.5b projected out of the bottom into the vessel to a distance of 1.3 cm.

2.1.4. Air Flow Line

Air was supplied by a 3 HP rotary compressor-cum-vacuum pump manufactured by Messrs J.B. Sawant Engineering Works, Bombay. A rotary compressor is a constant volume device and hence the flow rate is constant with respect to time. Throttling of air inlet into the compressor allowed gross control of the flow rate. Air from the compressor was first passed through an oil filter (Figure 2.6) containing coarse and fine glass wool and then through a 3 meter long pipe of 20 cm diameter which acted as a surge tank

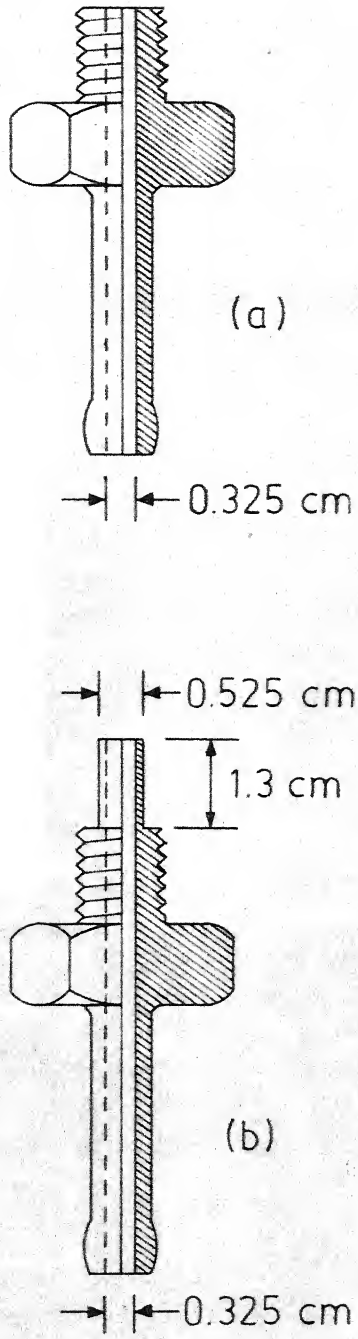

Fig. 2.5 Tuyeres for experiments with multiple tuyeres; (a) tuyere flush with bottom (b) tuyere projection = 4 d_j

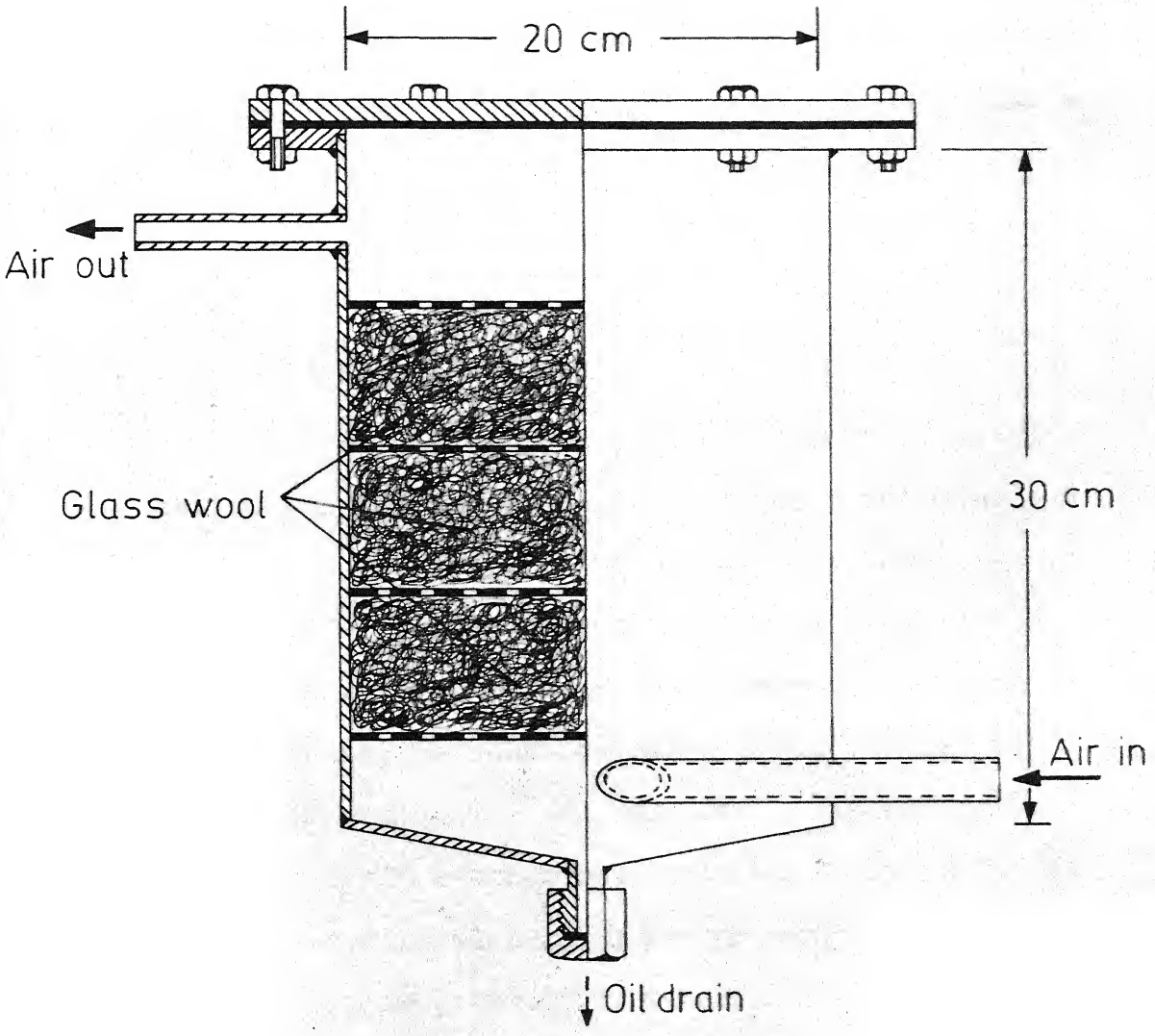

Fig. 2.6 Air filter

eliminating small pressure fluctuations. A 5 cm i.d. pipe, next in the flow-line, had a gauge to measure the pressure in the flow-line and a needle valve for blowing off air to effect finer adjustments in air flow rates.

The temperature of air was measured with a thermometer in a 10 cm dia and 25 cm long chamber, which was next in the flow-line.

Flow rates of air were measured with an orifice meter fabricated in the laboratory. An orifice meter was chosen for this purpose, because of its simplicity, standardized design, and wide range of flow rates that could be measured with accuracy. ASME specifications[35,36] were applied throughout, so that the meter could be used without recourse to time-consuming calibrations. Dimensional details of the orifice-meter are shown in Figure 2.7. It consisted of a square edged orifice of required size placed between two circular pipes of constant cross-section. Pressure difference between points 2.5 cm away on the upstream and downstream side from the respective faces of the orifice plate was measured. The total pressure on the upstream side was also simultaneously measured. With these data the flow rate can be calculated using standard tables.[35,36] The equation used for calculating the flow rate is the following (after conversion into metric units):

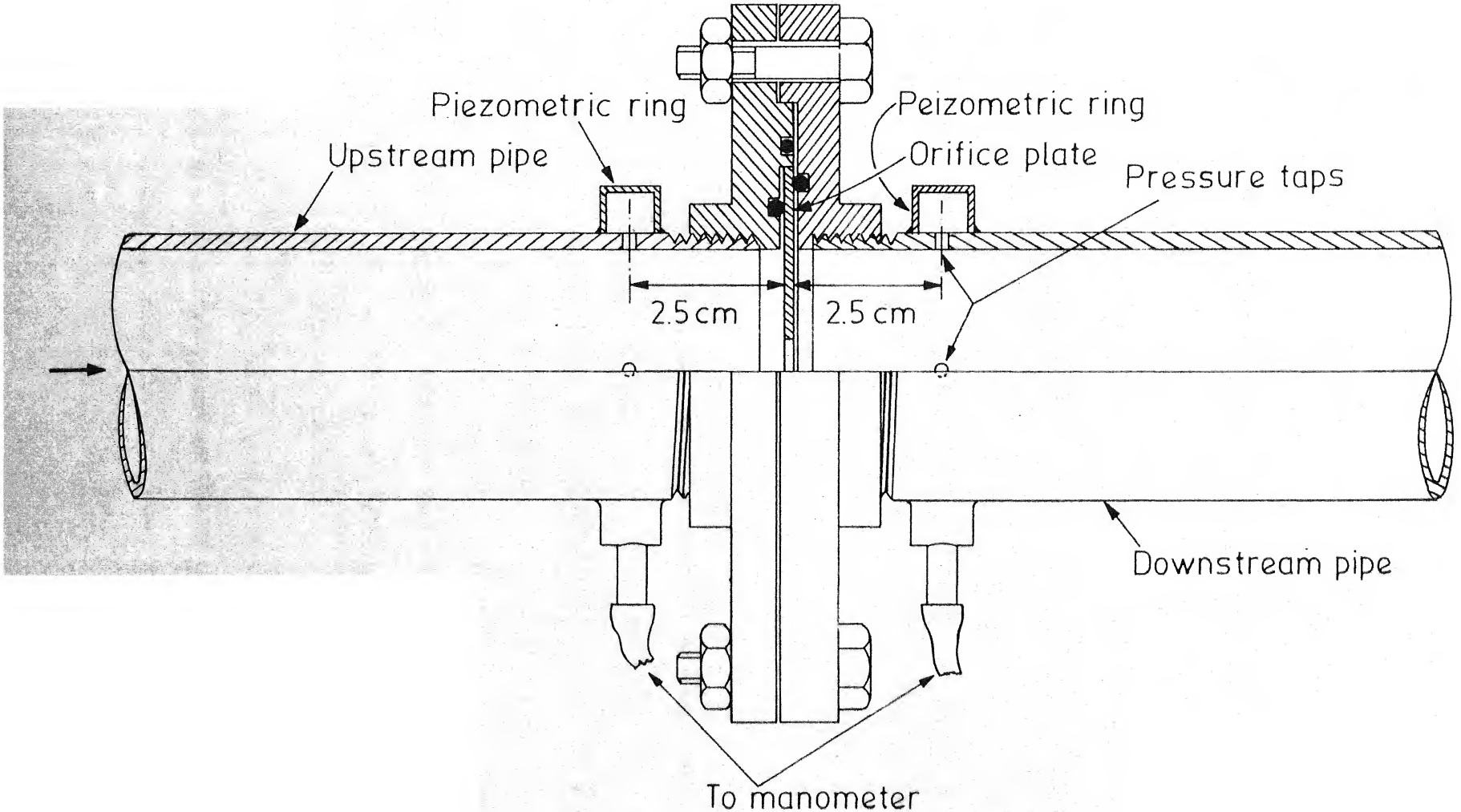

Fig. 2.7 Orifice meter

$$W = 34.77\ (D_2)^2\ KY_1\sqrt{\rho_1\ h_w} \qquad 2.3$$

where

W = mass flow rate of air, gm/sec

D_2 = orifice diameter, cm

K = flow coefficient = $C/\sqrt{1 - \beta^4}$, dimensionless

β = ratio of orifice diameter to pipe diameter, dimensionless

Y_1 = expansion factor, dimensionless

ρ_1 = density of metered fluid at upstream pressure tap conditions, gm/cc

h_w = pressure difference across the orifice, cm of water

C = coefficient of discharge, dimensionless.

Values of flow coefficient K[35] or coefficient of discharge C[36] are available in standard tables. It can also be calculated using empirical equations.[35] Values for the expansion factor Y_1 for various gases in terms of pressure difference h_w and β are also available in the literature.[35,36] The mass flow rate so obtained is converted to volume flow rate at the tuyere exit. Procedure for the calculation of flow rates is given in Appendix I.

The orifice meter pipes were of brass, 3.75 cm i.d. and was polished to brightness on the inside. The upstream side was about 60 cm long and the downstream side,

30 cm. The two were joined with flanges, with the orifice plate in between. Four pressure holes, 90° from each other, were provided both upstream and downstream of the orifice plate at a distance of 2.5 cm. Piezometric rings were soldered to the pipe outside to eliminate pressure variations along the perimeter of the pipe. These two piezometric rings were connected to the two ends of a manometer. A pressure tap was also provided on the upstream side to measure the total pressure. Flanges were carefully fitted to the pipes to give axial alignment of the latter. A step was provided in one of the flanges into which the orifice plate fitted tightly so that the latter is also axially aligned and orifice plates of different orifice diameters could be used.

The orifice plate was made of 0.15 cm thick stainless steel sheet. The dimensions of the orifice plates as shown in Figure 2.8 conformed to ASME specifications. The square edges were carefully machined and checked under a magnifying glass for imperfections.

In single tuyere experiments, air from the orifice meter was directly fed to the tuyere. In multi-tuyere experiments, however, air was distributed equally to various tuyeres with the help of a feeder shown in Figure 2.9.

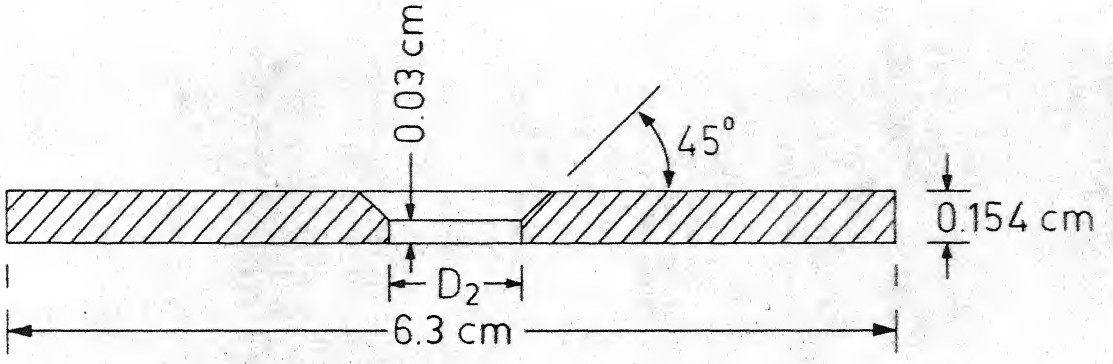

Fig. 2.8 Orifice plate

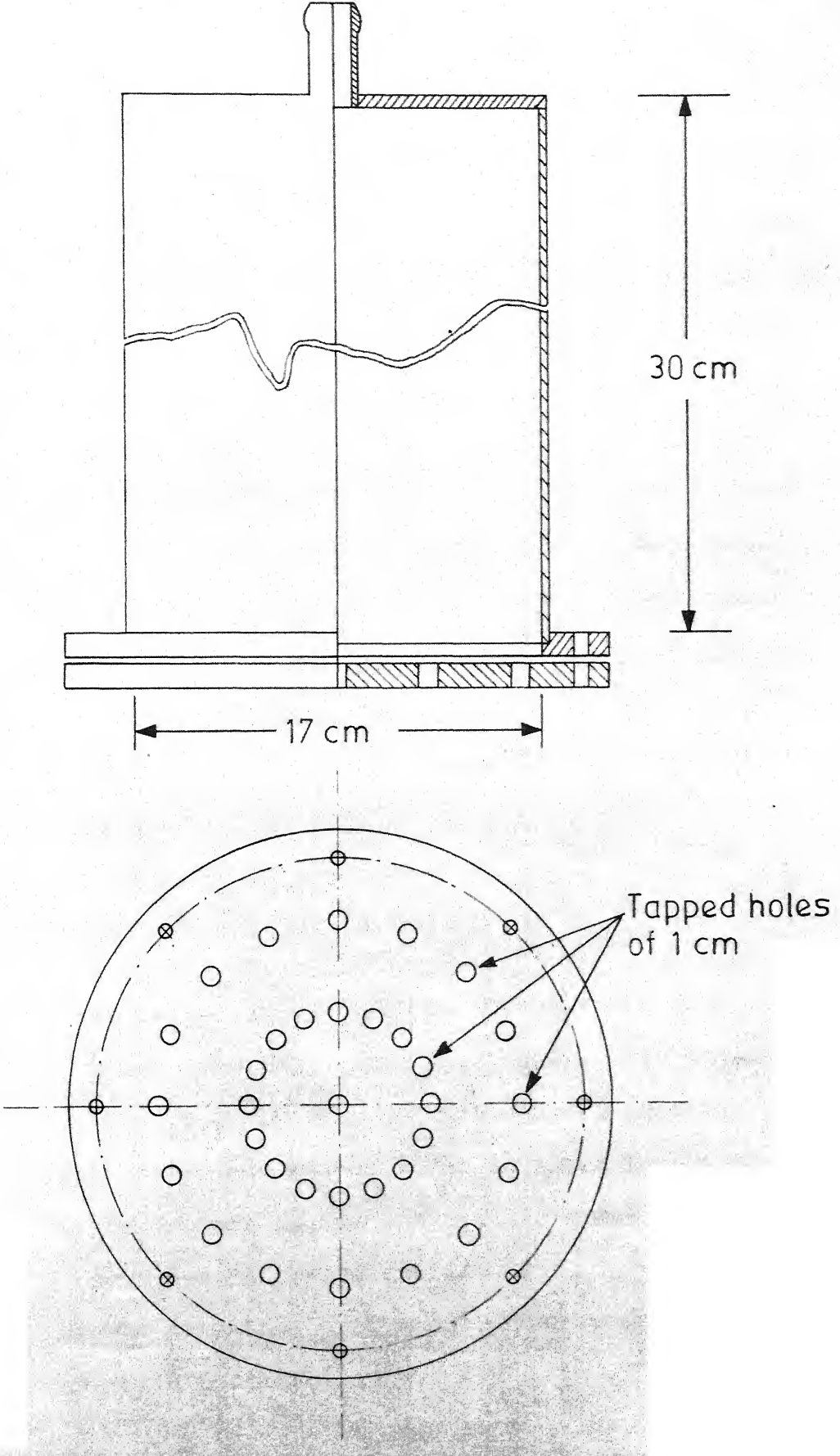

Fig. 2.9 Gas feeder to multiple tuyeres.

2.1.5. Flow-Line for Shrouding Gas

The flow-line for the shrouding gas is also shown in Figure 2.1. Carbon dioxide was supplied from a cylinder. The flow rate was adjusted with the help of a needle valve. The temperature of the gas was measured in a manner similar to the one employed for air. For mass transfer coefficient and shear stress measurements part of the air from the air flow-line was bifurcated to the flow-line for the shrouding gas.

The flow rates of the shrouding gas were measured with a Rotameter (for higher flow rates) or a capillary flow meter (for smaller flow rates). These had been precalibrated with a precision Wet-Test meter.

2.2. STUDIES OF GAS MIXING IN THE JET

Gas mixing in the jet was investigated only in the single-tuyere assembly since the results thus obtained are expected to be applicable to multi-tuyere assembly too. Air from the compressor was employed to simulate oxygen and carbon dioxide from cylinders employed to simulate the shrouding gas. Concentration profiles were taken at various heights from the tuyere exit. Gas analysis was done by gas-solid chromatography.

2.2.1. Sample Probe Assembly and the Drying Column

Gas sampling was done by a probe comprising of a 20 ml hypodermic syringe attached to a rigid arm. The plunger of the syringe was pulled by means of a wire connected to its head. The probe is shown in Figure 2.10. For sampling at various locations in the field of the jet, it is necessary to move the probe along two normal horizontal axes as well as in the vertical direction. Moreover, the exact location of the probe tip was to be known with fair accuracy. These were achieved by hanging the rigid arm from a metal platform which could be moved in the two horizontal directions. The rigid arm, which held the probe, could be moved up and down. Figure 2.11 presents a sketch of the assembly.

The gas sample thus collected was wet and was next dried over 3:1 sulphuric acid in the dryer shown in Figure 2.12. Drying is essential; otherwise water vapour would get adsorbed on the silica gel column in the chromatograph changing its characteristics.

2.2.2. Gas Analysis

Gas analysis was done with a gas chromatograph manufactured by Messrs Chromatographic Instruments Corporation, Baroda, India, and a 1 mV recorder (Sergeant,

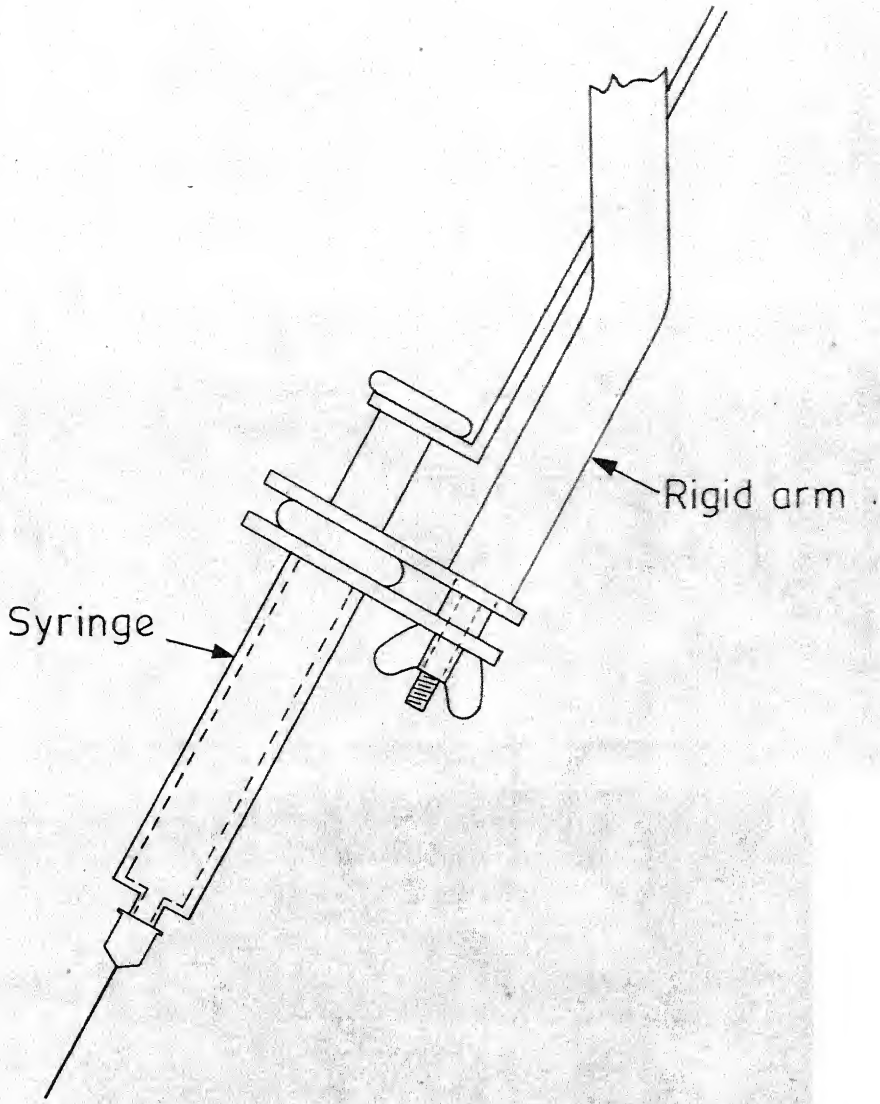

Fig. 2.10 Probe for gas sampling.

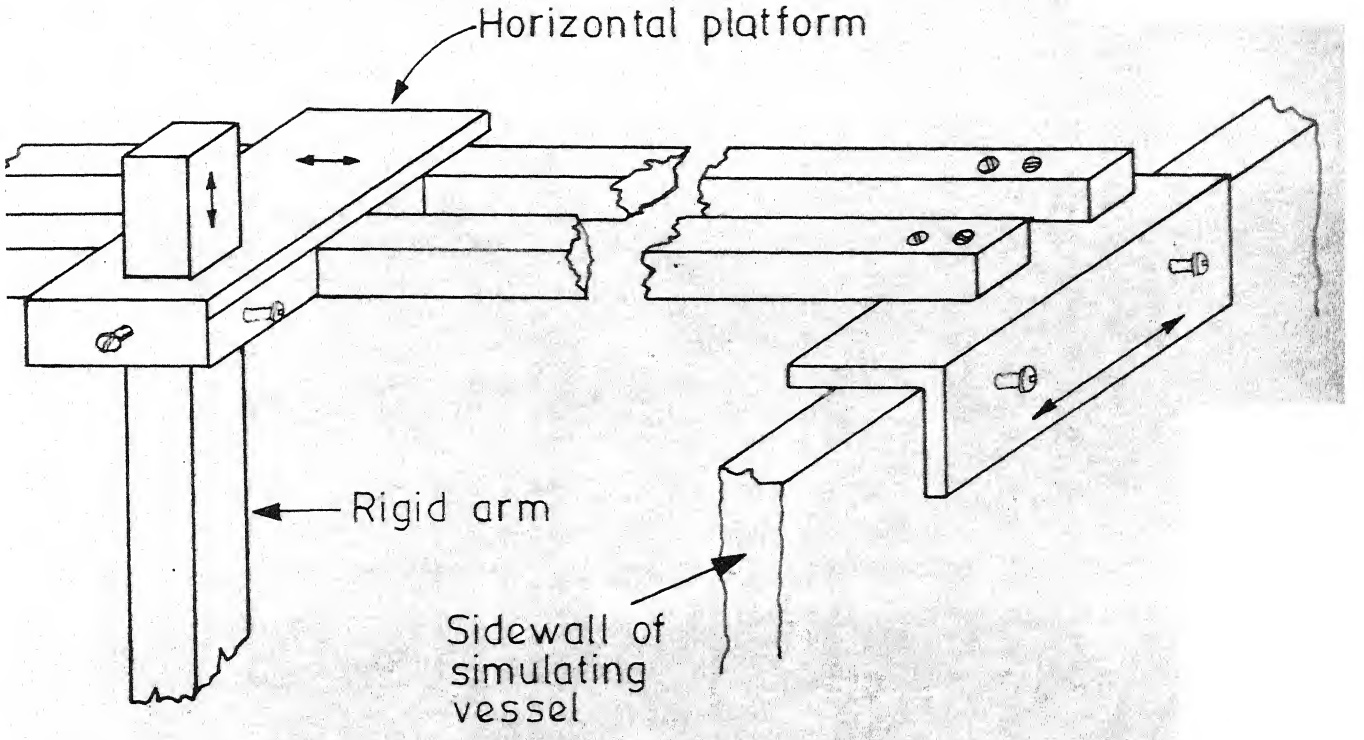

FIG. 2.11 Three dimensional traverse for gas sampling probe.

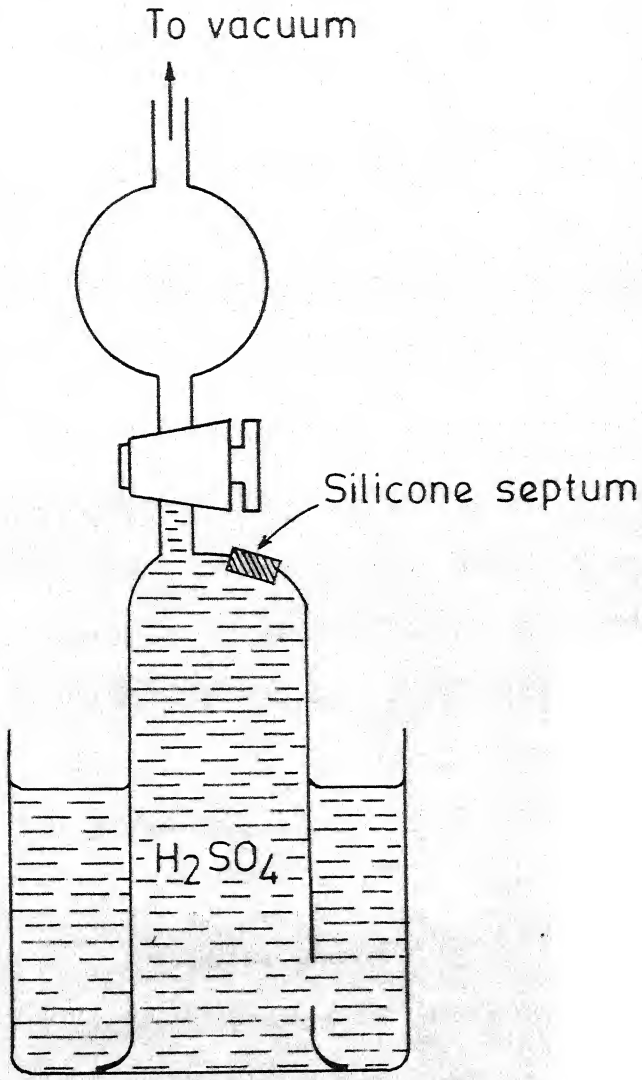

Fig. 2.12 Dryer for gas sample

U.S.A.). Silica gel was used as the stationary phase and hydrogen as the carrier gas. After much trial and error, the column temperature was fixed at 110°C and hydrogen flow rate at 40 cc/min. The detector was of the thermal conductivity type.

Injection of the sample with syringes did not give satisfactory reproducibility of analysis. Hence a sample introducing device, shown in Figure 2.13 was fabricated. This allowed a fixed amount of sample to be introduced every time and the rate of injection of the sample was constant. Using this device, the reproducibility of peak area as well as peak heights was good. Hence ratio of peak heights itself was used for the analysis, resulting in considerable saving of time. A calibration chart of ratio of peak heights vs. ratio of concentrations was drawn. On each day of experimentation, this calibration was checked to guard against any changes in column or detector behaviour.

2.2.3. Experimental Procedure for Gas Mixing Studies

The simulation vessel was filled with tap water. Blowing of air and carbon dioxide was started and adjusted to the required value. A sample of gas was taken at distance of about 20 cm. downstream from the tuyere exit, where the mixing was complete, and analysed to check whether the average concentration of carbon dioxide was that expected.

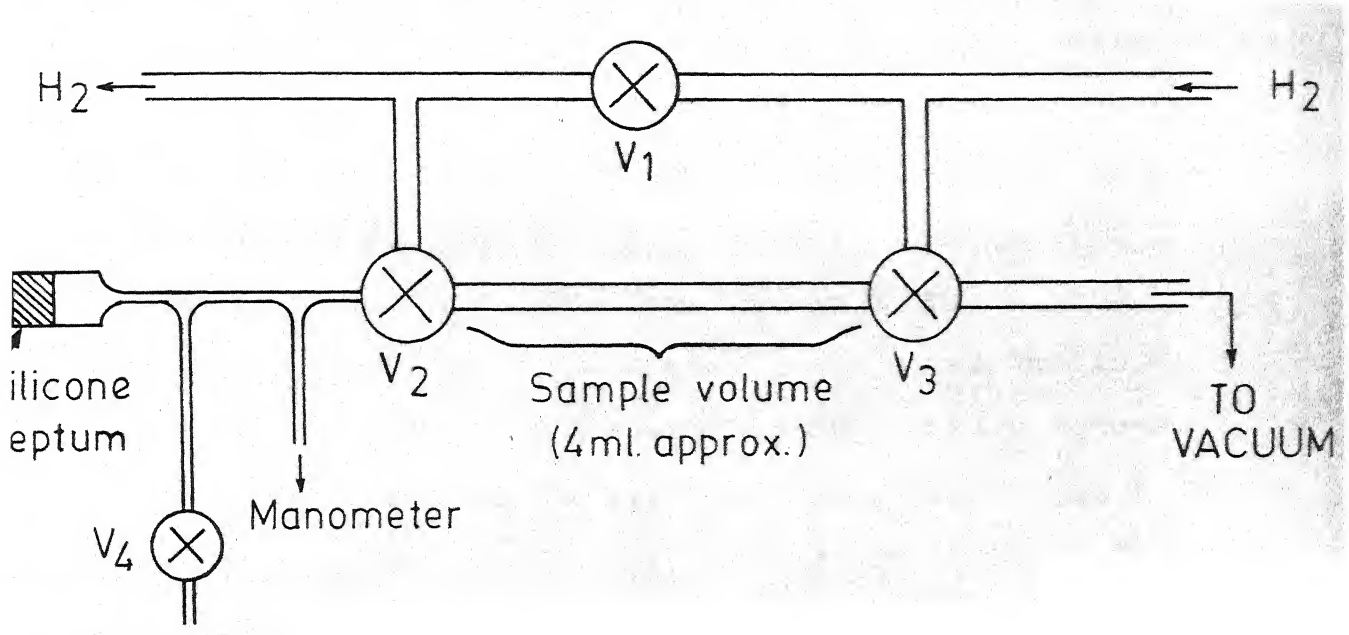

Fig. 2.13 Sample introduction device

The probe was then fixed at the required height and radial position. A sample of about 20 cc was taken into the syringe. The probe was then taken out. A small amount of the sample was injected into the dryer to bring the CO_2 concentration in the sulphuric acid nearer to the value which would be in equilibrium with the sample. After about one minute, this gas was sucked out and the sample injected into the dryer. The sample introducing device was by-passed from the carrier gas line and evacuated. About 4 ml of the sample was then taken from the dryer in a gas-tight syringe and introduced into the device through the silicone septum (see Figure 2.13). The mercury manometer indicated the pressure of gas in the sample tube, from which the amount of sample could be calculated. The carrier gas was then made to pass through the sample tube taking the sample along with it to the chromatograph. The heights of the peaks in the chromatogram corresponding to air and carbon dioxide were measured and the composition read from the calibration chart.

2.3. DEVELOPMENT OF TECHNIQUE FOR STUDYING FLUID FLOW NEAR THE WALLS

2.3.1. Efforts to Measure Flow Velocities

The study of fluid flow with reference to the bottom wear is a tricky problem. Originally, it was thought that flow profiling could be done in the near-bottom region

which could later be related to mass transfer and wall shear stress at the bottom. The following methods were tried out:

a) Tracking of particles with density very near that of water. This method had been used by Davenport et al[37] to measure flow velocities in a water model of the top-blown steelmaking process.

b) Hydrogen Bubble Technique[38]: This involves placing thin platinum wire cathodes in the flow field and producing streaks of tiny hydrogen bubbles. These bubbles could then by photographed to reveal the necessary information.

c) Thymol-Blue Method[39]: Here one employs the fact that the liquid very near a cathode in an electrochemical circuit becomes rich in OH^- ions, increasing the pH. Hence if a solution containing thymol blue indicator is maintained at a pH just less than 8 and a platinum wire cathode is placed in the flow field, a short pulse of current through the cathode would make a streak of blue to appear next to the cathode, which would move with the fluid. The streak could be followed photographically and necessary information obtained.

All the above three methods failed to yield relevant information, because the fluctuations in the flow are quite large. To locate the particles in the direction

of sighting was difficult. Moreover in (b) and (c) the streak of bubbles or thymol blue were hazy as they emerged from the cathode and were dissipated within a very short distance..

Apart from these, measurement of flow velocities using a pitot tube was also tried. However, changes in the total pressures were very small. Moreover, the pitot tube cannot give an idea of the fluctuations in flow which are important. In addition to that, the surface of water was not steady and so itself would contribute to the change of static pressure.

Finally, however, it was decided that the most relevant information could be obtained by measuring the mass transfer coefficient and the wall shear stress at the bottom directly by the electrochemical technique. The method is described in greater detail in the following sub-section.

2.3.2. The Electrochemical Technique — A Brief Review

In diffusion-limited electrochemical transfer of a species from an electrolyte to an electrode, the current becomes constant (limiting current, i_d) beyond a particular applied voltage and this current depends only on the mass transfer coefficient and bulk concentration of the species being transferred from the electrolyte to the electrode.

If across such a diffusion-limited electrode, the electrolyte is made to flow, the mass transfer coefficient and hence the current would be dependent on the velocity gradient. This is the principle behind the electrochemical technique to measure the mass transfer coefficient and the wall shear stress. An excellent review of the method, by Mizushina[40], exists in the literature, so only the highlights of the method and some of its applications will be noted here.

Figure 2.14 is a schematic plot of current vs. voltage at various flow rates across the electrode. At any given flow rate, as the voltage is continuously raised, a point is reached beyond which current remains constant on further increase of electrode potential. This region of constant current is the limiting current region. On further increase, however, a second reaction like hydrogen evolution would start causing current to increase drastically. So the shear stress measurements are done in the voltage range corresponding to the constant current region. Figure 2.14 also illustrates the effect of flow of the electrolyte. As the velocity of flow of the electrolyte increases, the mass transfer coefficient, and hence the current, increases due to decrease in the concentration boundary layer thickness. At very high flow rates, however, the reaction rate at the electrode surface becomes comparable to the rate of mass transfer and the plateau region in the current vs. voltage

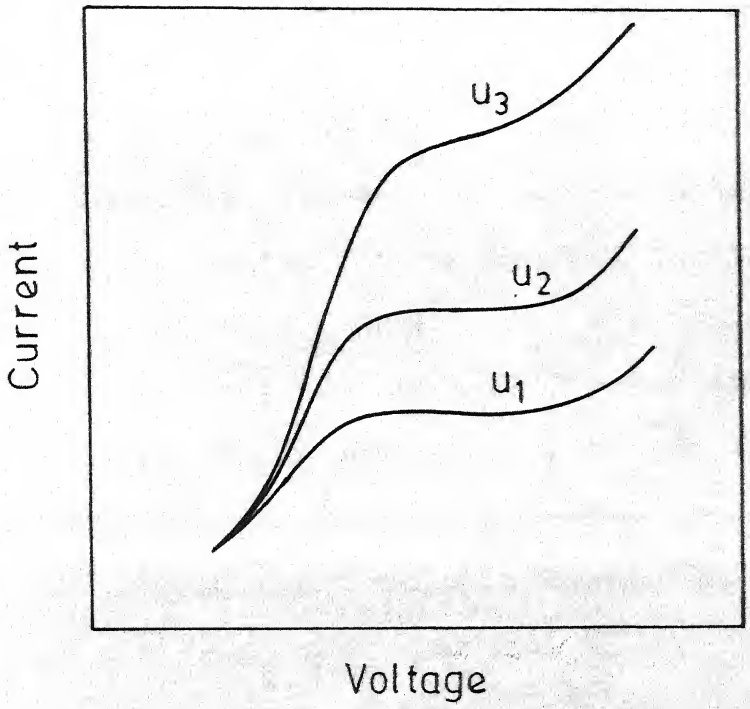

Fig. 2.14 Plot of current vs voltage at various flow rates u_i of the liquid across the electrode; $u_3 > u_2 > u_1$.

plot disappears. This upper limit to flow rate is called the "critical flow rate" and is a limit beyond which the electrochemical method cannot be employed.

Such an electrochemical method for measuring the mass transfer coefficient, the velocity gradient and therefrom wall shear stress has some inherent advantages. The electrode can be mounted flush with the wall so that the measuring process does not disturb the flow as in other techniques. Electrodes can be very small enabling one to measure local values of shear stress and mass transfer coefficient. Since the response of the cathode is very fast, one can measure both the time-averaged and fluctuating components of these quantities. The output signal can be processed in an analog device to yield the required information.

There are, however, certain limitations of the process. At very high flow rates, as mentioned earlier, the method is not applicable. Moreover, only certain kinds of electrolytes, in which a diffusion-limited reaction occurs, can be employed.

When current is passed through an electrochemical circuit, ions from the bulk of the electrolyte are transferred to the electrode surface by

a) diffusion aided by convection, i.e., by convective mass transfer through the concentration boundary layer, and

b) migration due to electrical potential gradient.

In the presence of a large concentration of an indifferent electrolyte, migration would be negligible at the boundary layer as compared to the convective mass transfer. Hence the standard equations for convective mass transfer to phase boundary would be applicable here as follows:

$$N_A = k(C_b - C_i) \qquad 2.4$$

where

N_A = mass transfer rate for component A,

k = mass transfer coefficient, which is dependent on the thickness of the effective boundary layer,

C_b = concentration of A in the bulk of the electrolyte, and

C_i = concentration of A at the electrode surface.

The current at the electrode (i) is given as

$$\frac{i}{AnF} = N_A \qquad 2.5$$

where

i = electrode current,

n = number of electrons involved in the reaction, and

F = Faraday constant.

At limiting current (i_d), C_i becomes zero and hence from Eqs. 2.4 and 2.5, one obtains:

$$k = \frac{i_d}{AnFC_b} \qquad 2.6$$

If at any instant the mass transfer coefficient is fluctuating, the current would also fluctuate. If $\bar{i}_d$ and i'_d are the time-averaged value and the fluctuating component of the instantaneous current, one can write:

$$\bar{k} = \frac{\bar{i}_d}{AnFC_b} \qquad 2.7$$

and

$$k' = \frac{i'_d}{AnFC_b} \qquad 2.8$$

where $\bar{k}$ and k' are the time-averaged and the fluctuating components of the mass transfer coefficient.

Reiss and Hanratty[41] have related the mass transfer measurements using small circular electrodes with the wall shear stress at the electrode surface. The following assumptions were made:

1. The scale of fluctuations is large compared to the electrode diameter so that the flow is uniform over the electrode surface.

2. The concentration boundary layer thickness is smaller than the laminar sub-layer thickness.

3. The local turbulence intensities in the two directions parallel to the wall are small.

4. The fluid properties are constant.

With these assumptions, they derived the following relationship between the instantaneous mass transfer coefficient (k), time averaged wall velocity gradient ($\bar{s}$) and the fluctuating component of the wall velocity gradient (s') as follows:

$$k = \frac{3}{2\Gamma(4/3)9^{1/3}} \left(\frac{D^2\bar{s}}{L_e}\right)^{1/3} \left(1 + \frac{s'}{\bar{s}}\right) - \frac{0.505171}{4} (9^{1/3}) \left(\frac{L_e D}{\bar{s}}\right)^{1/3} \frac{\partial \left(\frac{s'}{\bar{s}}\right)}{\partial t} \qquad 2.9$$

where

D = diffusion coefficient of the species being transferred, $cm^2/sec.$,

L_e = effective length of the electrode in the direction of the mean flow = $0.8131\ d_e$, cm,

t = time, sec,

Γ = gamma function, and

d_e = diameter of the electrode, cm.

The time average of this equation is

$$\bar{k} = \frac{3}{2\Gamma(4/3)9^{1/3}} \left(\frac{D^2\bar{s}}{L_e}\right)^{1/3} \qquad 2.10$$

and the fluctuating velocity gradient is given by

$$k' = \frac{1}{2\Gamma(4/3)9^{1/3}} \left(\frac{D^2\bar{s}}{L_e}\right)^{1/3} \left(\frac{s'}{\bar{s}}\right) - \frac{0.505171}{4} (9^{1/3}) \left(\frac{L_e D}{\bar{s}}\right)^{1/3} \frac{\partial\left(\frac{s'}{\bar{s}}\right)}{\partial t} \qquad 2.11$$

From Eqs. 2.10 and 2.11 one obtains:

$$3\frac{k'}{\bar{k}} = \frac{s'}{\bar{s}} - t^* \frac{\partial\left(\frac{s'}{\bar{s}}\right)}{\partial t} \qquad 2.12$$

where $$t^* = \frac{0.505171\,\Gamma(4/3)9^{2/3}}{2} \left(\frac{L_e^2}{D\,\bar{s}^2}\right)^{1/3}$$

is the time constant of the concentration boundary layer, by analogy with RC electrical circuits.

Average value of the shear stress, $\bar{\tau}$ can be calculated from Eqs. 2.7 and 2.10. However, Eq. 2.12 relating k' and s' is a differential equation and can only be solved if one knows the frequency distribution of the mass transfer coefficient. However, as a first approximation the second term in Eq. 2.12 can be ignored. This approximation is meaningful when the time constant for the concentration boundary layer t^* is small, i.e., the electrode diameter (d_e) becomes small. In such a case one can write for the r.m.s. value of s'

$$\frac{3\sqrt{\overline{k'^2}}}{\bar{k}} = \frac{\sqrt{\overline{s'^2}}}{\bar{s}} \qquad 2.13$$

Using Eqs. 2.8 and 2.13, the r.m.s. value of the fluctuating component of the velocity gradient can be obtained from the r.m.s. value of the fluctuating component of the current.

The time-averaged and the r.m.s. value of the fluctuating component of the wall shear stress can be calculated from the following relationships:

$$\bar{\tau} = -\mu_1 \bar{s} \qquad 2.14$$

and

$$\sqrt{\overline{\tau'^2}} = -\mu_1 \sqrt{\overline{s'^2}} \qquad 2.15$$

where

$\bar{\tau}$ = time-averaged value of the wall shear stress, dynes/cm^2,

τ' = fluctuating component of the wall shear stress, dynes/cm^2, and

μ_1 = fluid viscosity, poise.

In the measurement of mass transfer coefficient and wall shear stress, large anodes and small cathodes are used. Because of the difference in area, polarization at the anode would be negligible and the measurement would yield the

required values of the quantities at the cathode location. Platinum and nickel electrodes have been used extensively for these experiments.

Application of this method to measurement of mass transfer coefficient and wall shear stress has been quite extensive. Only some of them will be mentioned below.

In the measurement of mass transfer coefficient and wall shear stress, redox type of solutions are normally employed. One system widely employed by various workers is the equimolar aqueous solution of potassium ferrocyanide and potassium ferricyanide. The electrode reactions are

$$Fe(CN)_6^{3-} + e^- \longrightarrow Fe(CN)_6^{4-} \quad \text{at the cathode} \qquad 2.16$$

$$Fe(CN)_6^{4-} \longrightarrow Fe(CN)_6^{3-} + e^- \quad \text{at the anode} \qquad 2.17$$

Large amounts of sodium hydroxide and/or potassium chloride are used as indifferent electrolytes.

Hanratty and coworkers[44], Ito and Ogawa[45], Runchal[46], Berger and Hau[47], and Maruyama et al[48] have all studied mass transfer in pipe flows using the above system. Forced convection across cylinders has been investigated by Son[49] and Dimopoulos and Hanratty[50]. Mass transfer fluctuations in turbulent boundary layers have been studied by Dworak and Wendt.[51,52]

Shear stress measurements have been done by Reiss and Hanratty[41], Mitchell and Hanratty[53], Sircar and Hanratty[54] in pipe flows. Son[49], and Dimopoulos and Hanratty[50] have studied velocity gradients and shear stress at the walls of cylinders kept crosswise in flow.

The following cathodic reaction has been used by Fench and Tobias[55] in their mass transfer studies on horizontal plates.

$$Cu^{2+} + 2e \longrightarrow Cu \qquad 2.18$$

Schutz[56] did similar measurements on cylindrical and spherical surfaces.

The present investigation did not permit the use of the above electrolyte systems, because the electrolyte cannot be kept free of oxygen. Therefore, oxygen dissolved in water was employed as the transfer species in the electrochemical system. The electrode reactions were

$$O_2 + 4e^- + 2H_2O \longrightarrow 4OH^- \quad \text{at the cathode} \qquad 2.19$$

$$4OH^- \longrightarrow 2H_2O + O_2 + 4e^- \quad \text{at the anode} \qquad 2.20$$

Large amount of sodium hydroxide or potassium hydroxide was used as the indifferent electrolyte. This system had been employed by Postlethwaite and Holdner[57,58] in their mass transfer studies in pipes carrying slurries. Lin et al[59]

compared various electrode reactions for the study of mass transfer in pipe flows. The behaviour of oxygen as the transfer species was found to be satisfactory by these workers.

2.4. MEASUREMENT OF MASS TRANSFER COEFFICIENT AND WALL SHEAR STRESS

Mass transfer coefficient and wall shear stress measurements were made at the bottom of the simulating vessel, when blowing with single and multiple tuyeres, using the electrochemical technique. Some measurements were also made along the sidewalls in experiments with single tuyeres. The details of the experimental arrangement, equipments and procedure are discussed in this section.

2.4.1. Electrode Preparation

Platinum electrodes of circular cross section were employed for measurement. The diameter of the electrodes was selected to be about 0.25 mm. This was found to be adequate because the amplitude of flow fluctuations was large and frequency small. Moreover, the currents obtained with this electrode were in the easily measurable range.

In a circular disc of perspex a 0.4 mm hole was made in the center and the platinum electrode wire was fixed in it with Araldite so that a small portion of the wire

projected from the surface. The disc was then carefully faced on a lathe; the feed was kept to a minimum each time to minimise electrode distortion. It was then polished sequentially on emery papers of increasing fineness. The electrodes were inspected under a microscope for geometrical irregularities. Electrodes which had rough edges, large striation or distorted cross-sections were further polished. The electrode diameters were then measured under the microscope using a calibrated eyepiece. These were then fitted to the bottom and sides of the vessel using chloroform so as to be flush with the vessel surface. Any small projections were removed by polishing with fine emergy paper. The electrode construction is shown in Figure 2.15.

The anode employed was a large platinum sheet kept far from the cathode in the simulating vessel.

2.4.2. Electrolyte

Oxygen dissolved in water constituted the transfer species. Distilled water with 0.1 mole/liter of sodium or potassium hydroxide dissolved in it constituted the electrolyte. The physical properties of this solution are given in Appendix II.

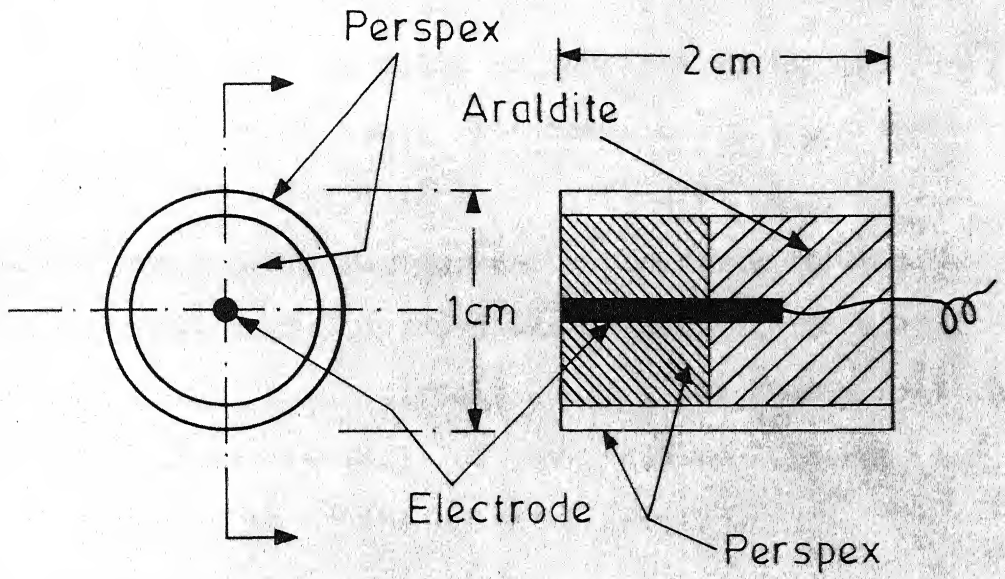

Fig. 2.15 Electrode construction.

2.4.3. Electrical Circuit

The electrical circuit consisted of two parts as follows:

a) The first part was meant for application of the required potential across the electrochemical cell and the conversion of the cell current to a voltage signal. This part may be termed as the electrode circuit.

b) The second part processed the output voltage signal from the electrode circuit to give the average and the root mean square value of the signal. This part may be referred to as the output circuit.

The electrode circuit is shown in Figure 2.16 and is similar to the one used by Son.[47] The anode was grounded to the water pipes in the laboratory and a voltage relative to the anode was applied to the cathode with the help of two 1.5 V dry-cells connected in parallel and a 100 Ω potentiometer. The other end of the potentiometer was connected to the inverting terminal of a FET-input operational amplifier, IM 8007, used in the current-to-voltage converter mode. The noninverting terminal was grounded along with the anode. The op. amp. allowed the voltage across the electrodes to remain steady when the current in the circuit was fluctuating. In the feed-back was connected a 100 kΩ, 0.1 pct. metal film resistor. The output voltage (V) from the op. amp.

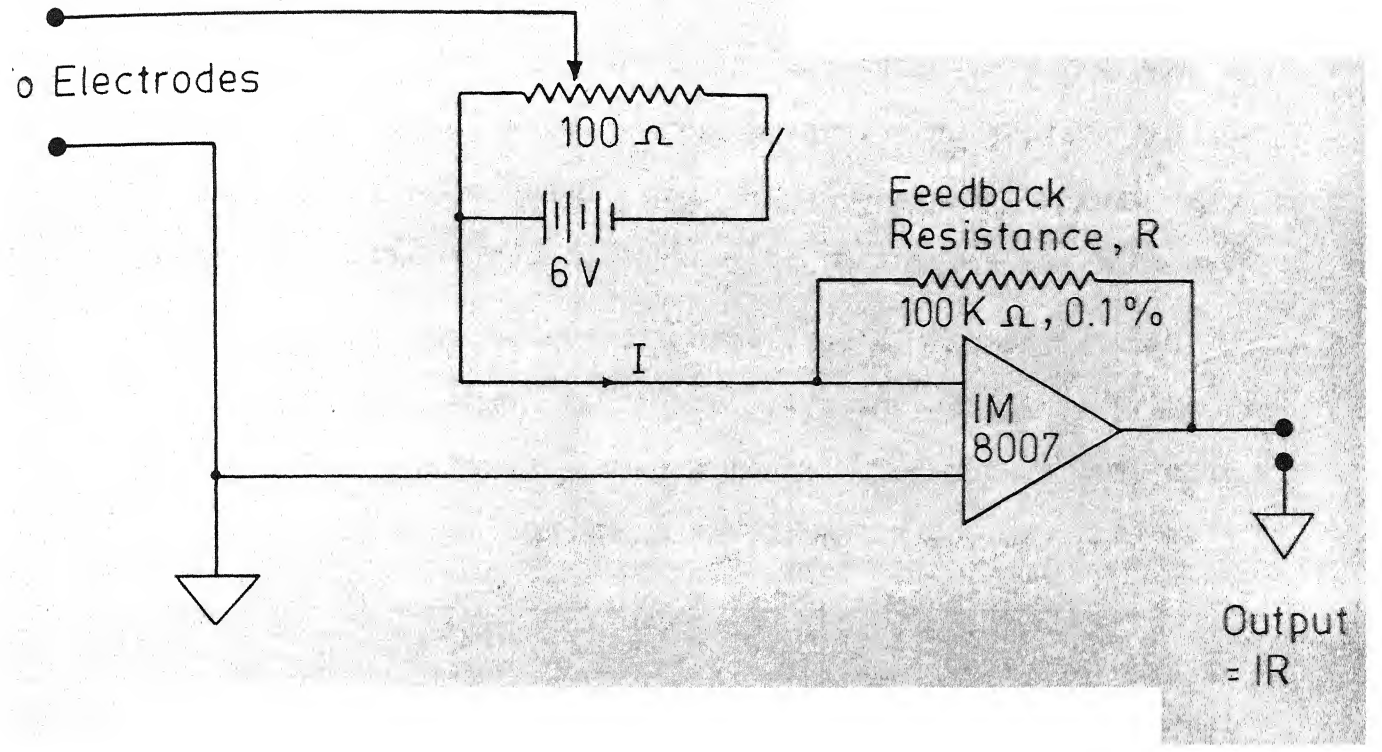

Fig. 2.16 Electrode cicuit.

would be equal to the product of the current in the circuit i and the feedback resistance, i.e.,

$$V = 10^5 i \qquad 2.21$$

All ground connections were made with thick copper wires, and all other external wires were shielded. The battery and the potentiometer were housed in a grounded aluminium box. All these precautions were necessary to minimise noise pick up.

The output circuit consisted of two parts. In the first part, shown in Figure 2.17, the output from the electrode circuit was passed through a low-pass filter with a time constant of 100 secs, which had an op. amp., FET-input IM 8007, as the active element. Output from this op. amp. was the average value of the signal. This average was subtracted from the original signal to separate the fluctuating component of the original signal.

The fluctuating component of the signal so obtained was the input to the second part of the output circuit, shown in Figure 2.18. This signal was first amplified to the required value in a preamplifier. It was then filtered of any DC components in a simple RC filter followed by an op. amp. as buffer. The output from the buffer was squired in an Analog Devices Multiplier, AD 530. The squared signal was averaged in a low-pass filter to get the mean square of the fluctuations. The root-mean-square value was then

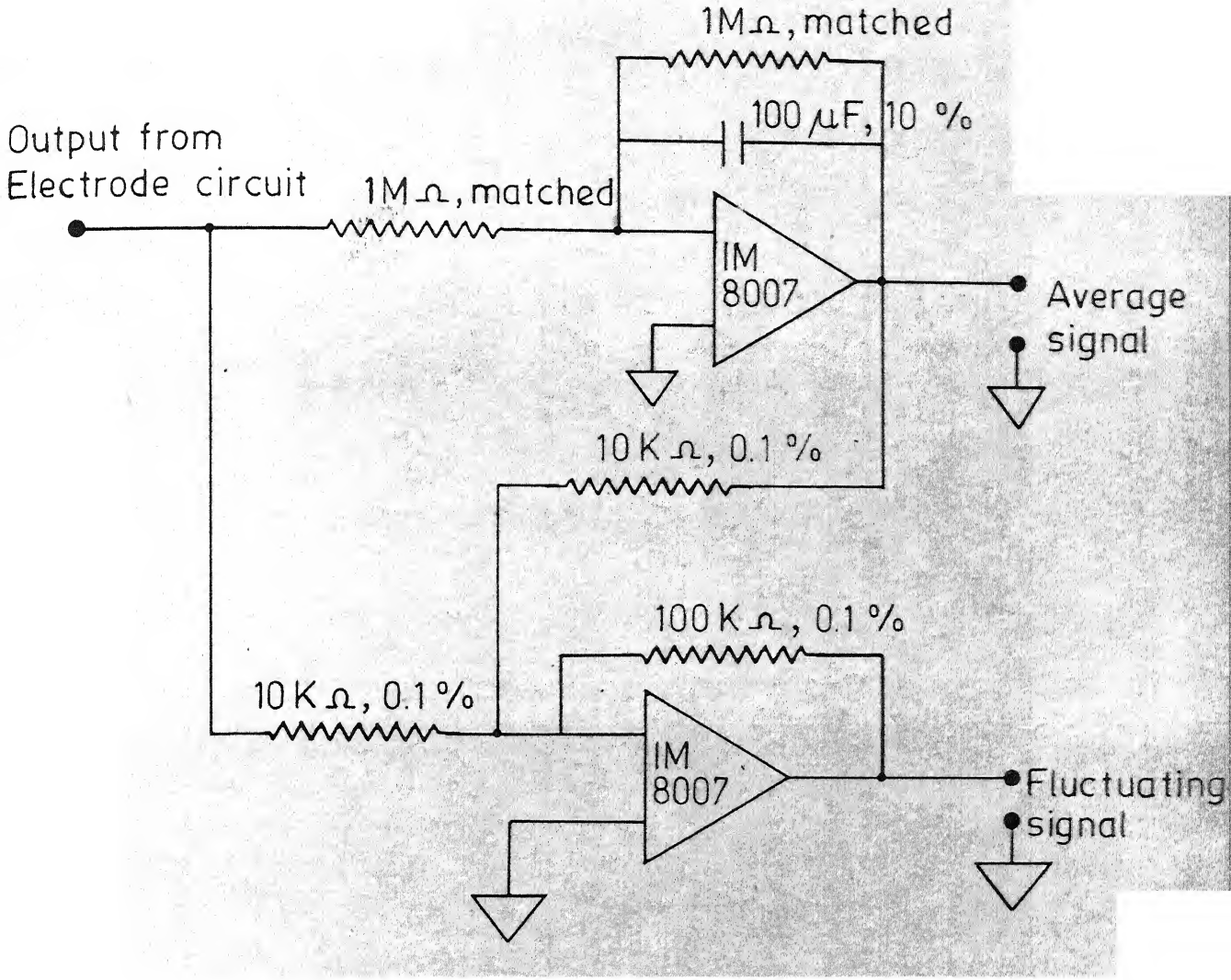

Fig. 2.17 Output circuit for measuring the average current.

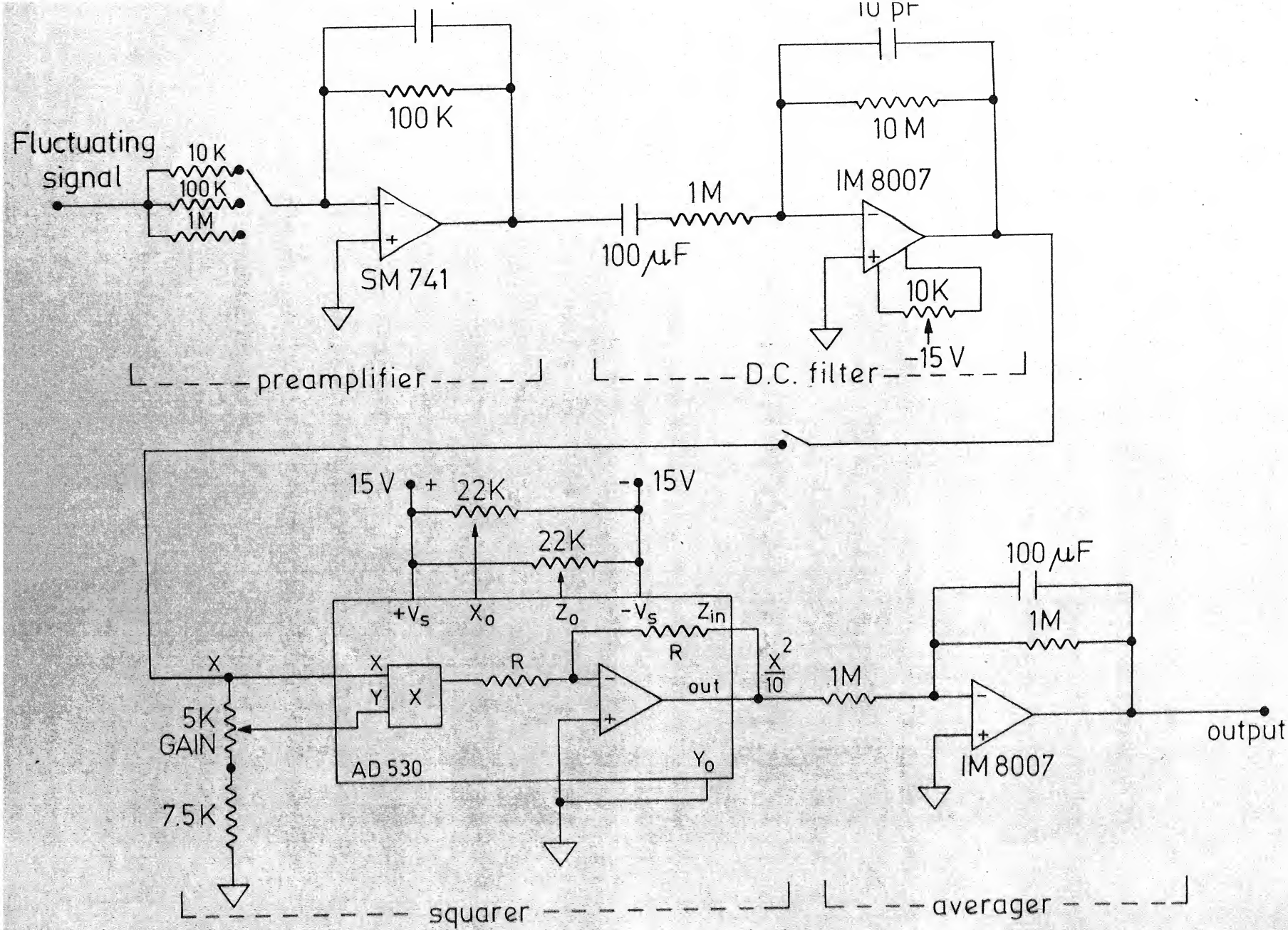

Fig. 2.18 Mean square circuit for measuring mean square of fluctuations in current.

calculated from this, taking into account the amplification in the circuit. Small capacitances were incorporated in the feed-back loop of all the operational amplifiers to avoid any oscillation problems due to capacitive coupling.

2.4.4. Experimental Procedure

The simulation vessel was thoroughly cleaned with soap water and rinsed with tap water. After drying, the electrodes were cleaned with fine emery paper. The vessel was then rinsed with distilled water and filled with it upto the desired height. Either sodium hydroxide or potassium hydroxide was added to get a concentration of 0.1 moles/liter.

Each cathode was pretreated in the following manner before measurements:

(i) The electrode was kept at +1.0 V for about 15 seconds to oxidise any impurity on its surface.

(ii) Polarity was reversed and the electrode was kept at -1.1 V for about 30 minutes. This was expected to reduce any platinum oxide or adsorbed oxygen on the electrode surface.

(iii) The electrode was then kept at -0.8 V for about two hours for obtaining a stable electrode surface during experiments.

This pretreatment was arrived at, after many trials, to obtain reproducible results.

Blowing of air, was then started and the flow rate was adjusted to the required value. Total flow rate was measured with the orifice meter. When studying the effect of the flow rate of shrouding gas, the total flow rate was kept constant and the required percentage of this flow was directed through the annular space. This way, the effect of total air input was separated from the effect of distribution of air in the two parts of the tuyere. Flow rate of gas through the annular space was measured with a rotameter.

The electrochemical cell was then switched on. It took about 10 minutes for the average of the output from the electrode circuit to become steady. This was measured with a Philips DC-Microvoltmeter and was also plotted in a millivolt recorder to observe its stability. Once the average of the signal was steady, the mean square of the fluctuations was measured. This took about another 15 minutes. Throughout the measurement period, the fluctuating component of the signal was monitored on an oscilloscope to make sure that no stray noises were picked up and the operational amplifiers in the circuit were not saturated.

From these data, the mass transfer coefficient and the wall shear stress were calculated. The calculation procedures are given in Appendix I.

2.4.5. Arrangement of Electrodes in Experiments with Single and Multiple Tuyeres

Distribution of the electrodes along the bottom and the sidewalls for experiments with single tuyere are shown in Figure 2.19. Five electrodes were placed at the bottom along a radius at intervals of 4 cm. Six electrodes were placed on the sidewalls along a vertical line at intervals of 8 cm.

The electrode distribution in the multi-tuyere bottom is shown in Figure 2.20. Electrodes were placed along two radii perpendicular to each other. This was essential for measuring the shear stress distribution when blowing with asymmetric tuyere arrangements.

2.5. VISUALIZATION OF FLOW

The flow patterns in the simulating vessel during bottom blowing with a single tuyere were visualized using dust particles and polystyrene beads. In general lighting, the picture of flow was quite confusing and difficult to understand. Therefore an arrangement was made to light only a slit of about 2 cm width in the flow field. The lighting arrangement employed is shown in Figure 2.21. It consisted of two 1000 W bulbs kept one above the other inside a cylindrical reflector made of aluminium. The light from the slit in the reflector was passed through

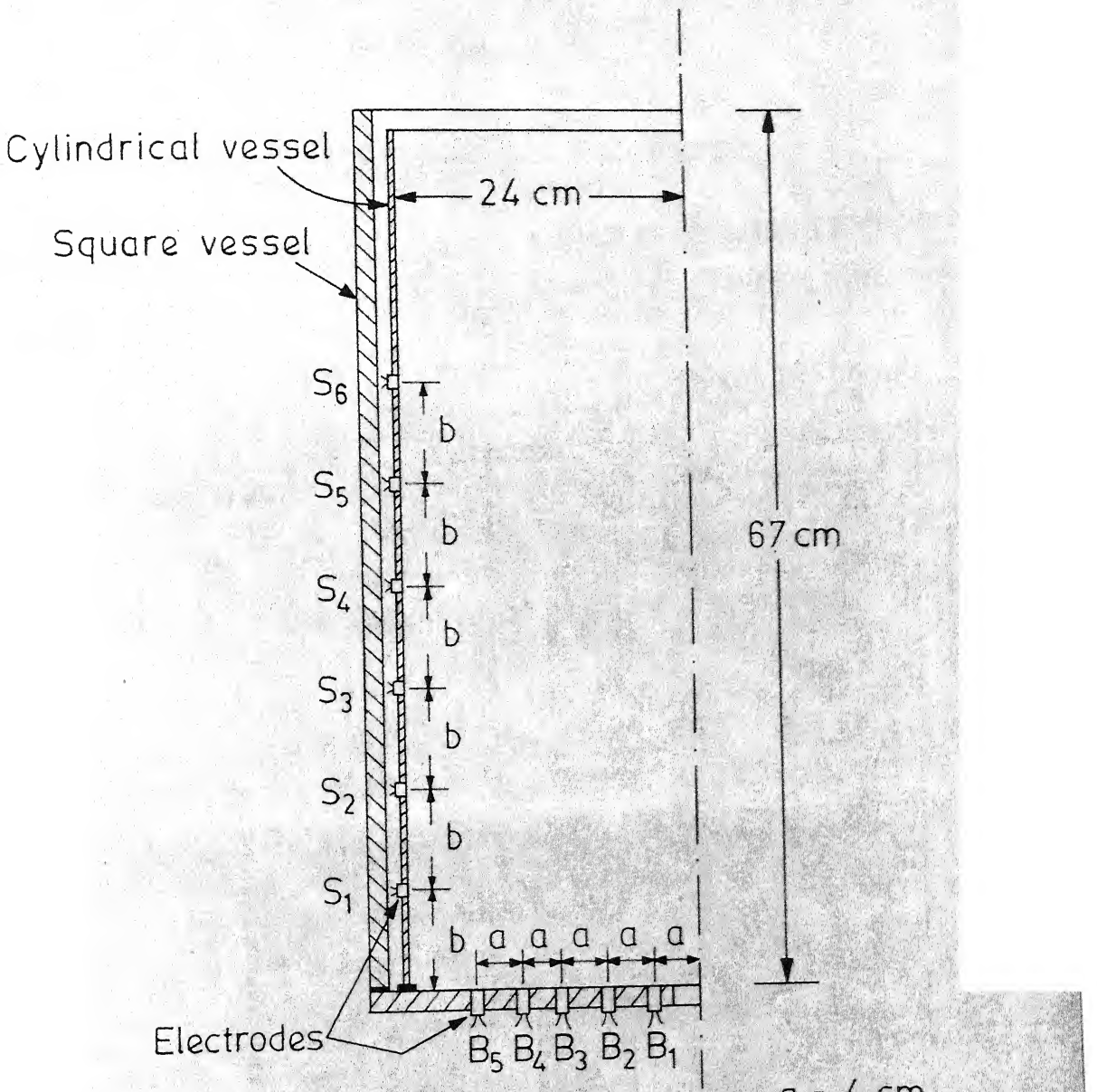

Fig. 2.19 Positions of electrodes for experiments with single-tuyeres.

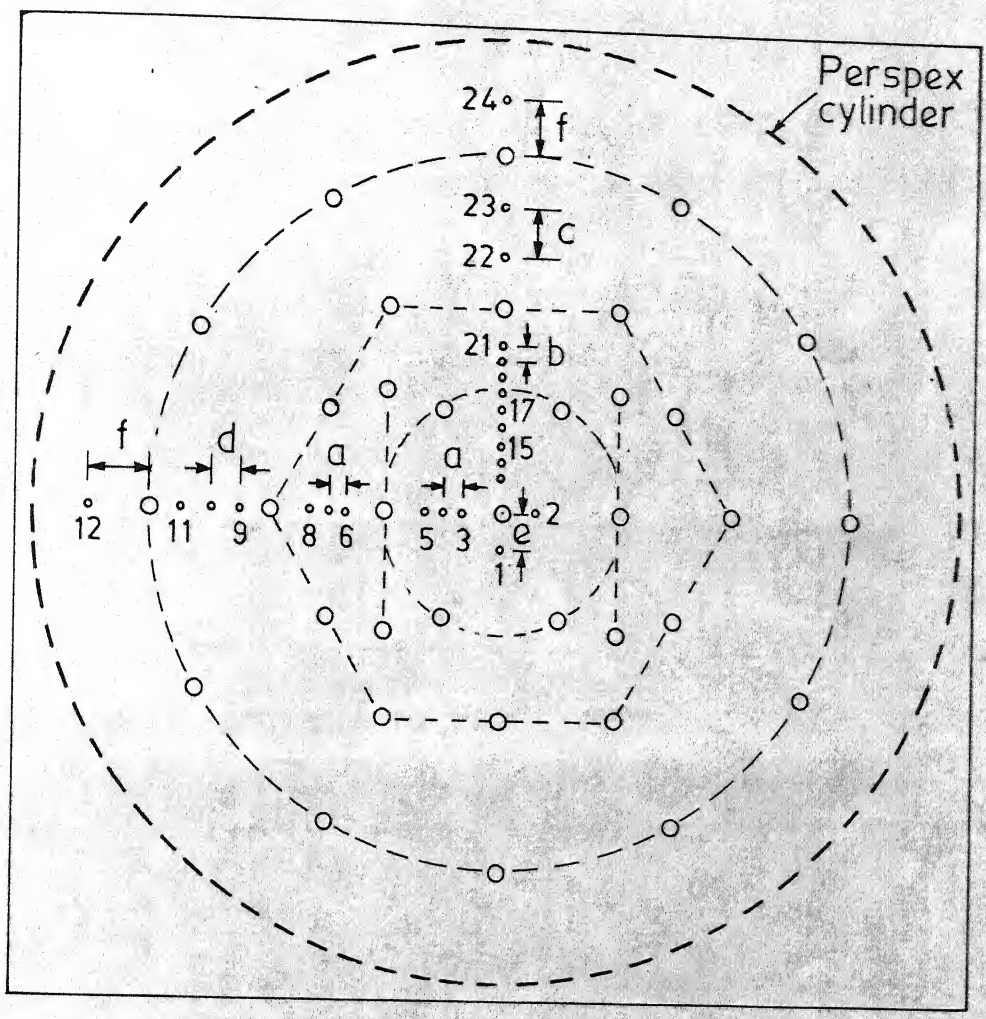

a = 1 cm
b = 0.86 cm
c = 2.5 cm
d = 1.5 cm
e = 2.0 cm
f = 3.0 cm
o tuyeres
∘ electrodes

Fig. 2.20 Positions of electrodes for experiment with multiple tuyeres.

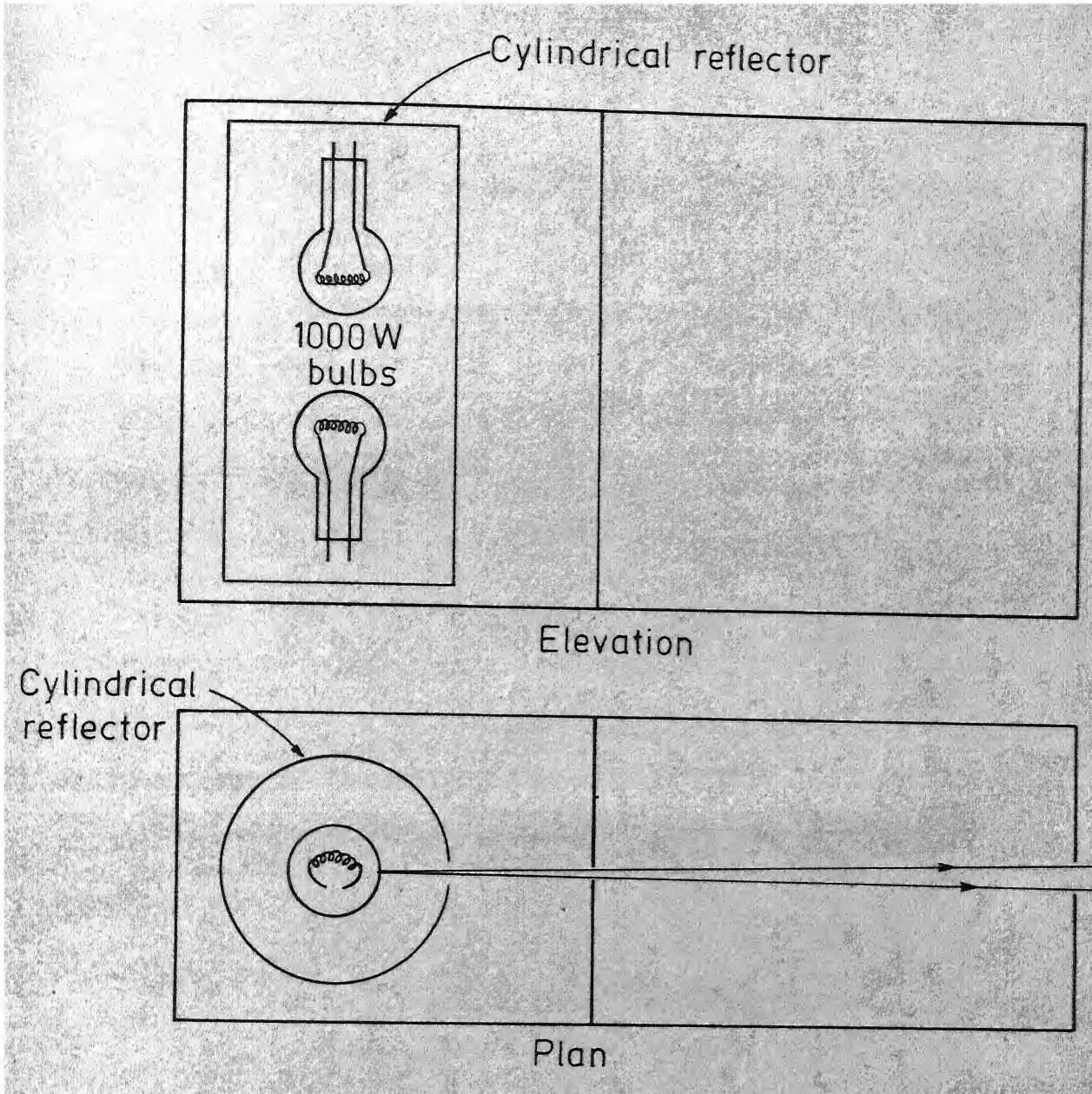

Fig. 2.21 Arrangement for slit lighting.

two more slits at a distance of 30 cms from each other, so that the light emerging from these lighted a vertical section of only about 2 cm width.

In visual observations, dust particles present in the tap water were sufficient to enable one to trace the flow pattern. Some important flow patterns were photographed using polystyrene beads of 0.25 mm diameter as tracers. The time of exposure was 0.25 sec. at full aperture.

Apart from these the behaviour of a single jet in water were visualized. The jet cone angle was determined by taking photographs with 1 sec exposure time. Moreover, a movie at 64 frames per second were taken to study the emergence of the jet from the tuyere and its subsequent break up.

CHAPTER 3

RESULTS AND DISCUSSION

The first section in this chapter contains a discussion on errors and reproducibility in the measurements. Qualitative observations from visualization of the flow pattern are presented in Section 3.2. Results of the gas mixing studies with a single centrally placed coaxial tuyere are discussed in Section 3.3. Section 3.4 contains the results and discussion of the measurement of the wall shear stresses with a single coaxial tuyere. Results of experiments with multiple tuyeres are discussed in Section 3.5. A discussion of bottom refractory wear in bottom-blown oxygen processes in the light of the findings in the present study appears in Section 3.6.

3.1. ERRORS IN RESULTS

Errors in results can arise due to the following reasons: limits of reproducibility of the measurement, accuracy of calibration, least counts of the measuring instruments and accuracy of the standard data used in calculations. Sources of errors and their estimates for different measurements are discussed in this section.

3.1.1. Errors in Measurement of Gas Flow Rate

The orifice meter which was used to measure the flow rates of air, was designed according to ASME specifications and was fabricated with good care. Values of discharge coefficients were taken from the standard tables.[35] Error due to the use of these tabulated data is not expected to be more than 1 pct. The inaccuracy in the measurement of the pressure difference across the orifice would be about 1 mm. This would contribute an error of 1.25 pct. at the lowest flow rate, where this error is the maximum. The diameter of the orifice was measured to within 0.02 mm. It appears as a square term in the equation for flow rate calculation and hence the error in the flow rate contributed by this inaccuracy is about 0.4 pct. for the smallest orifice. The temperature was measured to within $\pm 0.5^{\circ}C$ and its contribution to the error in the flow rate measurement should be negligible. Combining all these, maximum error in the measurement of the flow rates of air is about 2.65 pct. The accuracy of the measurement at lower flow rates was tested using a precision wet-test meter and the errors were found to be well within this limit.

The flow rates of carbon dioxide were measured with a rotameter or a capillary flow meter, both of which were previously calibrated against a precision wet-test meter.

The accuracy of measurement is estimated to be $\pm$ 5 pct.

3.1.2. Errors in the Measurement of Gas Composition

Gas samples in the studies on mixing of two jets were analysed in a gas-chromatograph. The chromatograms were calibrated by analysing known mixtures of carbon dioxide and air. Figure 3.1 is the calibration curve with the ratio of concentrations of the two gases as the ordinate and the ratio of the respective peak heights as the abscissa. The curve was drawn using 67 different gas mixtures. The least square fit for the calibration is:

$$\frac{\text{pct. } CO_2}{\text{pct. air}} = 1.14 \frac{\text{height of } CO_2 \text{ peak}}{\text{height of air peak}} \qquad 3.1$$

The maximum error in gas analysis by using this equation is about 5 pct. of the total of concentration. To ensure the stability of the chromatograph, gas mixtures of known compositions were analysed everyday during the measurement period.

3.1.3. Errors in Measurements of Mass Transfer Coefficient and the Wall Shear Stress

The following formulae, discussed in Chapter 2 have been used to calculate the average mass transfer coefficients $\bar{k}$ and the average shear stress $\bar{\tau}$:

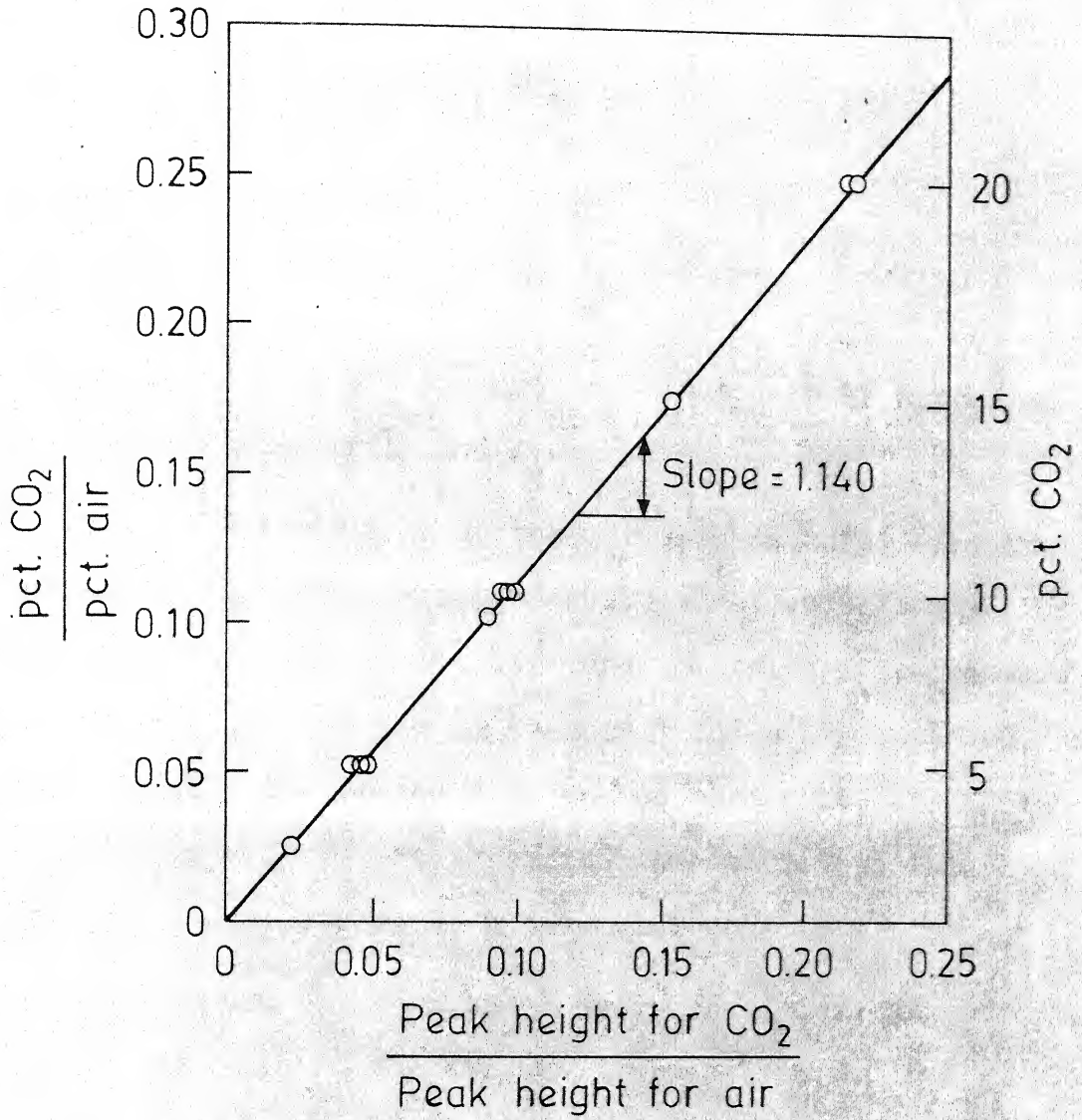

Fig. 3.1 Calibration curve for gas analysis using gas-chromatograph in CO_2-air mixtures.

$$\bar{k} = \frac{4\bar{i}_d}{\pi n F C_b d_e^2} \qquad 3.2$$

$$\bar{\tau} = \text{const.} \frac{\bar{k}^3 d_e \mu_l}{D^2} \qquad 3.3$$

Random errors in $\bar{k}$ and $\bar{\tau}$ are contributed to by errors in the measurement of $\bar{i}_d$ and d_e.

To ensure that the currents measured were truly diffusion currents, plots of current vs. voltage were obtained for each electrode. One such plot is reproduced in Figure 3.2. It can be seen that the average current and the r.m.s. value of the fluctuations are quite steady between -0.5 V and -0.9 V. Measurements were therefore done by keeping the electrode at a potential of -0.8 V.

The error in the conversion of current to voltage and in determining the average is less than 0.5 pct. The output voltage was measured with a Philips DC-Microvoltmeter with a least count of 1 pct. of full scale.

To check the reproducibility of current measurement, experiments with identical experimental conditions were repeated at different times. In Table 3.1 are presented the current values that were measured with one such set of conditions. It can be seen that the reproducibility is about ± 2 pct. Hence the errors in the measurement of current

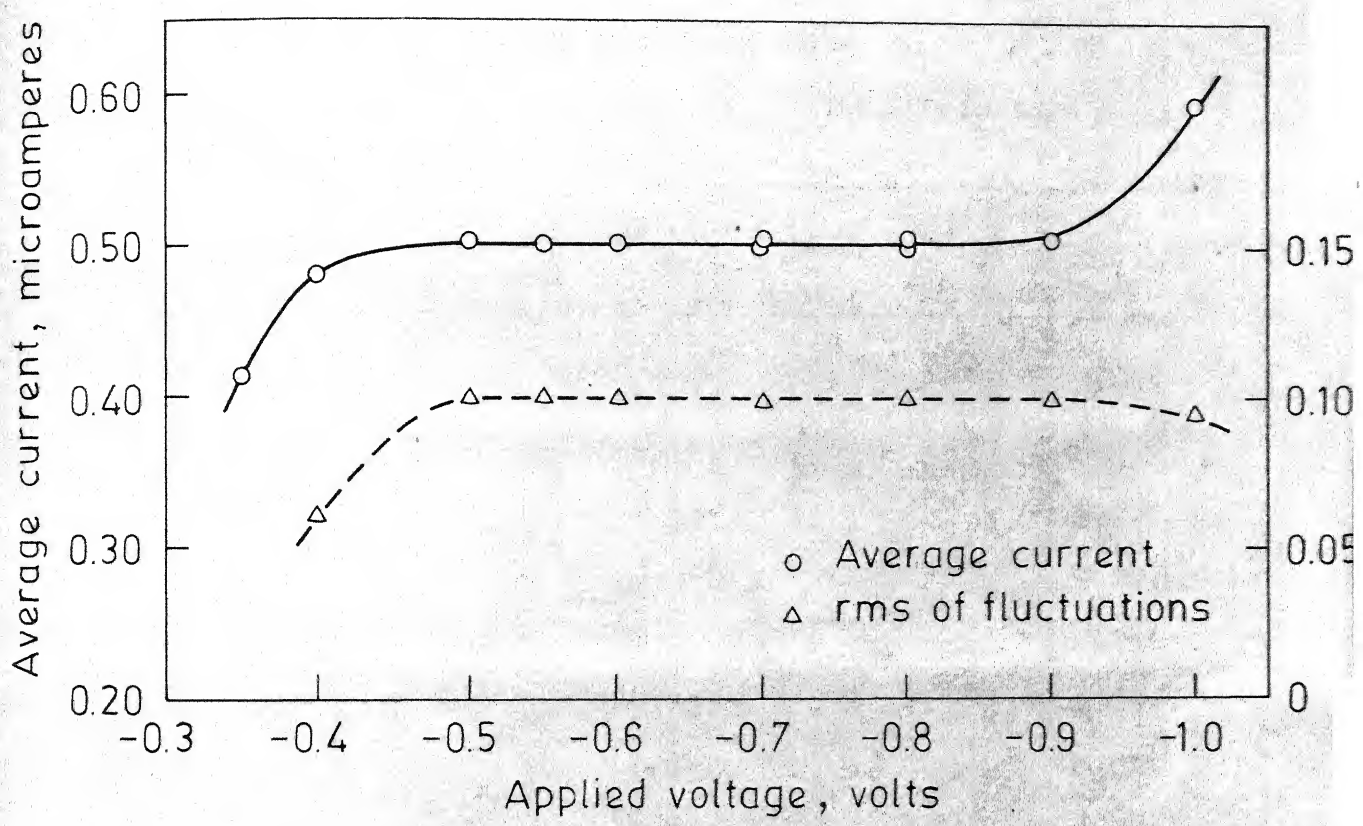

Fig. 3.2 Variation of average current and rms value of current fluctuations with applied voltage for electrode B_1; Q_j = 100 litres/min, Q_s = 0, l = 0 and h = 40 cm.

Table 3.1

Current Values Measured with Electrode B1 to Check Reproducibility of measurement d_j = 0.65 cm, h = 40 cm, l = 0, $\dot{Q}_s$ = 0, $\dot{Q}_j$ = 100 liters/min.

Experiment No.	Average current, A	R.M.S. of fluctuations, A
1	0.500	0.057
2	0.500	0.058
3	0.490	0.056
4	0.505	0.062
5	0.500	0.058
6	0.495	0.057
7	0.495	0.057
8	0.500	0.055
9	0.505	0.057
10	0.50	0.057
Mean	0.499	0.0575
Standard deviation	0.004	0.002

contributes a maximum error of about 2.5 pct. in the mass transfer coefficient values and 7.5 pct. in the shear stress values.

As mentioned in Chapter 2, electrode diameters were measured under the microscope using a calibrated eye-piece and were accurate within 1 pct. This would contribute an error of 2 pct. in the mass transfer coefficient values and 5 pct. in the shear stress values.

Hence, the total random error in the measurement of the mass transfer coefficients is within about 4.5 pct. It would be within about 12.5 pct. in the measurement of shear stresses.

Apart from these, systematic errors were contributed to by uncertainties in the values of D, μ_l, C_b and the constant in Eq. 3.3. As can be seen in Appendix II, the errors in the values of D, μ_l and C_b are 5 pct, 1 pct and 1 pct respectively. These would contribute an error of 1 pct in mass transfer coefficient values and 14 pct in shear stress values.

Experiments were conducted to ascertain whether the water flow in the vessel when blowing with a centrally located tuyere was axially symmetric or not. The tuyere employed in these experiments was of 0.325 cm diameter and was flush with the bottom of the vessel (Figure 2.5a).

Height of the water bath was 40 cm. The flow rate of air was varied between 50 and 100 liters/min. There was no shrouding. Shear stresses were measured at the bottom along two radii orthogonal to one another. The results are plotted in Figure 3.3. It is evident from the plot that the shear stress values along the two radii matched well within the experimental errors mentioned above. Therefore, the flow was taken to be axially symmetric and all consequent measurements were done along a single radius only.

3.2. FLOW VISUALIZATION

The flow patterns in the vessel when blowing with a single tuyere were visualised with the help of the slit-lighting arrangement shown in Figure 2.21. Particles of dust and polystyrene beads were employed as tracers in these visual observations. Some streak photographs were also taken using polystyrene beads. Figure 3.4 shows two such photographs of streak lines near the bottom for high and low flow rates of air. Based on these photographs and the visual observations, the general flow patterns were obtained and are shown in Figure 3.5. The stream surfaces were torus-shaped with the liquid going up in the inner region and coming down in the outer region. Velocities along the free surface at the top and the top part of the sidewall were quite high.

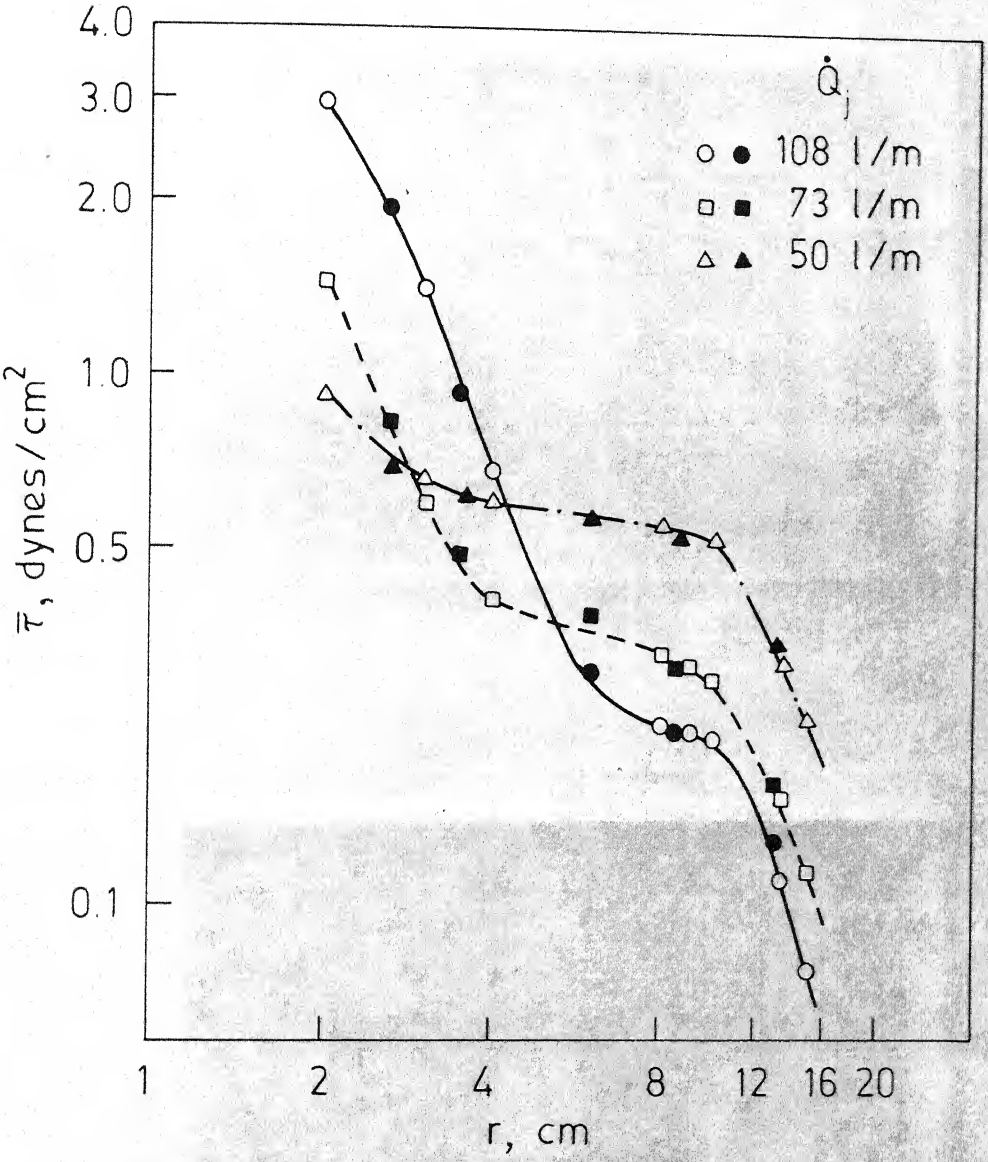

Fig. 3.3 Log-log plot of average shear stress $\bar{\tau}$ at the bottom vs the radial distance r from the tuyere axis in experiment with a single tuyere. The unfilled and the filled symbols stand for measurement along two radii orthogonal to each other; $d_j = 0.325$ cm, $l = 0$, $\dot{Q}_s = 0$ and $h = 40$ cm.

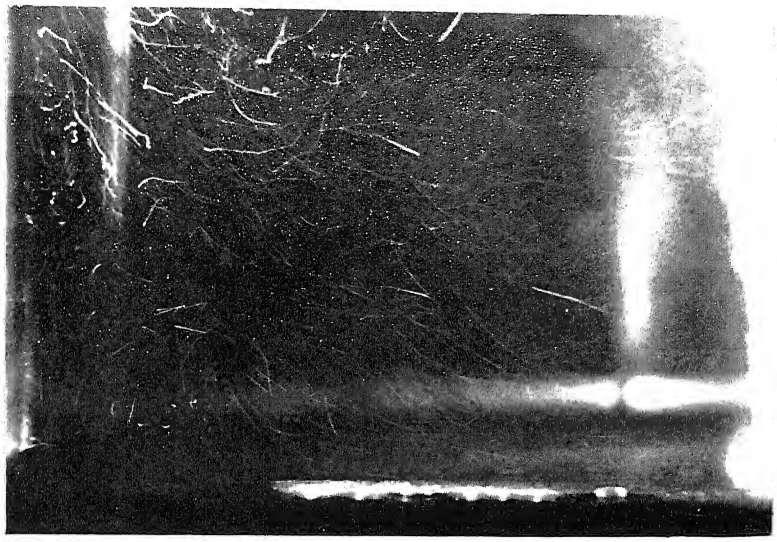

(a)

(b)

Figure 3.4. Photographs showing the streak lines near the bottom in experiments with a single tuyere; d_j = 0.65 cm, h = 40 cm, time of exposure - 0.25 sec; a) $\dot{Q}_j$ = 200 liters/min, and b) $\dot{Q}_j$ = 50 liters/min

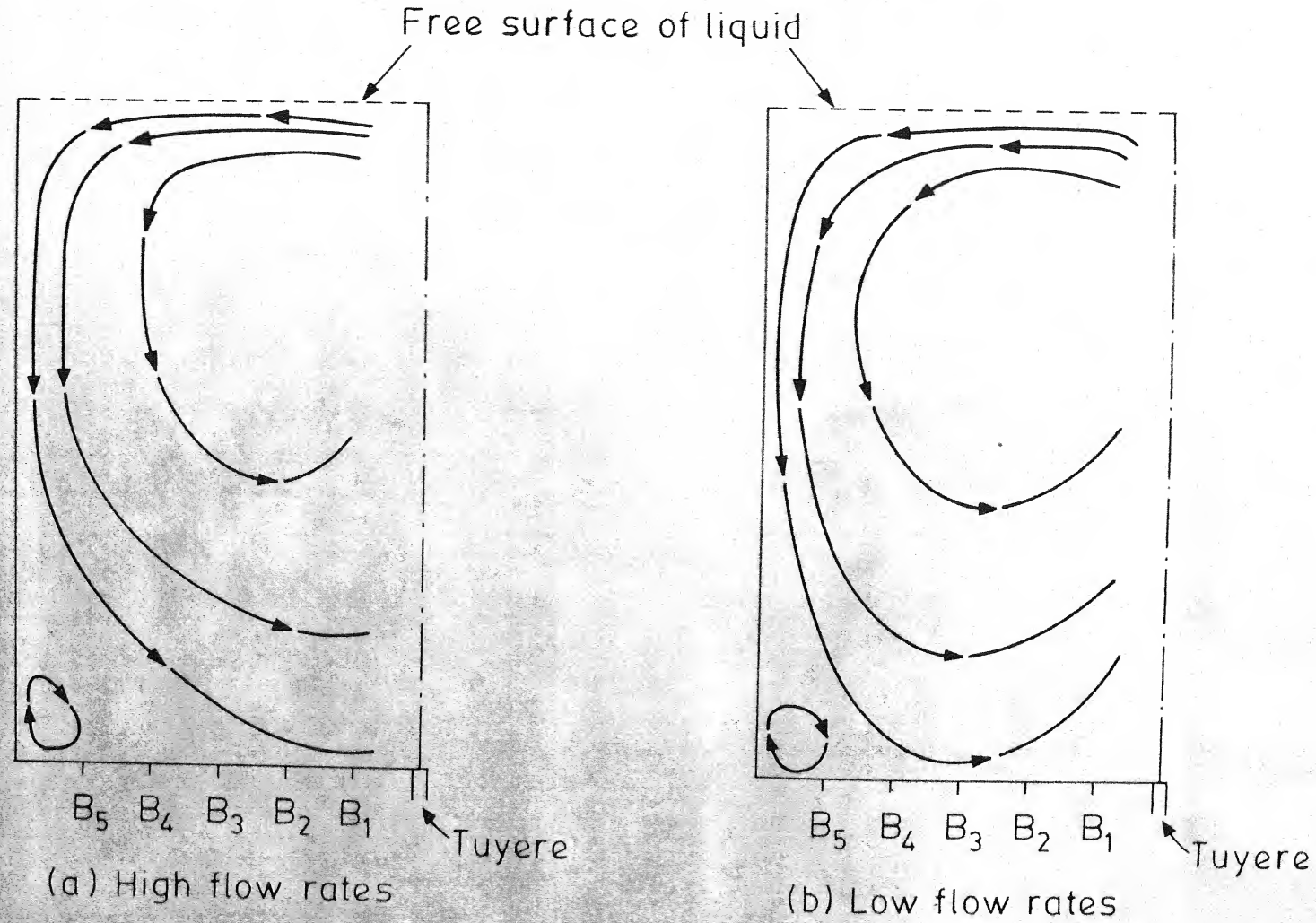

Fig. 3.5 General pattern of the flow of the liquid in experiments with a single tuyere; (a) high flow rates of air, (b) low flow rates of air.

Near the bottom, the liquid velocity had a downward component at points far from the tuyere and an upward component near the tuyere. There was a small region in between where the flow of the liquid was parallel to the bottom surface. This region was nearer to the tuyere at high flow rates of air and moved away as the flow rate was decreased. There was some secondary recirculation near the corner where the sidewall meets the bottom.

Time exposure photographs were taken of the gas jet near the tuyere exit in single tuyere experiments. Figure 3.6 is one such photograph for time of exposure 1 sec. The tuyere diameter d_j was 0.65 cm and the flow rate of air $\dot{Q}_j$ was 100 liters/min. There was neither any shrouding ($Q_s = 0$) nor any projection of the tuyere ($l = 0$) into the vessel. The jet cone angle was measured from these photographs and was found to be $20° \pm 2°$. This compares well with the values reported in the literature.[19,31]

Movie photographs of the jet were taken at 64 frames per second speed. A series of photographs are reproduced in Figure 3.7. As can be seen the jet as it came out of the tuyere oscillated vigorously; it seems as though the jet consisted of a series of gas pulses discharged rapidly into the liquid. This instability is probably due to the large difference in density between the gas and the

Figure 3.6. Time exposure photograph of time of exposure - 1 sec.

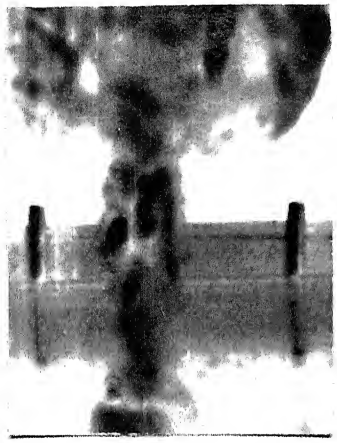

0

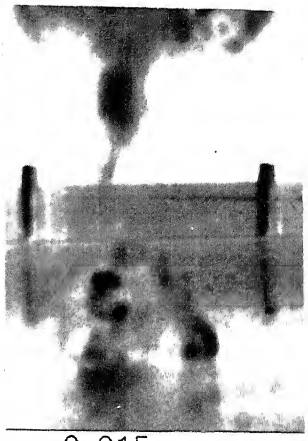

0.015 sec

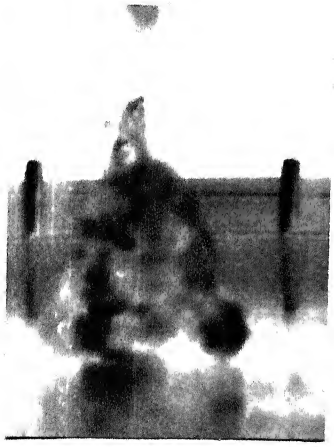

0.031 sec

0.046 sec

0.062 sec

0.078 sec

Figure 3.7. Sequence of movie photographs of the jet.

liquid. This kind of behaviour have been observed by other workers also.[19,20]

3.3. GAS MIXING IN EXPERIMENTS WITH SINGLE TUYERE

Experimental conditions for study of the mixing of two coaxial gas jets submerged in water are presented in Table 3.2.

Table 3.2

Experimental Conditions in Gas Mixing Studies

Height of the water bath	$= h = 40$ cm
Diameter of the water bath	$= d_b = 48$ cm
Diameter of the inner pipe	$= d_j = 0.65$ cm
Thickness of the annulus	$= t_s = 0.075$ cm
Flow rate of air	$= \dot{Q}_{air} = 50$, 100 and 150 liters/min.
Flow rate of carbon dioxide	$= \dot{Q}_{CO_2} = 5$, 10 and 15% of $\dot{Q}_{air}$
Sampling distance downstream from the tuyere exit	$= z = 1$, 3 and 5 cm

Tuyere placed axially in the cylindrical vessel.

Tables of results for the determination of concentration profiles at various z values are listed in Appendix A3.1. Some of the concentration profiles are shown in Figures 3.8 to 3.12.

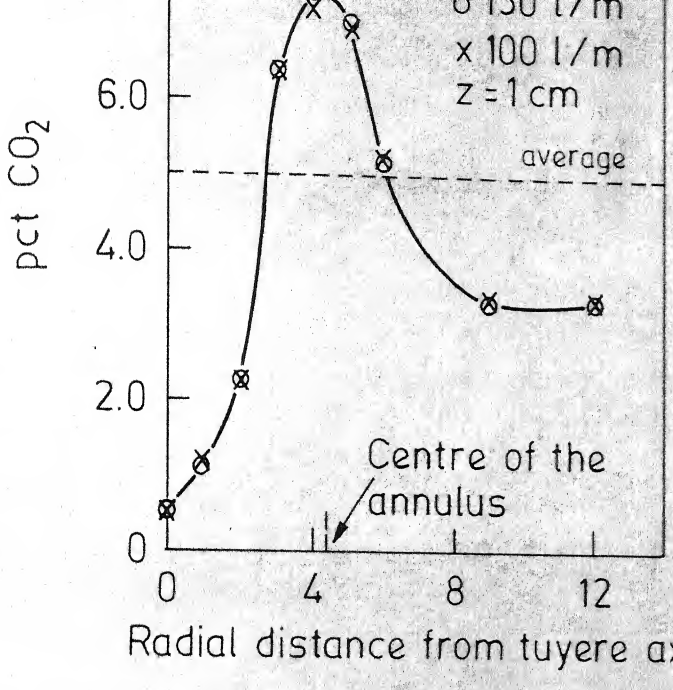

Fig. 3.8 Concentration profile at a distance of 1 cm downstream from the tuyere exit; $\dot{Q}_{CO_2}$ = 5 pct of $\dot{Q}_{air}$.

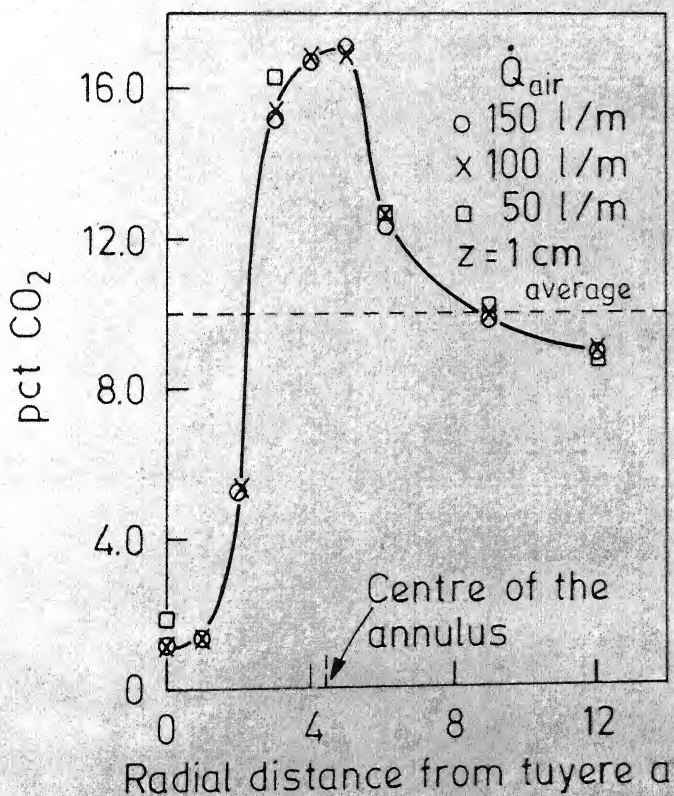

Fig. 3.9 Concentration profile at a distance of 1 cm down stream from the tuyere exit; $\dot{Q}_{CO_2}$ = 10 pct of $\dot{Q}_{air}$.

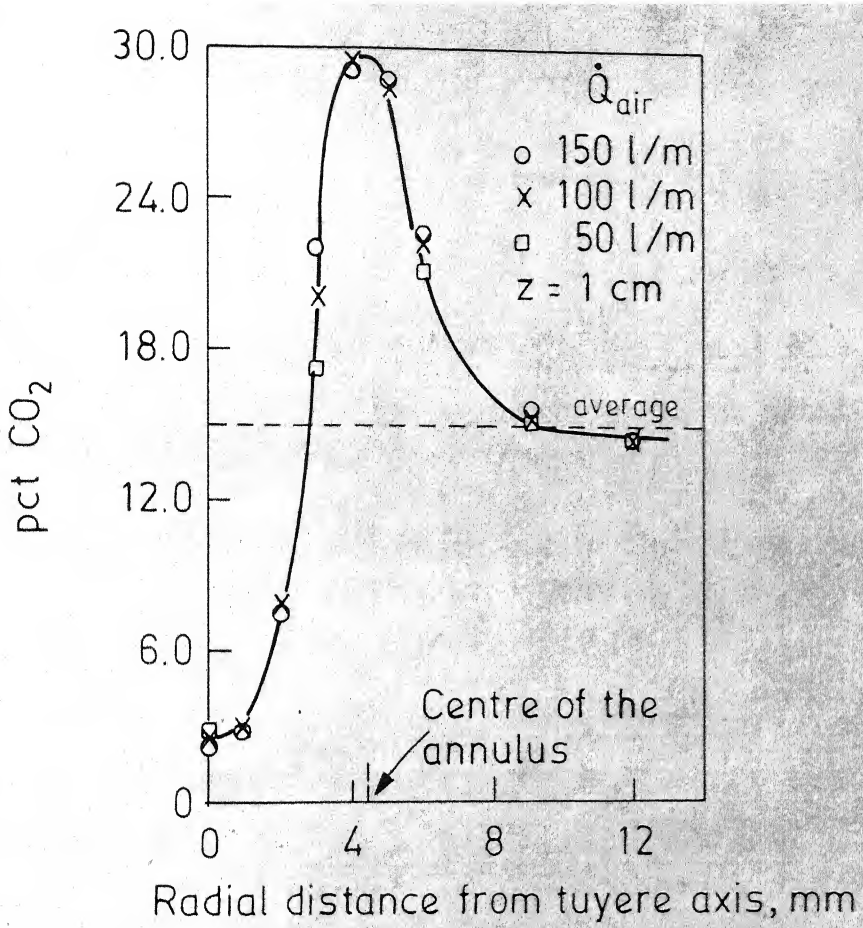

Fig. 3.10 Concentration profile at a distance of 1 cm downstream from the tuyere exit, $\dot{Q}_{CO_2}$=15 pct of $\dot{Q}_{air}$

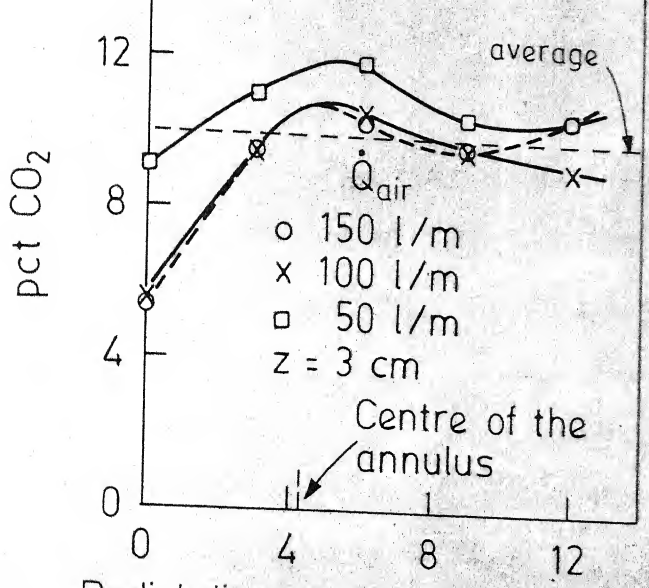

Fig. 3.11 Concentration profile at a distance of 3 cm downstream from the tuyere exit; $\dot{Q}_{CO_2}$ = 10 pct of $\dot{Q}_{air}$.

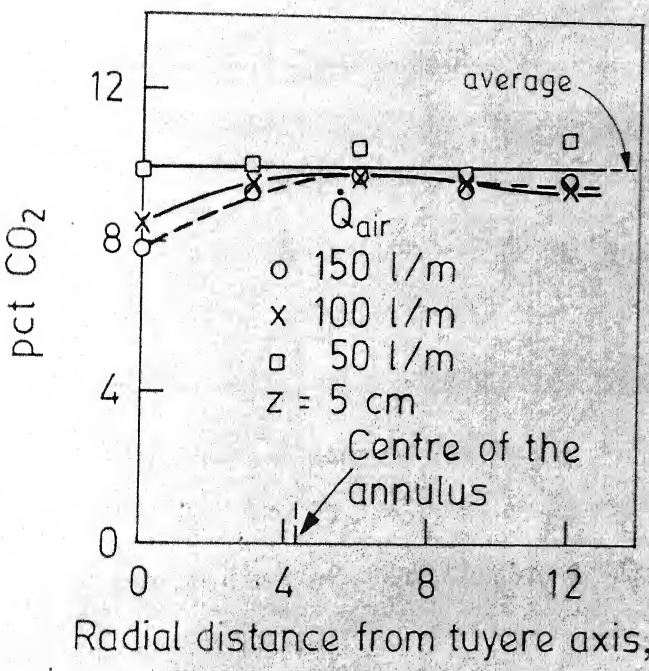

Fig. 3.12 Concentration profile at a distance of 5 cm downstream from the tuyere exit; $\dot{Q}_{CO_2}$ = 10 pct of $\dot{Q}_{air}$.

It is evident from Figures 3.8 to 3.12 that the concentration of air was appreciable even at the jet/water interface. This was true even when z was small (i.e., z = 1 cm). It means that CO_2 introduced through the annulus was ineffective in preventing air from coming into contact with water surrounding the jet even very near the tuyere exit. This behaviour can be explained on the basis of the movie photographs shown in Figure 3.7. The inner jet as it comes out of the tuyere is oscillating laterally and at times expands to about three tuyere diameters. This makes it spread beyond the shrouding jet.

Figures 3.8 to 3.10 present pct. CO_2 in the jet as a function of radial distance from the axis for various flow rates of air ($\dot{Q}_{air}$) and various ratios of flow rates of CO_2 and air ($\dot{Q}_{CO_2}/\dot{Q}_{air}$) at z = 1 cm. It may be noted that at a fixed $\dot{Q}_{CO_2}/\dot{Q}_{air}$, the profiles are independent of $\dot{Q}_{air}$. The dynamics of the mixing process very near the tuyere is, therefore, not significantly affected by the absolute values of the flow rates of the two gases, but only by their relative magnitudes. At greater distances downstream however the profiles did change with change in $\dot{Q}_{air}$ (Figures 3.11 and 3.12).

The three curves, Figures 3.8 to 3.10, are plotted together in Figure 3.13 which shows the variation

of the normalised concentration of carbon dioxide $C^*_{CO_2}$ with radial distance for various $(\dot{Q}_{CO_2}/\dot{Q}_{air})$. Here the normalised concentration is defined as

$$C^*_{CO_2} = \frac{\text{pct. } CO_2}{\dot{Q}_{CO_2}/\dot{Q}_{air}} \qquad 3.4$$

It may be noted that the maximum concentration was always found just above the annulus. This indicates that the carbon dioxide jet was not significantly deflected by the presence of the air jet.

Dependence of maximum $C^*_{CO_2}$ on the ratio $\dot{Q}_{CO_2}/\dot{Q}_{air}$ is shown in Figure 3.14. In the range studied, the relationship is linear and is given as:

$$(C^*_{CO_2})_{max} = 5.5 \frac{\dot{Q}_{CO_2}}{\dot{Q}_{air}} + 1.15 \qquad 3.5$$

If there is no interaction between the jets, i.e., if the final concentration profile is obtained by a summation of the two undisturbed jet profiles one through the inner pipe and the other through the annulus, the maxima in $C^*_{CO_2}$ should have been independent of $(\dot{Q}_{CO_2}/\dot{Q}_{air})$ at a fixed $\dot{Q}_{air}$. This is because of the fact that for a planar turbulent jet, to which the thin annular jet can be approximated, the velocity at any point is proportional to the square root of the jet momentum[60], and therefore, the maximum velocity is proportional

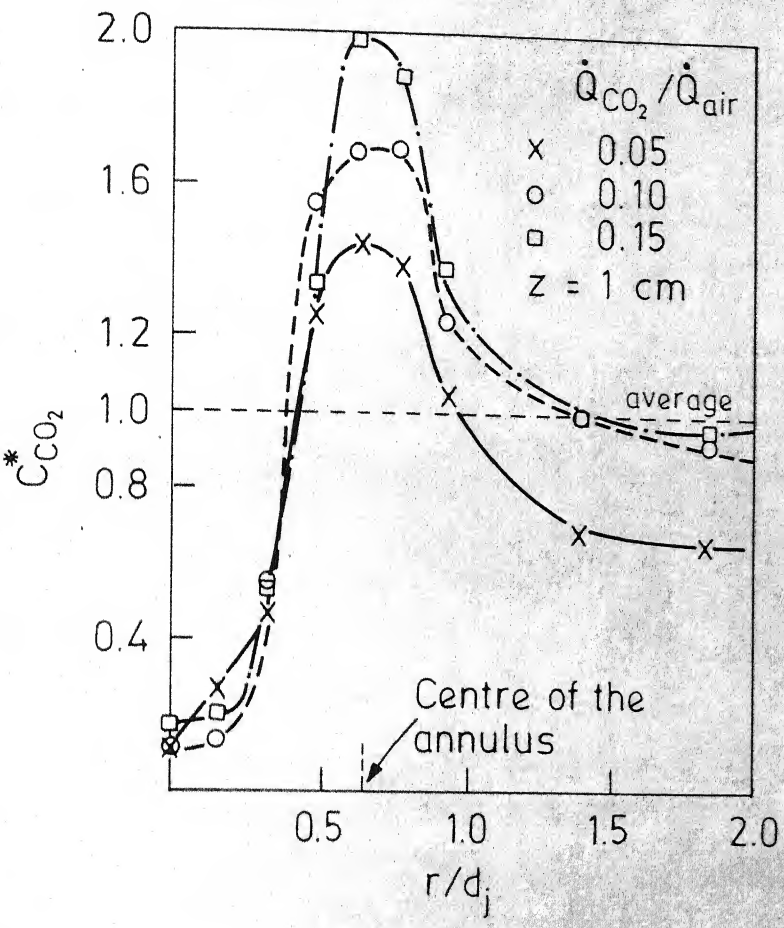

Fig. 3.13 Plots of normalised concentration $C^*_{CO_2}$ vs dimensionless distance from the tuyere axis at a distance of 1 cm downstream from the tuyere.

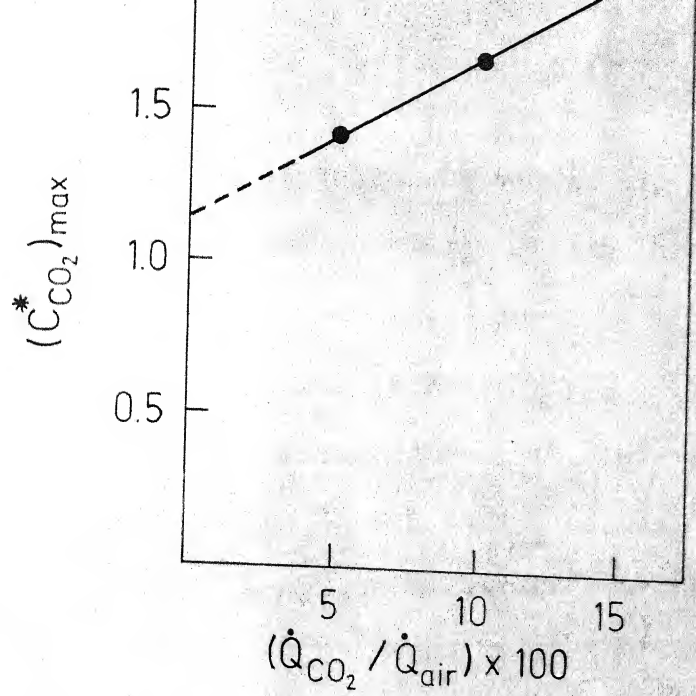

Fig. 3.14 Dependence of maxima in concentration $z = 1$ cm on $\dot{Q}_{CO_2} / \dot{Q}_{air}$.

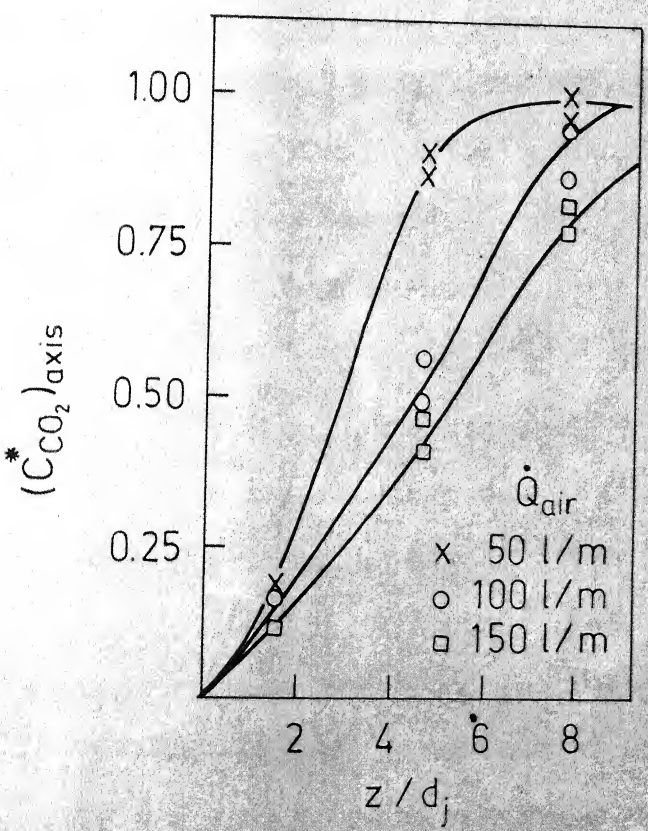

Fig. 3.15 Dependence of the normalized concentration at tuyere axis on distance downstream from the tuyere.

to the flow rate. The dependence given in Eq. 3.5 can only be explained with a better knowledge of annular gas jets submerged in liquid.

The plot of normalised axial concentration vs. the dimensionless axial distance from the tuyere exit (z/d_j) is shown in Figure 3.15. As may be noted, mixing was almost complete at $z/d_j \approx 7$ for $\dot{Q}_j$ = 50 liters/min. However, for $\dot{Q}_j$ = 150 liters/min., the point at which the two gases were completely mixed was farther downstream ($z/d_j \approx 10$).

3.4. MEASUREMENTS OF MASS TRANSFER COEFFICIENT AND WALL SHEAR STRESS IN EXPERIMENTS WITH SINGLE TUYERE

The experimental conditions employed in the measurement of mass transfer coefficient and wall shear stress along the bottom and the sidewall of the cylindrical vessel with a centrally placed single coaxial tuyere are presented in Table 3.3.

Results of the measurements of the average values and the rms values of the fluctuations of the mass transfer coefficient and the wall shear stress for experiments with single tuyere are presented in Appendix III, Table A3.2. Table A3.2a gives the results along the bottom and the sidewalls for the experiment in which $\dot{Q}_s$ = 0, l = 0 and h = 40 cm. It was found, while varying l and $\dot{Q}_s/(\dot{Q}_s + \dot{Q}_j)$,

Table 3.3

Experimental Conditions in Measurements of Wall Shear Stress Using Single Tuyere

Height of the water bath	$= h = 40$, 30 and 20 cm
Diameter of the water bath	$= d_b = 48$ cm
Diameter of the inner pipe	$= d_j = 0.65$ cm
Thickness of the annulus	$= t_s = 0.075$ cm
Projection of the inner pipe	$= l = 0$, d_j and $2d_j$
Total flow rate of air	$= \dot{Q}_s + \dot{Q}_j = 50$, 100, 150 and 200 liters/min.
Percent of air blown through the annulus	$= \frac{\dot{Q}_s}{\dot{Q}_s + \dot{Q}_j} \times 100 = 0$, 5 and 10

The tuyere was placed axially in the cylindrical vessel. Electrode positions are shown in Figure 2.19.

that the effect of these parameters at the electrodes along the sidewall and on the bottom far from the tuyere was not perceptible. Hence the results of experiments at electrodes with negligible change from those presented in Table A3.2a are not given in the succeeding tables. It is just mentioned that they are similar to those in Table A3.2a.

The values of the average mass coefficient $\bar{k}$ and the rms values of the fluctuations $\sqrt{\overline{k'^2}}$ are presented only

in Table A3.2a. As $\bar{k}$ and $\sqrt{\overline{k'^2}}$ are simply related to the average shear stress $\bar{\tau}$ and the rms of the fluctuations in shear stress $\sqrt{\overline{\tau'^2}}$ through Eqs. 2.10, 2.13-2.15. The discussions of the wall shear stress would qualitatively hold for the mass transfer coefficients also. Hence the mass transfer coefficient values have not been given for the rest of the experiments.

3.4.1. General Observations

The variation of the wall shear stress along the bottom at various total flow rates of air ($\dot{Q}_j + \dot{Q}_s$) are plotted for some of the experiments in Figures 3.16 to 3.18. Figure 3.16 corresponds to Table A3.2a where $l/d_j = 0$, $\dot{Q}_s = 0$ and $h = 40$ cm. The result of the experiment in which $\dot{Q}_s/(\dot{Q}_s + \dot{Q}_j) = 0.1$ is shown in Figure 3.17. In Figure 3.18 is shown the consequence of projecting the tuyere to a distance of $2d_j$ (i.e., $l/d_j = 2$).

The first thing that is quite apparent in these plots is the similarity of behaviour of both the average value of the shear stress $\bar{\tau}$ and the rms value of its fluctuations $\sqrt{\overline{\tau'^2}}$. It was felt that the two may be related by a simple relation which is characteristic of the system. Hence $\sqrt{\overline{\tau'^2}}$ was plotted against $\bar{\tau}$, as shown in Figure 3.19. It can be seen that $\sqrt{\overline{\tau'^2}}$ is directly proportional to $\bar{\tau}$. A least square fit of this curve gave the following expression

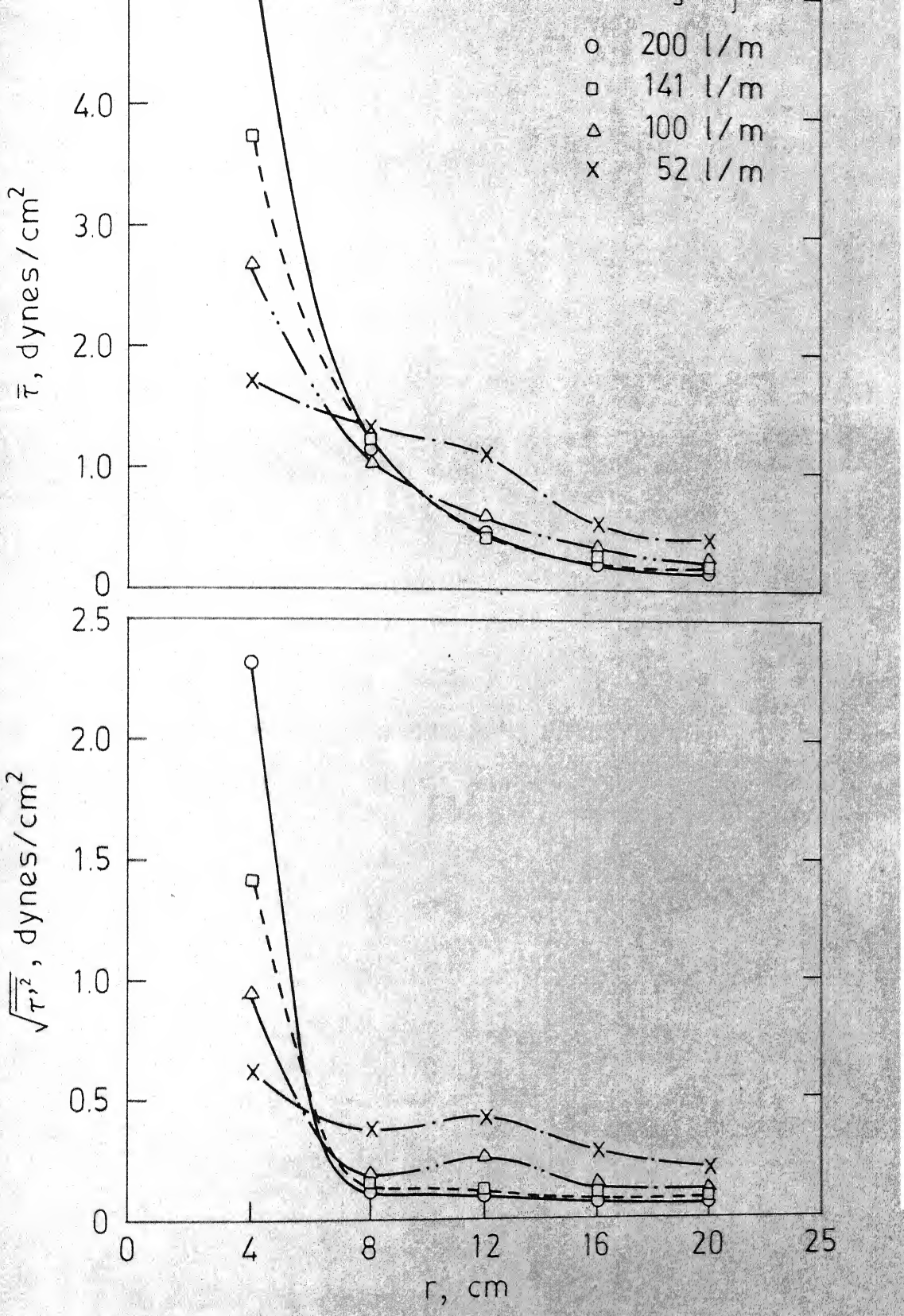

Fig. 3.16 Variation of average shear stress $\bar{\tau}$ and rms value of fluctuations in shear stress $\sqrt{\overline{\tau'^2}}$ with radial distance r from the tuyere axis in experiments with single tuyere; $l/d_j = 0$, $\dot{Q}_s = 0$ and $h = 40$ cm.

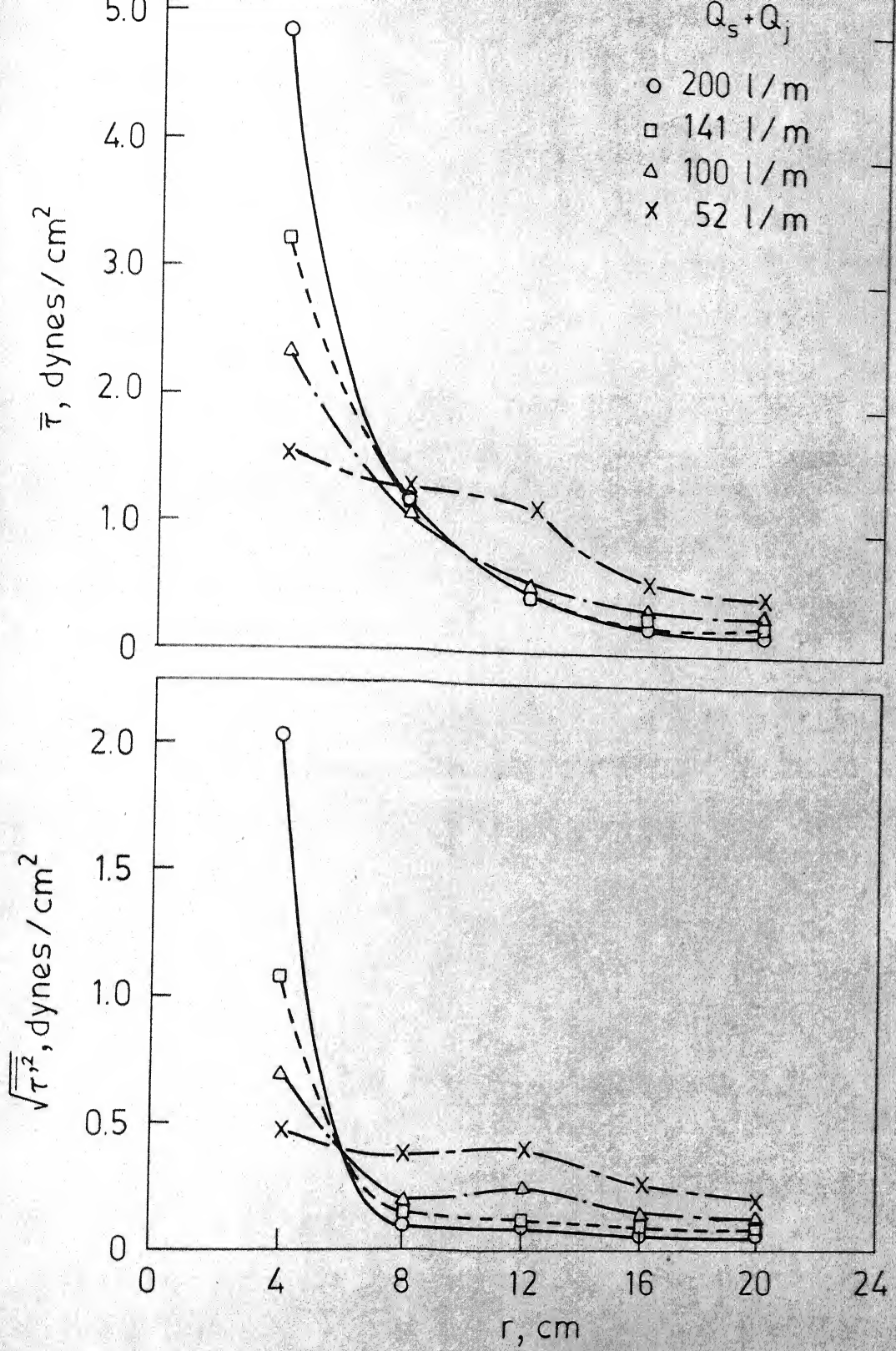

g. 3.17 Variation of the average shear stress $\bar{\tau}$ and rms value of fluctuations in shear stress $\sqrt{\overline{\tau'^2}}$ with radial distance r from the tuyere axis in experiments with single tuyere; $l/d_j = 0$, $\dot{Q}_s/(\dot{Q}_s+\dot{Q}_j) = 0.1$ and h= 40 cm.

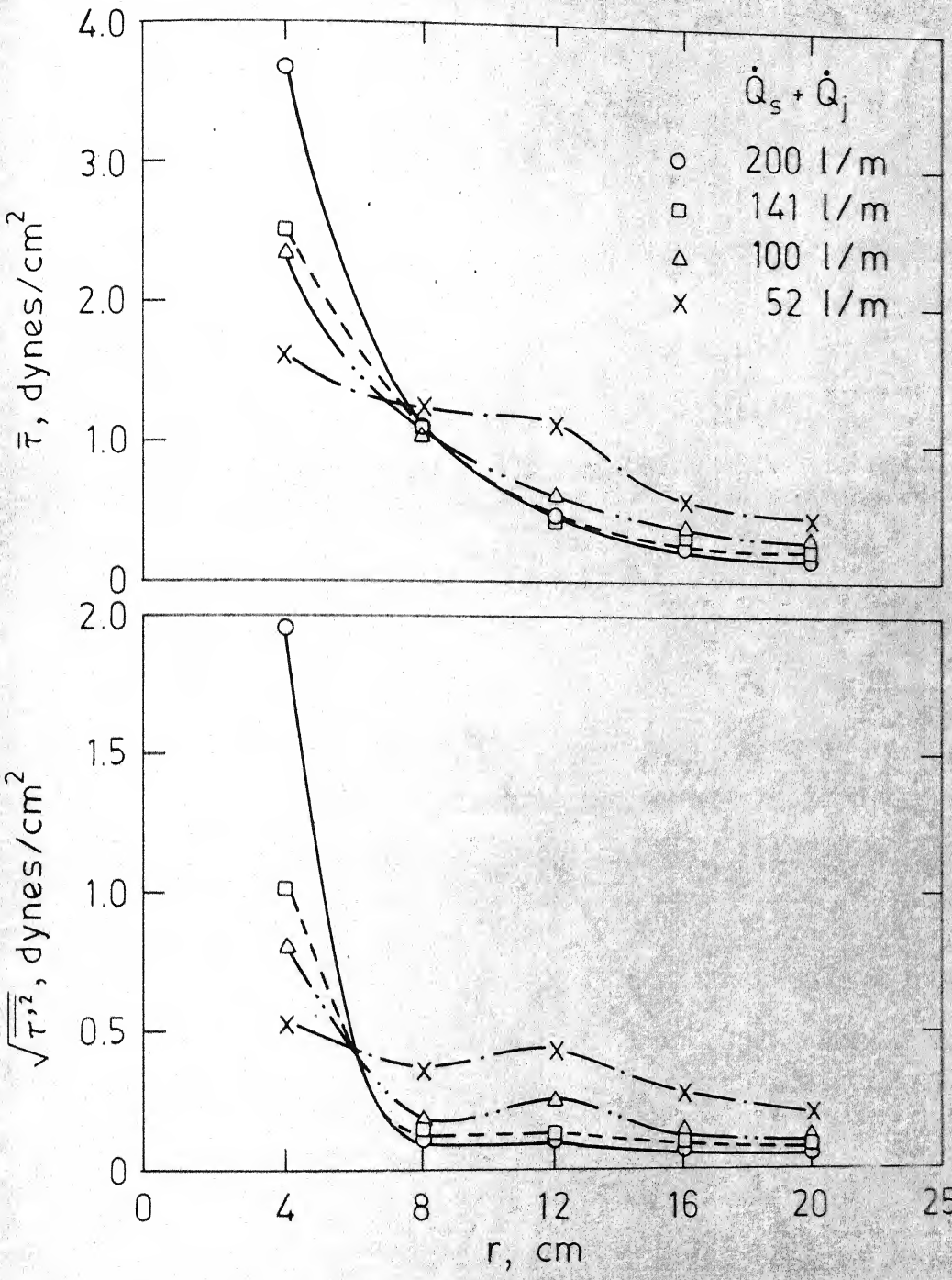

Fig. 3.18 Variation of average shear stress $\bar{\tau}$ and rms value of fluctuations in shear stress $\sqrt{\overline{\tau'^2}}$ with radial distance r from the tuyere axis in experiments with single tuyere; $l/d_j = 2$, $\dot{Q}_s = 0$ and $h = 40$ cm.

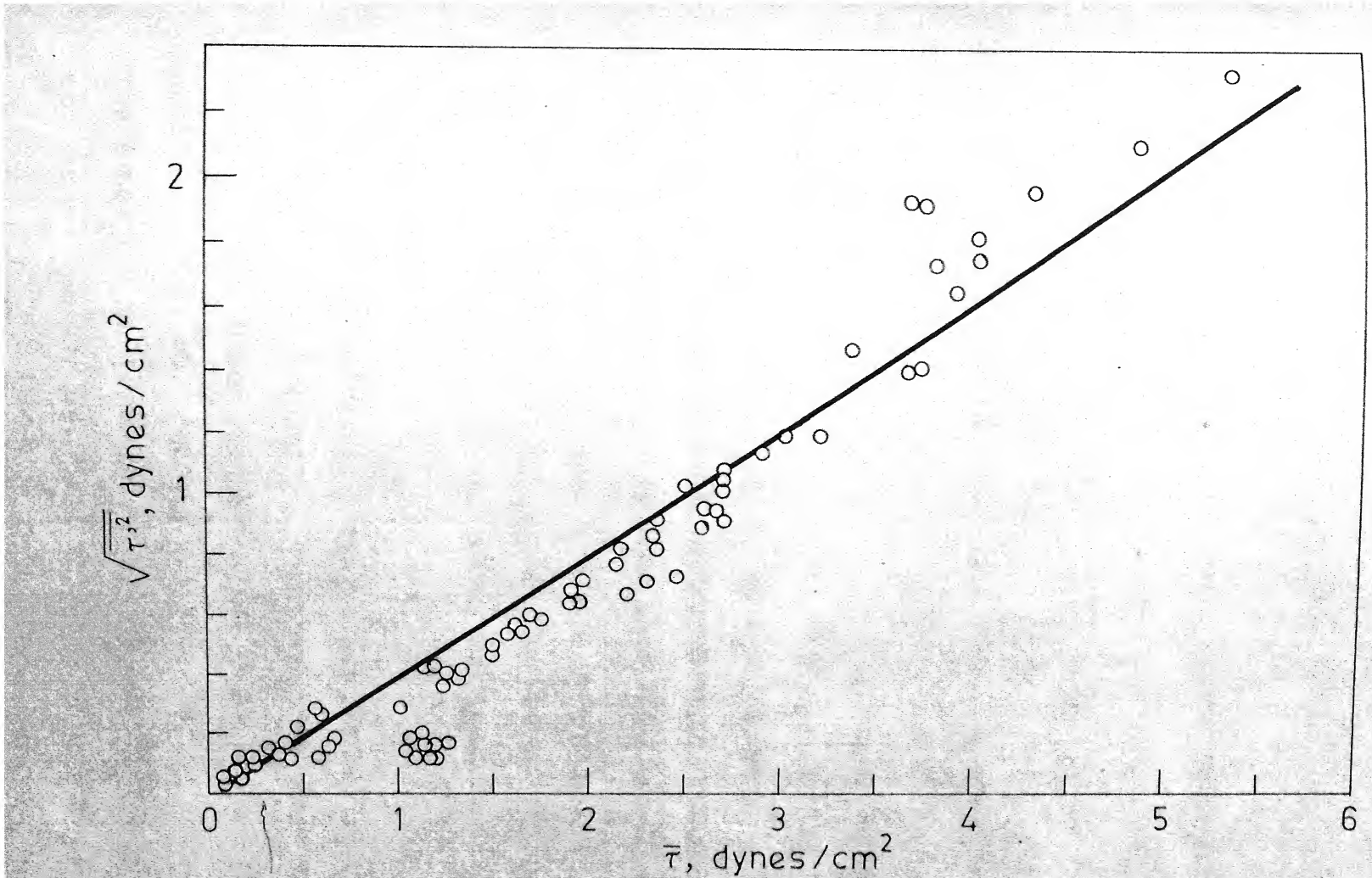

Fig. 3.19 Plot of rms value of fluctuations in shear stress $\sqrt{\overline{\tau'^2}}$ vs average shear stress $\bar{\tau}$ in experiments with single tuyere.

$$\sqrt{\overline{\tau'^2}} = 0.40\ \bar{\tau} \qquad 3.6$$

The standard deviation in the value of the slope is 1.1 pct.

Figure 3.20 shows two typical oscilloscope traces of the fluctuations in current. These fluctuations are obviously due to the fluctuations in the mass transfer coefficient and the wall shear stress. The photograph of the oscilloscope trace for electrode B_1 that is closest to the tuyere is presented in Figure 3.20a. Figure 3.20b corresponds to electrode B_5 which is farthest from the tuyere. It can be seen from these photographs that the density of high frequency fluctuations is large at electrode B_1 and is almost absent at electrode B_5. This seems to indicate that the high frequency flow fluctuations that are generated at the jet-water interface are dissipated in the liquid and the density of these fluctuations decreases as the distance from the jet increases.

Because of the straight line relationship between $\sqrt{\overline{\tau'^2}}$ and $\bar{\tau}$, correlations and discussion have been restricted to the average shear stress $\bar{\tau}$. All these interpretations would, however, hold equally well for the rms values of the fluctuations in shear stress $\sqrt{\overline{\tau'^2}}$, only difference being the changes in the numerical values of the constants.

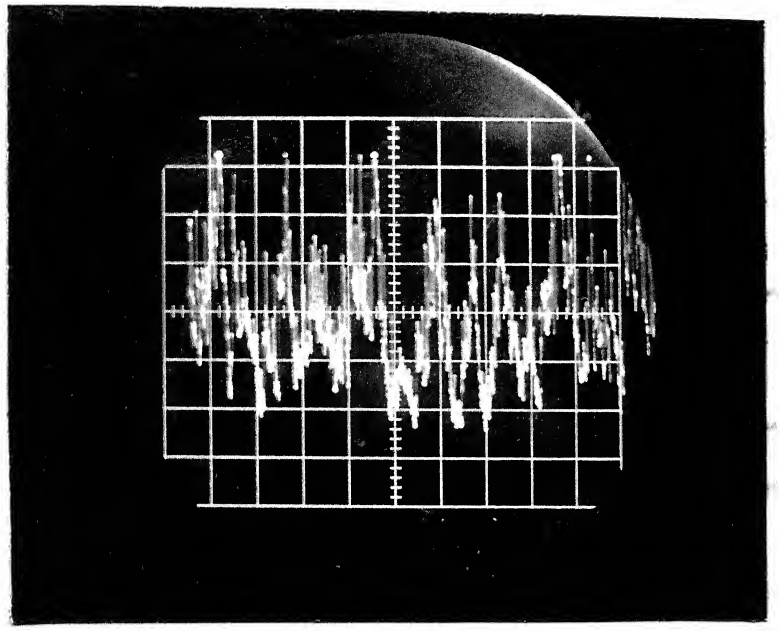

(a)

0.005V
0.5s

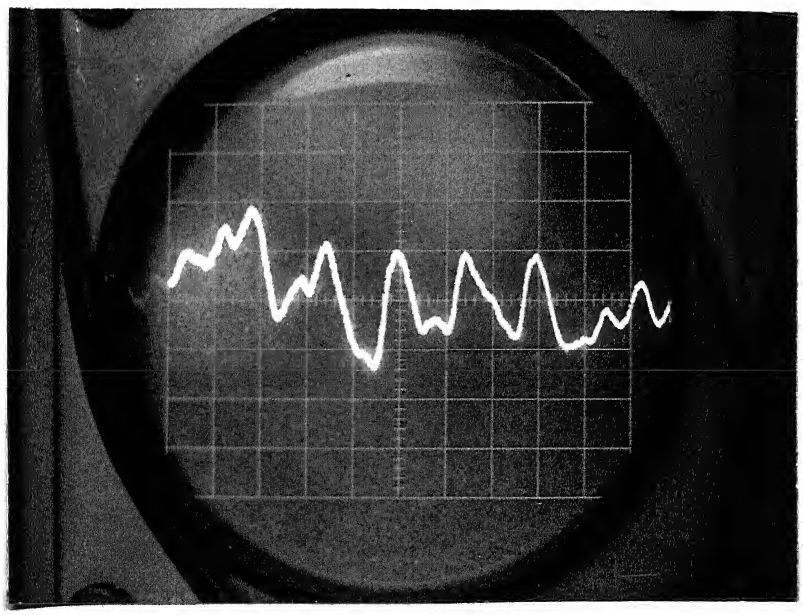

(b)

Figure 3.20. Oscillograms of fluctuations in current at a) electrode B_1 and b) electrode B_2

The variations of log $\bar{\tau}$ with the log of the radial distance r of the electrode from the tuyere axis, at various flow rates of air are plotted in Figures 3.21 and 3.22. Figure 3.21 depicts the situation when the bath height was 40 cm and Figure .22 when it was 30 cm. It is evident that the slopes of the curves at any air flow rate vary with r. Such a behaviour can be explained qualitatively with the help of the flow pattern shown in Figure 3.5 as follows.

When the fluid flow is parallel to a solid surface and is converging towards an axis perpendicular to the surface, the shear stress at the wall is expected to vary inversely as the distance r from the axis. This is due to the fact that as r increases, radial velocity v_r decreases in magnitude because of the increasing area of cross-section for the flow. That is, if

$$\tau \propto r^x \qquad 3.7$$

x = 1 for parallel flow. If the flow direction is towards the surface, as is the case near the bottom depicted in Figure 3.5a, x will be greater than 1 (from continuity considerations). If the flow is away from the bottom surface as in the region close to the tuyere in Figure 3.5b, x will be less than 1. Comparison of Figures 3.21 and 3.22 with Figure 3.5 demonstrates the fact that the behaviour observed is in accordance with the above explanation. That is, the

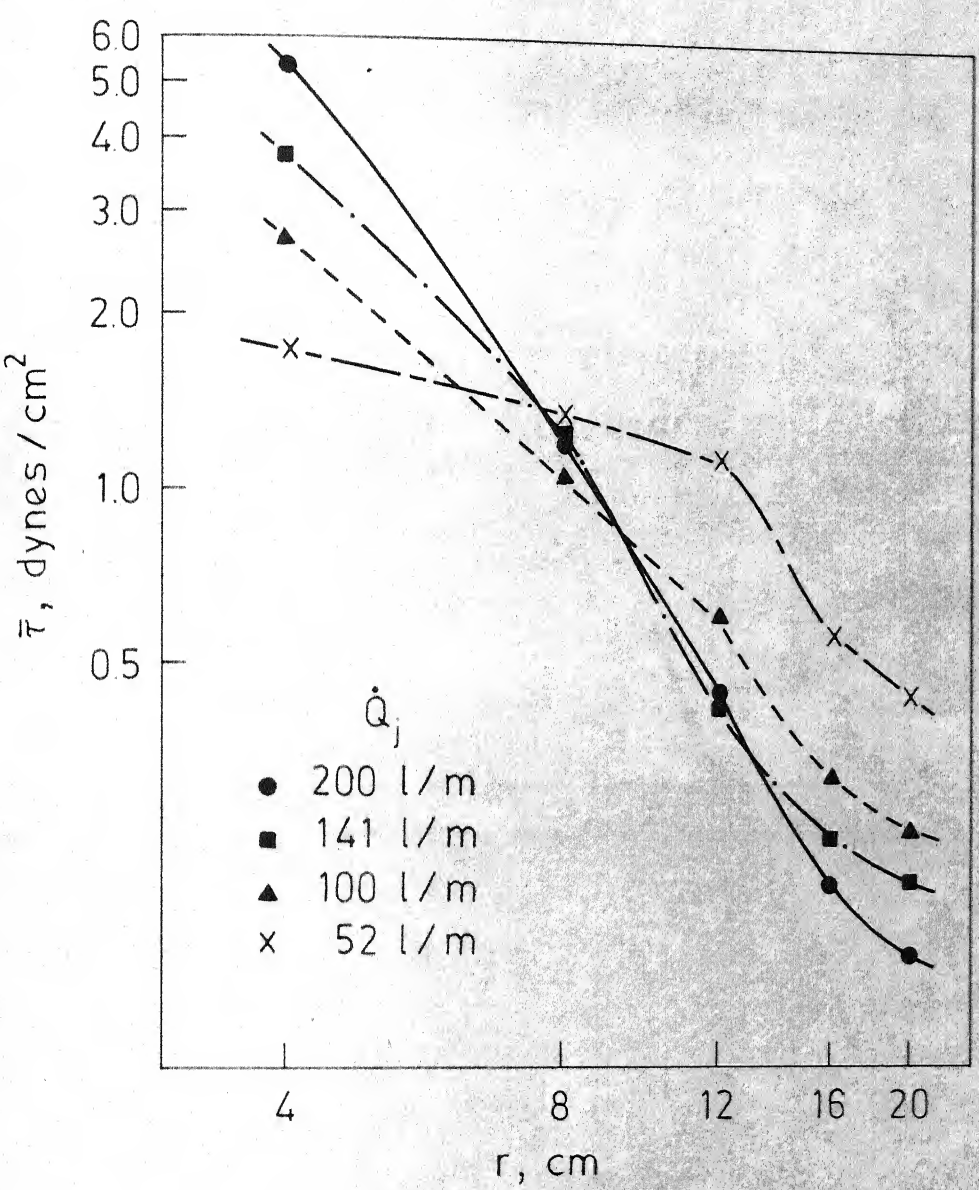

Fig. 3.21 Log-log plot of average wall shear stress $\bar{\tau}$ vs the radial distance r from the tuyere axis for experiments with single tuyere; $l/d_j = 0$, $\dot{Q}_s = 0$ and $h = 40$ cm.

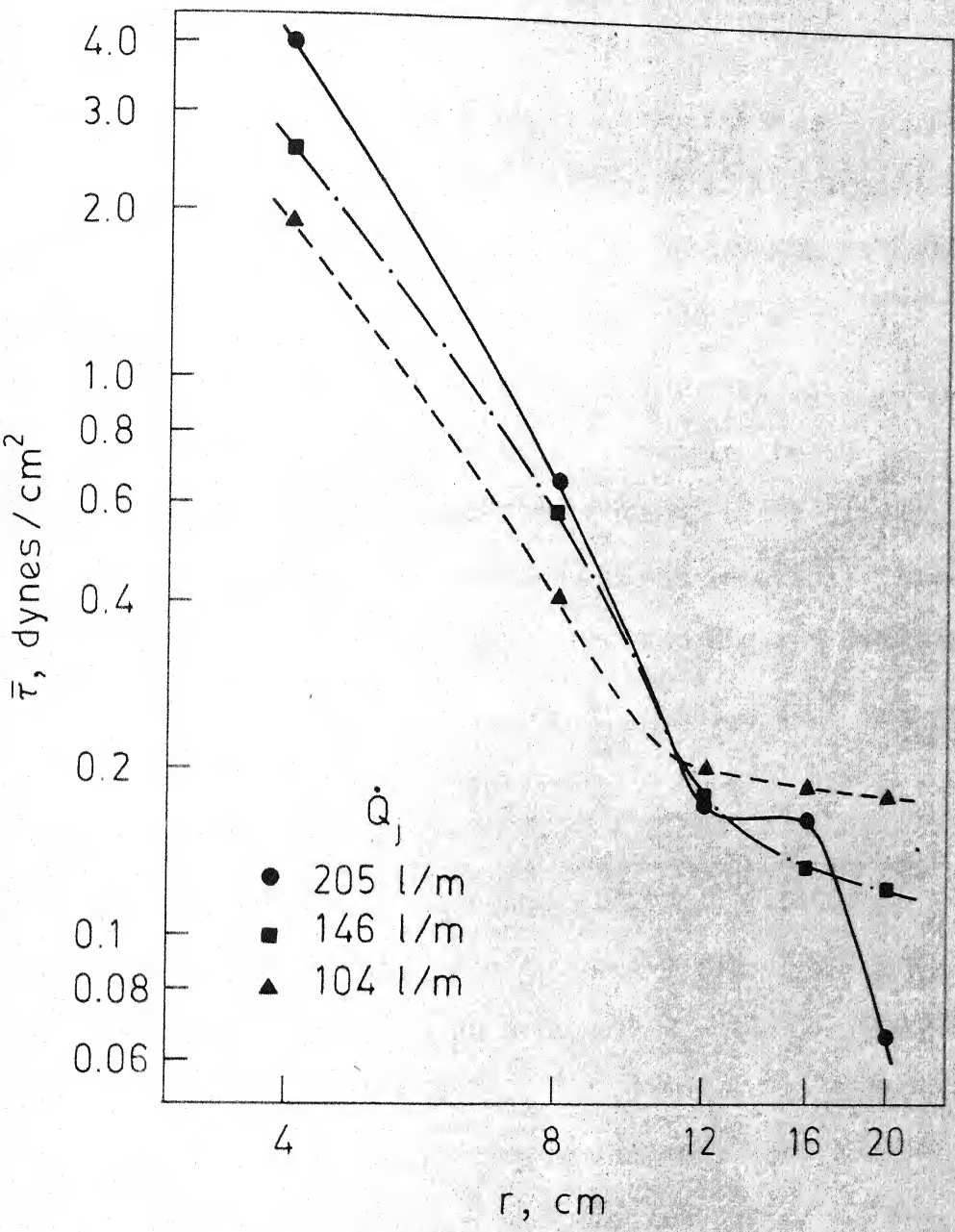

Fig. 3.22 Log-log plot of average wall shear stress $\bar{\tau}$ vs the radial distance r from the tuyere axis for experiments with single tuyere; $l/d_j = 0$, $\dot{Q}_s = 0$ and $h = 30$ cm.

point at which x is equal to 1, i.e., the flow is parallel to the bottom, moves towards the axis of the tuyere as the air flow rate is increased from 50 liters/min to 200 liters/min.

Another interesting consequence of the type of behaviour of the flow explained above is the increase of shear stress as the total flow rate of air decreases at the electrodes far from the tuyere. This is readily seen in Tables A3.2a, A3.2i and A3.2l and the Figures 3.16 to 3.19.

It can be seen from the tables that the shear stress level at all the electrodes along the bottom decreases as the height of the water bath decreases from 40 cm to 20 cm. At electrode B_1 (the electrode closest to the tuyere) the shear stress decreases as the length of projection of the tuyere l increases at constant $\dot{Q}_s$ and $\dot{Q}_j$. Increasing $\dot{Q}_s/(\dot{Q}_s + \dot{Q}_j)$ at constant $(\dot{Q}_s + \dot{Q}_j)$ and l has a similar effect at B_1. At other electrodes, however, the effects of increasing l and $\dot{Q}_s/(\dot{Q}_s + \dot{Q}_j)$ are not perceptible.

Correlations between the process variables have been obtained for the electrode B_1 and are discussed in Section 3.4.2. As the effects of l and $\dot{Q}_s/(\dot{Q}_s + \dot{Q}_j)$ are not perceptible at electrodes B_2 to B_5, no further analysis of the results at these electrodes has been attempted.

3.4.2. Dimensionless Correlation

When a gas is blown into a liquid, momentum put into the liquid per unit time is equal to $v_j^{o2} \cdot \frac{\pi d_j^2}{4} \cdot \rho_j^o$ where v_j^o is the mean velocity of the jet at tuyere exit and ρ_j^o is its density. This momentum is transferred to the walls. If τ is the shear stress at any point on the wall, $\int_A \tau \, dA$ is the total momentum transferred to the walls. Therefore, a quantity like $(\tau/v_j^{o2}\rho_j^o)(d_b^2/d_j^2)$ would characterize the system. As d_b and d_j were not varied in the present work, the dimensionless number $\bar{\tau}/(\rho_j^o v_j^{o2})$, which corresponds to the Euler number, N_{Eu}, that is,

$$N_{Eu} = \frac{\bar{\tau}}{v_j^{o2} \rho_j^o}, \qquad 3.7$$

may be accepted as a pertinent dimensionless group for correlation purposes.

Gravitational effects, like buoyancy, are expressed by the modified Froude number, $N_{Fr'}$, defined as

$$N_{Fr'} = \frac{v_j^{o2} \rho_j^o}{gh\,(\rho_l - \rho_j^o)} \qquad 3.8$$

where

g = acceleration due to gravity

h = height of the bath

and ρ_l = density of the liquid.

Here h is chosen as the characteristic length in preference to d_j because we are interested in the characteristics of the bath motion rather than those of the jet. In addition to that, the momentum contributed by the shrouding gas, which is an order of magnitude less than that contributed by the jet gas, has been ignored in these calculations. It is expected that N_{Eu} should decrease as $N_{Fr'}$ increases, as the gravitational effects are small for large $N_{Fr'}$.

Values of N_{Eu} and $N_{Fr'}$ for the various sets of results are presented in Appendix IV. Figures 3.23 to 3.25 are plots of the dependence of N_{Eu} on $N_{Fr'}$. It is evident that, in the range of investigation, log N_{Eu} is linearly related to log $N_{Fr'}$, i.e.,

$$N_{Eu} = a \cdot N_{Fr'}^{b} \qquad 3.9$$

where a and b are constants.

One interesting feature to be noted in these plots is that for a given $\frac{1}{d_j}$ and h, the points are on the same straight line for various values of $\dot{Q}_s/(\dot{Q}_s + \dot{Q}_j)$ upto a value of 0.1 for the latter. This seems to indicate that the decrease in the shear stress when a small part of the gas is diverted through the annular space is only due to the decreased amount of momentum input into the system. Therefore, total momentum input into the system is the major

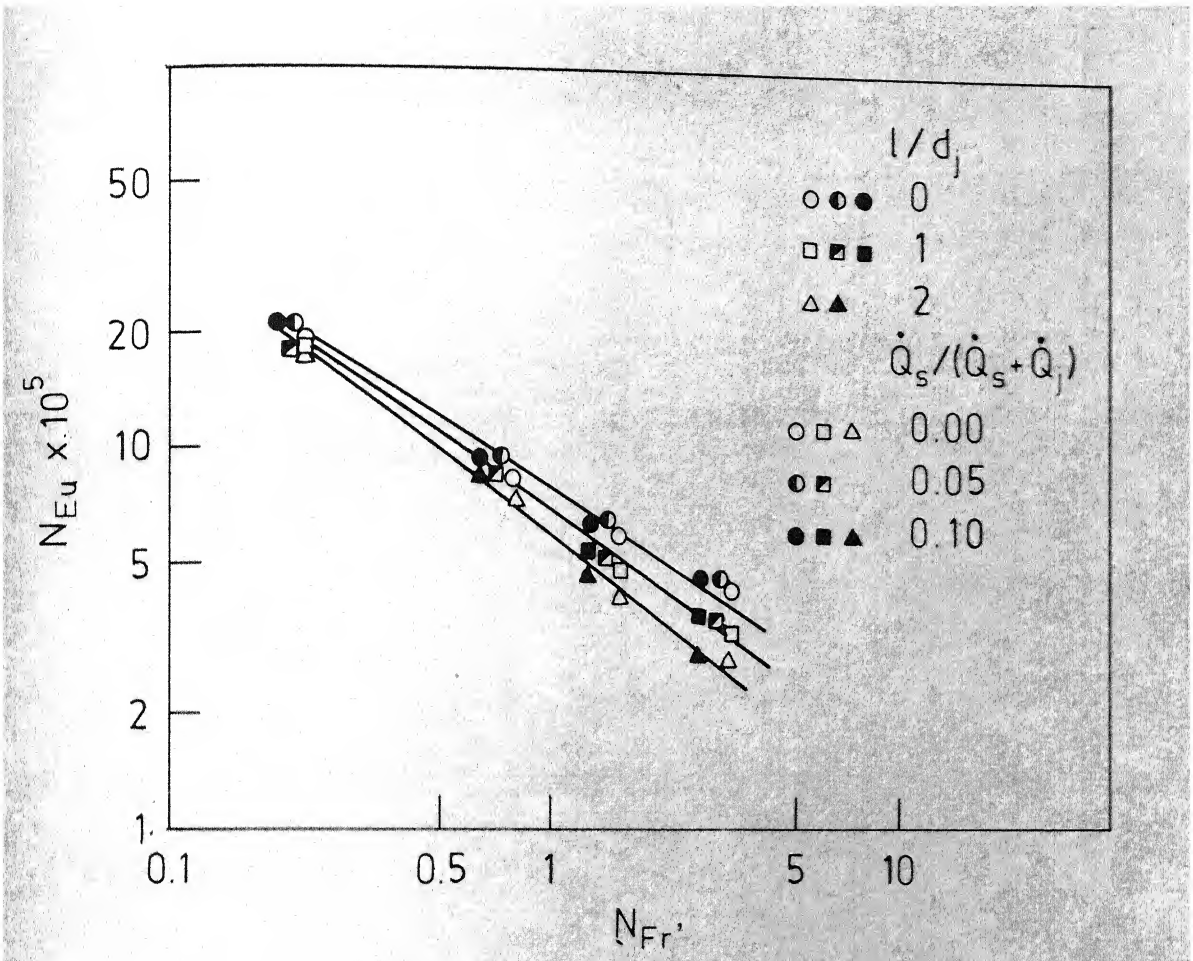

Fig. 3.23 Variation of Euler number N_{Eu} with modified Froude number $N_{Fr'}$ in experiments with single tuyere; h = 40 cm.

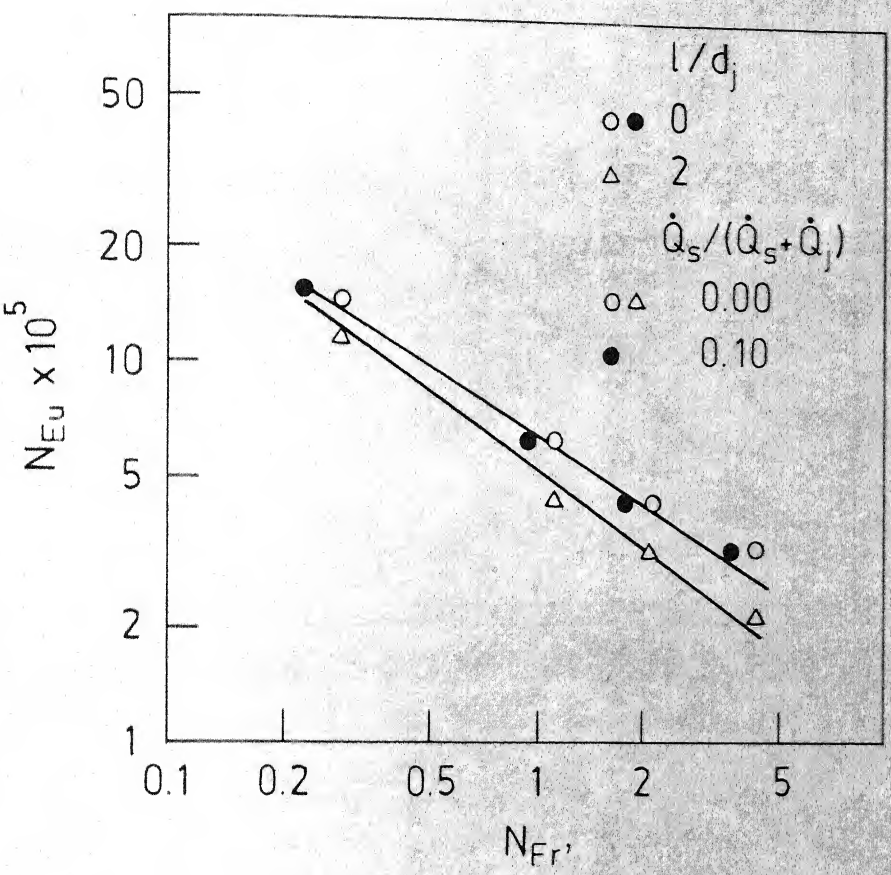

Fig. 3.24 Variation of Euler number N_{Eu} with modified Froude number $N_{Fr'}$ in experiments with single tuyere, h = 30 cm.

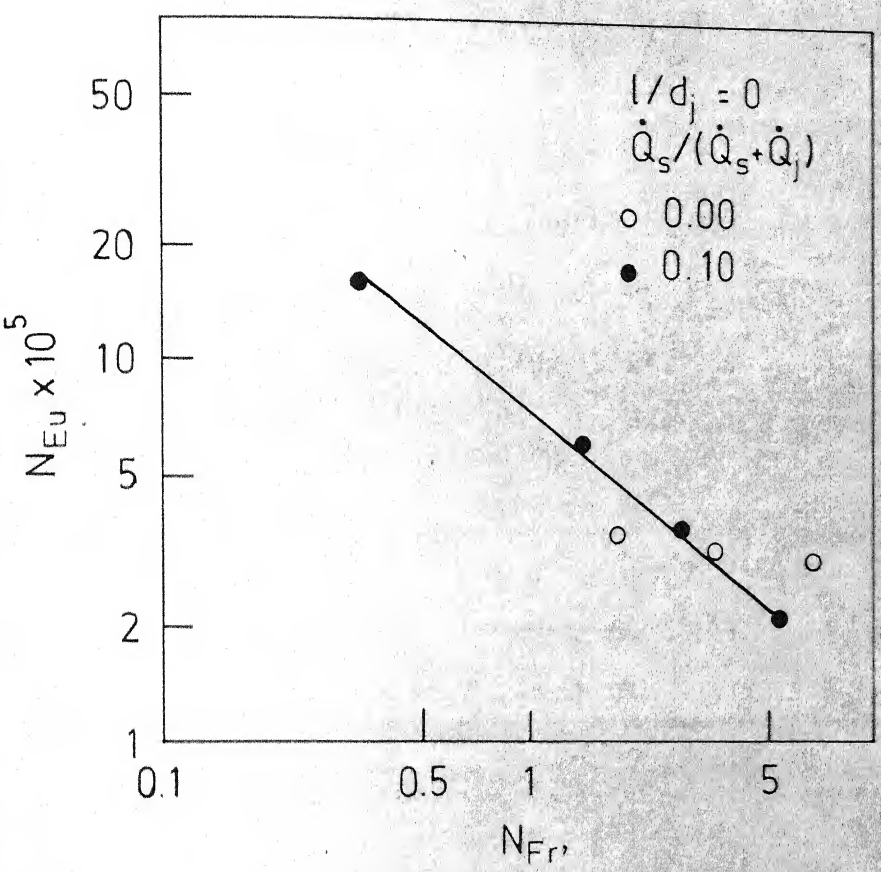

Fig. 3.25 Variation of Euler number N_{Eu} with modified Froude number N_{Fr}, in experiments with single tuyere; h = 20 cm.

criteria in determining the shear stress distribution along the wall.

The parameters a and b for the various lines in Figures 3.23 to 3.25 are presented in Table 3.4.

Table 3.4

Parameters 'a' and 'b' in Eq. 3.9 for Various Experimental Conditions

h, cm	$1/d_j$	a x 10^5	b
40	0	7.93	-0.58
40	1	6.90	-0.65
40	2	5.90	-0.77
30	0	6.22	-0.61
30	2	5.28	-0.62
20	0	7.09	-0.62

As may be seen from the above table, the parameter 'a', which is the value of N_{Eu} at $N_{Fr'} = 1$, decreases as $1/d_j$ increases. Similarly, the magnitude of the slope b increases with increasing $1/d_j$. Effect of the variation of the bath height on these parameters is not clear.

3.5. MEASUREMENTS OF WALL SHEAR STRESS IN EXPERIMENTS WITH MULTIPLE TUYERES

The experimental parameters in experiments with multiple tuyeres are presented in Table 3.5.

Table 3.5

Experimental Parameters in Measurements of Wall Shear Stress Using Multiple Tuyeres

Height of the water bath	= h = 40 cm
Diameter of the water bath	= d_b = 48 cm
Diameter of the tuyere	= d_j = 0.325 cm
Projection of the tuyere	= l = 0 and $4d_j$
Flow rate of air	= $\dot{Q}_j$ = varied between 150 and 350 liters/min.
Number of tuyeres employed	= 3, 6 and 12 in symmetric and asymmetric configurations

The tuyere positions are indicated along with the results in Table 3.6. The electrode positions are shown in Figure 2.20.

Results of the measurement of the average shear stress $\bar{\tau}$ and the rms value of the fluctuations in shear stress $\sqrt{\overline{\tau'^2}}$ are tabulated in Appendix III, Tables A3.3.

Arrangement of the results in these tables and the representation of these in the figures for the various experiments are presented in Table 3.6.

Table 3.6

Presentation of the Results of the Experiments with Multiple Tuyeres

No. of tuyeres	Tuyere positions (Refer Figure 2.3)	Symmetric or asymmetric	$\frac{l}{d_j}$	Table No. in Appendix III	Figure No.
3	1, 2, 5	Symmetric	0	A3.3a	3.26
3	1, 2, 5	Symmetric	4	A3.3b	3.27
3	1, 2, 12	Asymmetric	4	A3.3c	3.28
6	13, 15, 17, 19, 21, 23	Symmetric	4	A3.3d	3.29
6	27, 14, 16, 24, 1, 30	Asymmetric	0	A3.3e	3.30
6	27, 14, 16, 24, 1, 30	Asymmetric	4	A3.3f	3.31
12	13, 15, 17, 19, 21, 23, 2, 3, 4, 5, 6, 7	Symmetric	4	A3.3g	3.32

As in the case of experiments with single tuyere the rms value of the fluctuations in shear stress $\sqrt{\tau'^2}$ was found to be proportional to the average shear stress $\bar{\tau}$; i.e.,

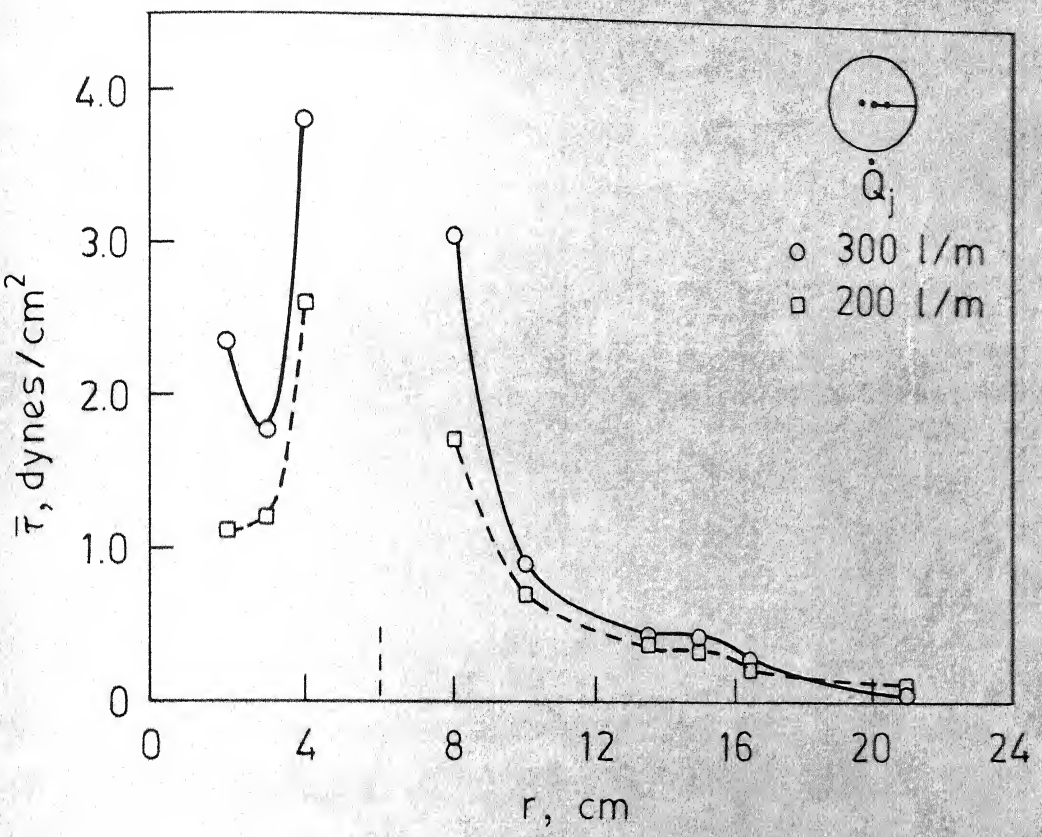

Fig. 3.26a Variation of the average shear stress $\bar{\tau}$ at the bottom with the radial distace r from the vessel axis when blowing with three symmetrically placed tuyeres; $l/d_j = 0$. The circle at the top right corner indicates the radius along which the measurements were made.

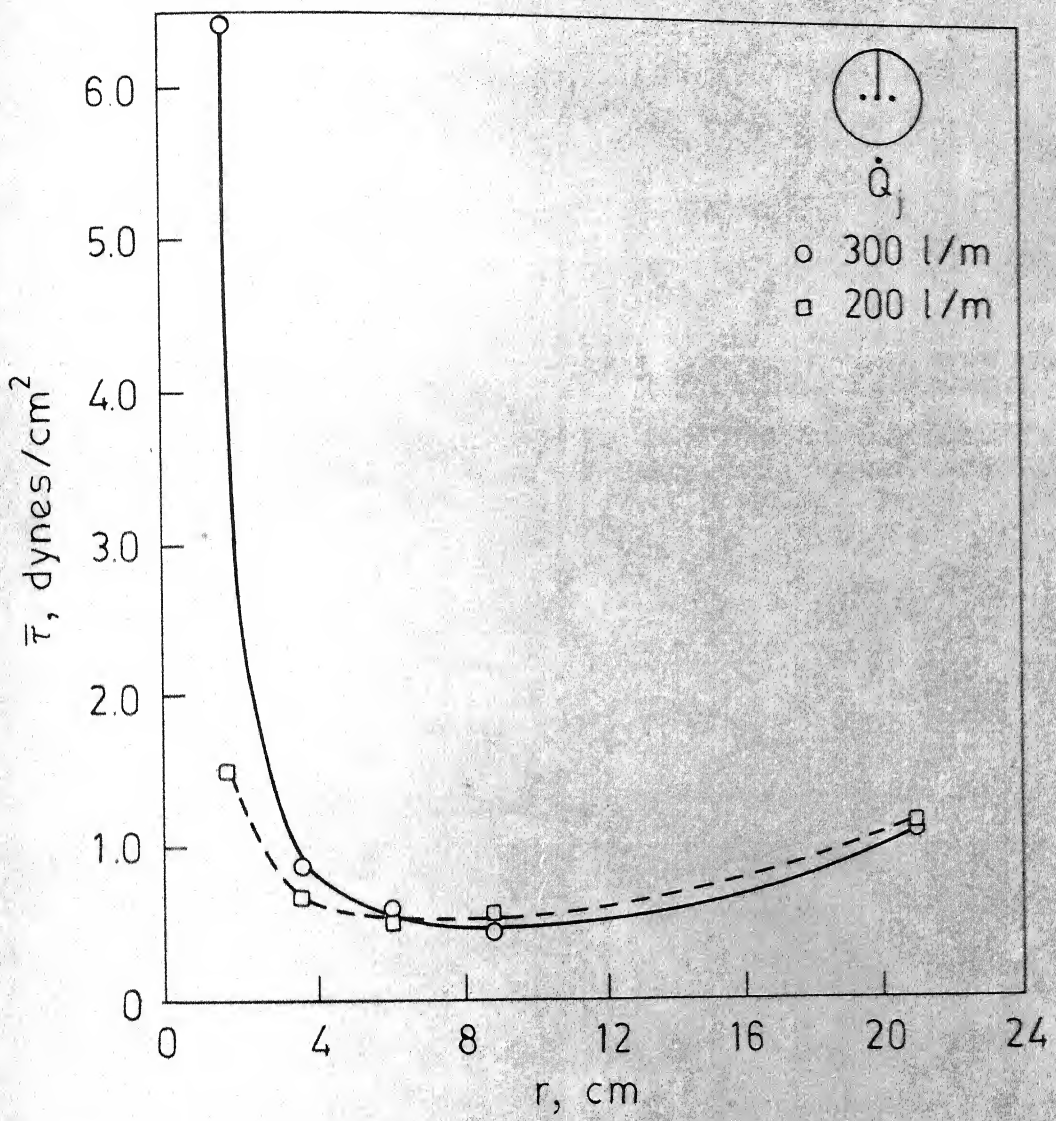

Fig. 3.26 b Variation of the average shear stress $\bar{\tau}$ at the bottom with the radial distance r from the vessel axis when blowing with three symmetrically placed tuyeres; $l/d_j = 0$. The circle at the top right corner indicates the radius along which the measurements were made.

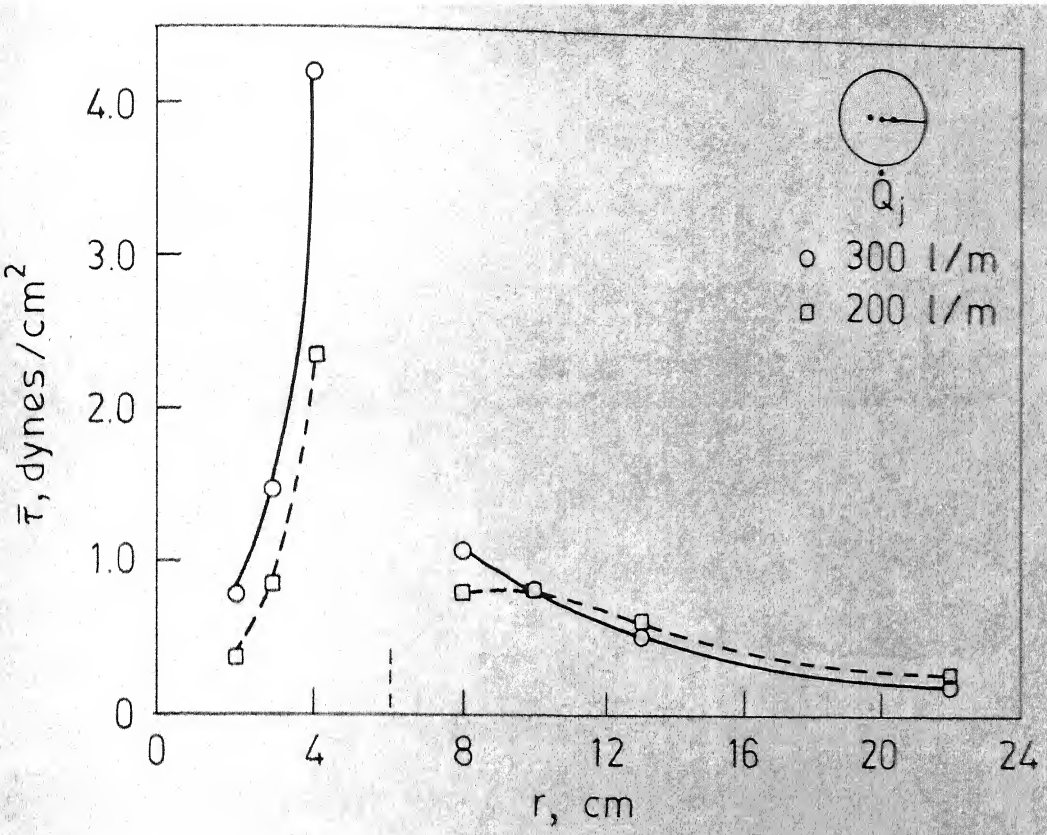

Fig. 3.27 a Variation of the average shear stress $\bar{\tau}$ at the bottom with the radial distance r from the vessel axis when blowing with three symmetrically placed tuyeres; $l/d_j = 4$. The circle at the top right corner indicates the radius along which the measurements were made.

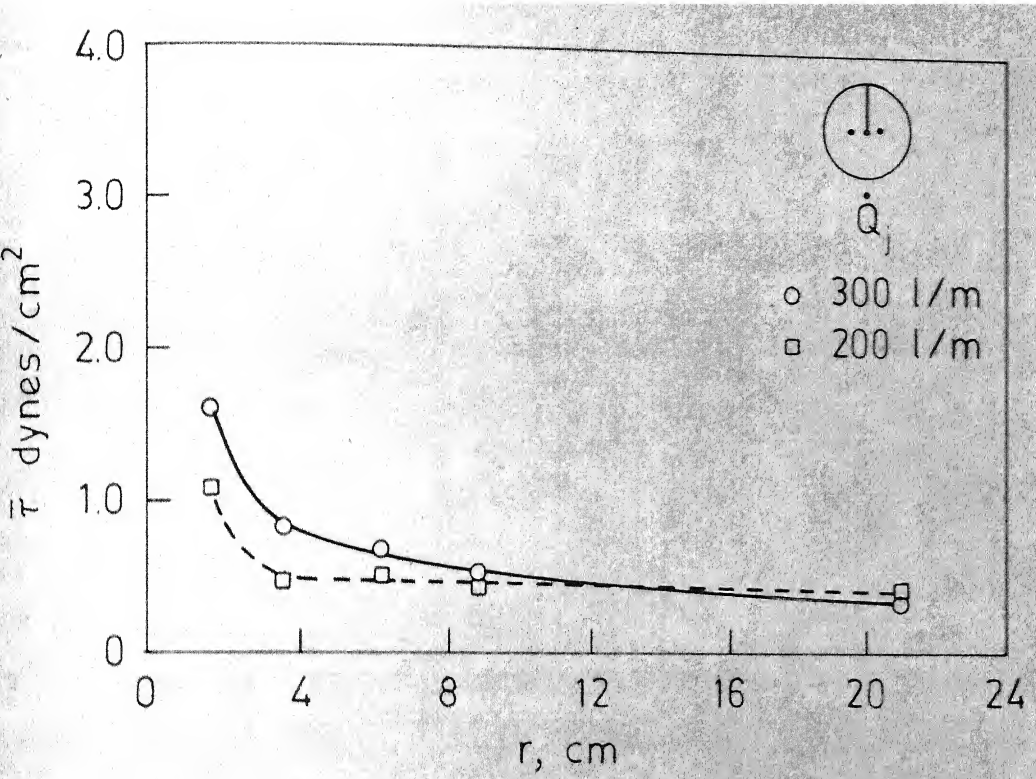

Fig. 3.27 b Variation of the average shear stress $\bar{\tau}$ at the bottom with the radial distace r from the vessel axis when blowing with three symmetrically placed tuyeres; $l/d_j = 4$. The circle at the top right corner indicates the radius along which the measurements were made.

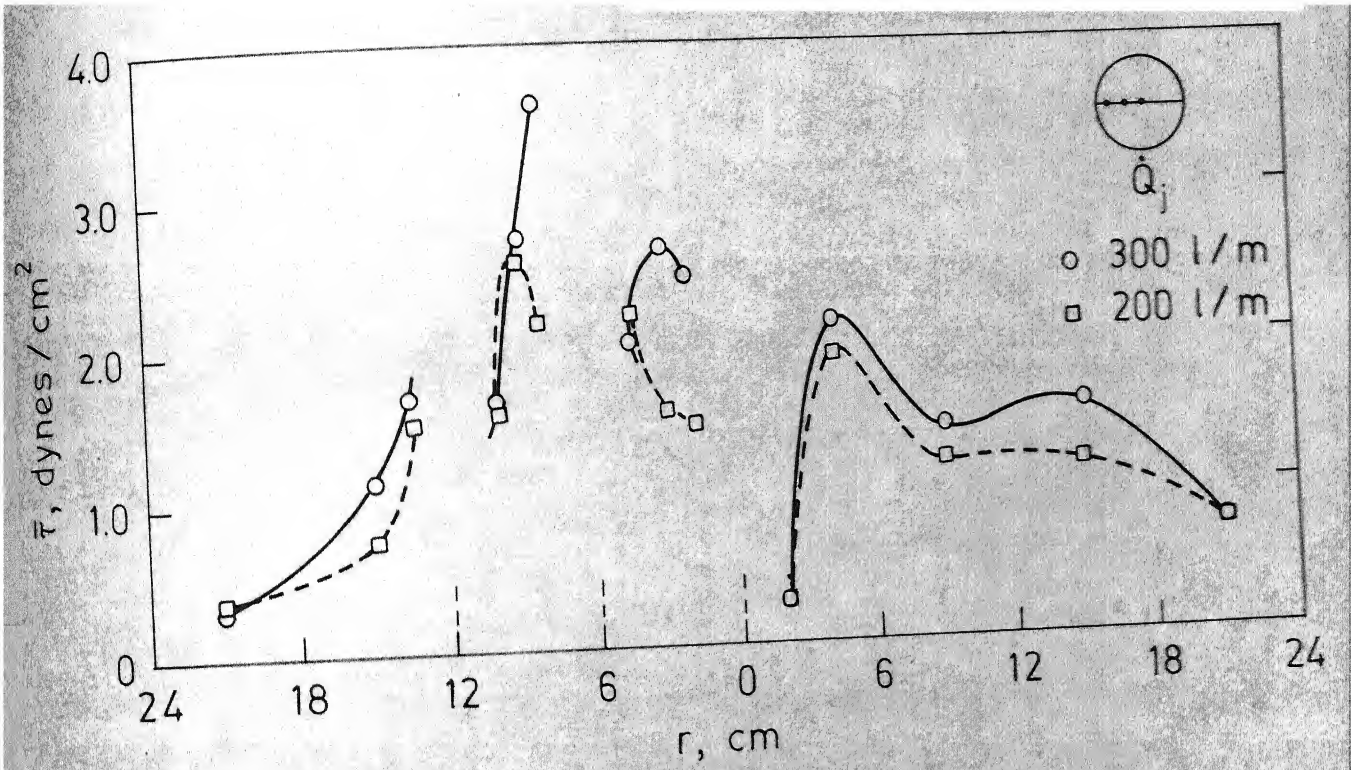

Fig. 3.28 a Variation of the average shear stress $\bar{\tau}$ at the bottom with the radial distance r from the vessel axis when blowing with three asymmetrically placed tuyeres; $l/d_j = 4$. The circle at the top right corner indicates the diameter along which the measurements were made.

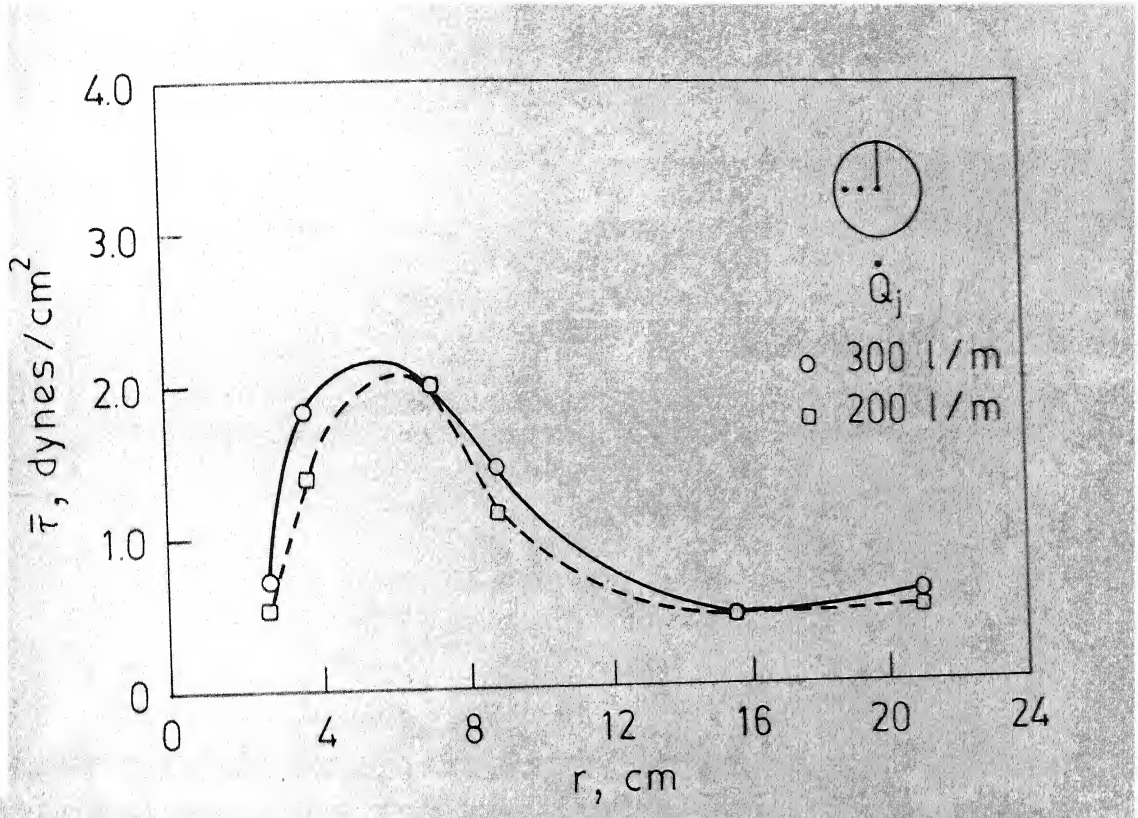

Fig. 3.28 b Variation of the average shear stress $\bar{\tau}$ at the bottom with the radial distance r from the vessel axis when blowing with three asymmetrically placed tuyeres; $l/d_j = 4$. The circle at the top right corner indicates the radius along which the measurements were made.

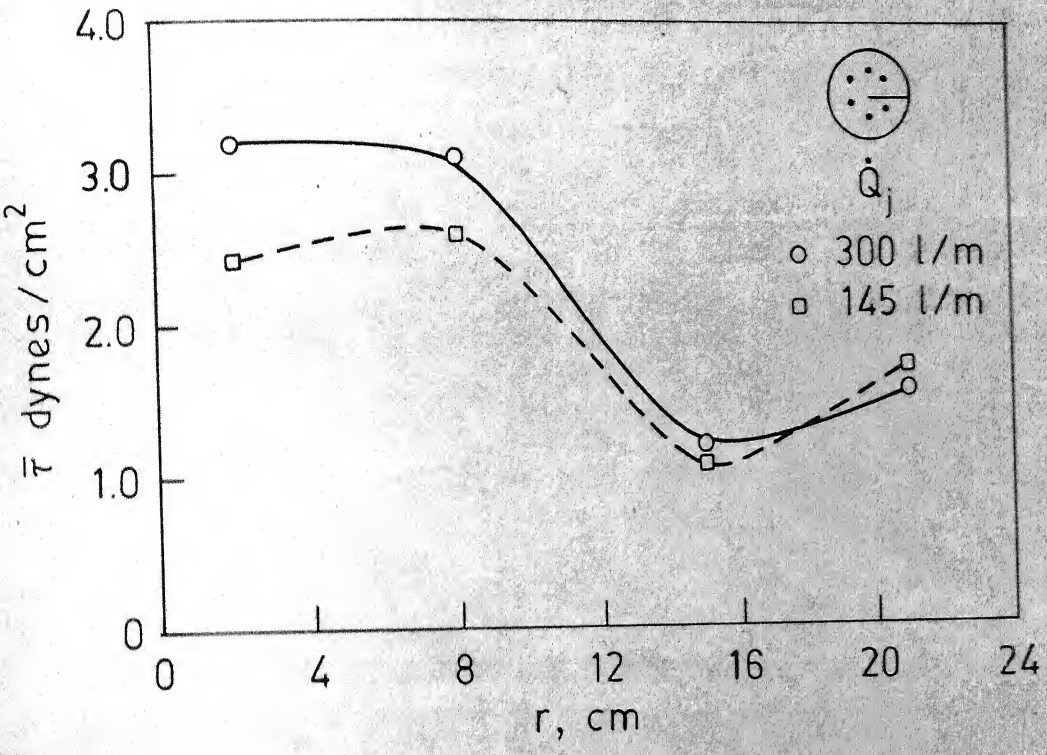

Fig. 3.29 a Variation of the average shear stress $\bar{\tau}$ at the bottom with the radial distance r from the vessel axis when blowing with six symmetrically placed tuyeres; $l/d_j = 4$. The circle at the top right corner indicates the radius along which the measurements were made.

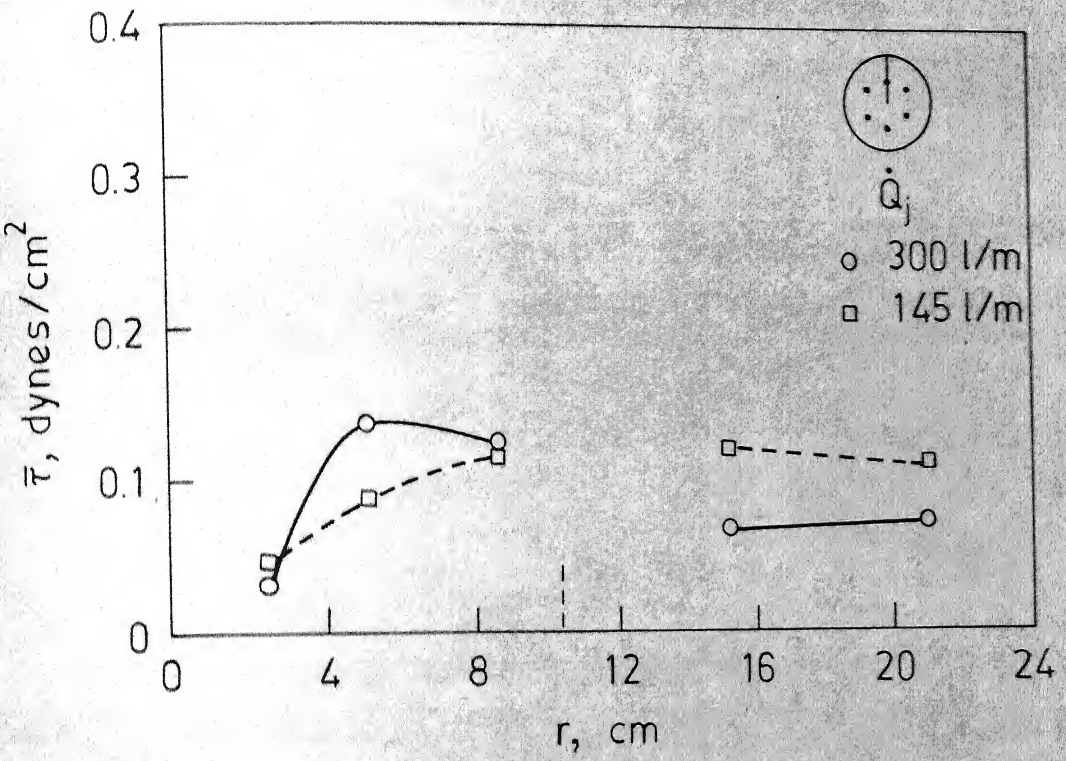

Fig. 3.29 b Variation of the average shear stress $\bar{\tau}$ at the bottom with the radial distance r from the vessel axis when blowing with six symmetrically placed tuyeres; $l/d_j = 4$. The circle at the top right corner indicates the radius along which the measurements were made.

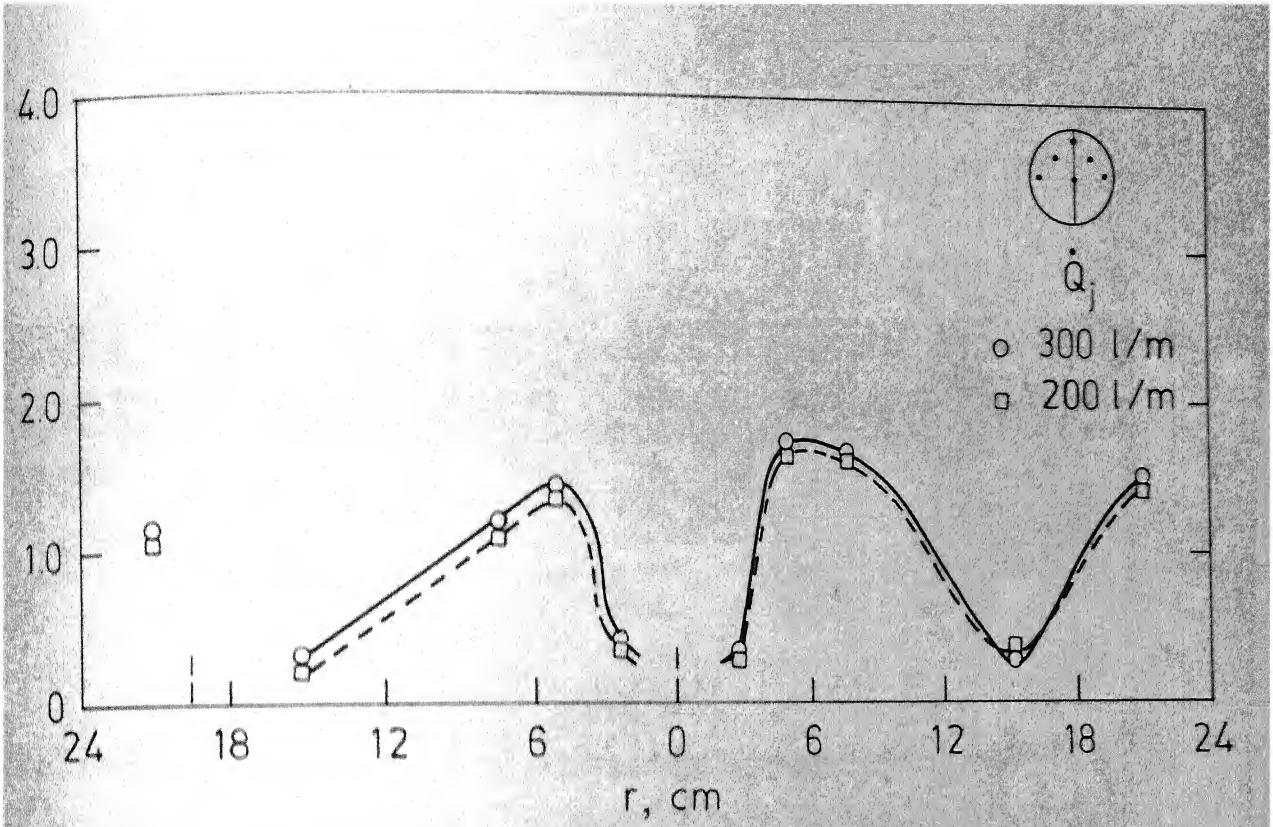

Fig. 3.30a Variation of the average shear stress $\bar{\tau}$ at the bottom with the radial distance r from the vessel axis when blowing with six asymmetrically placed tuyeres; $l/d_j = 0$. The circle at the top right corner indicates the diameter along which the measurements were made.

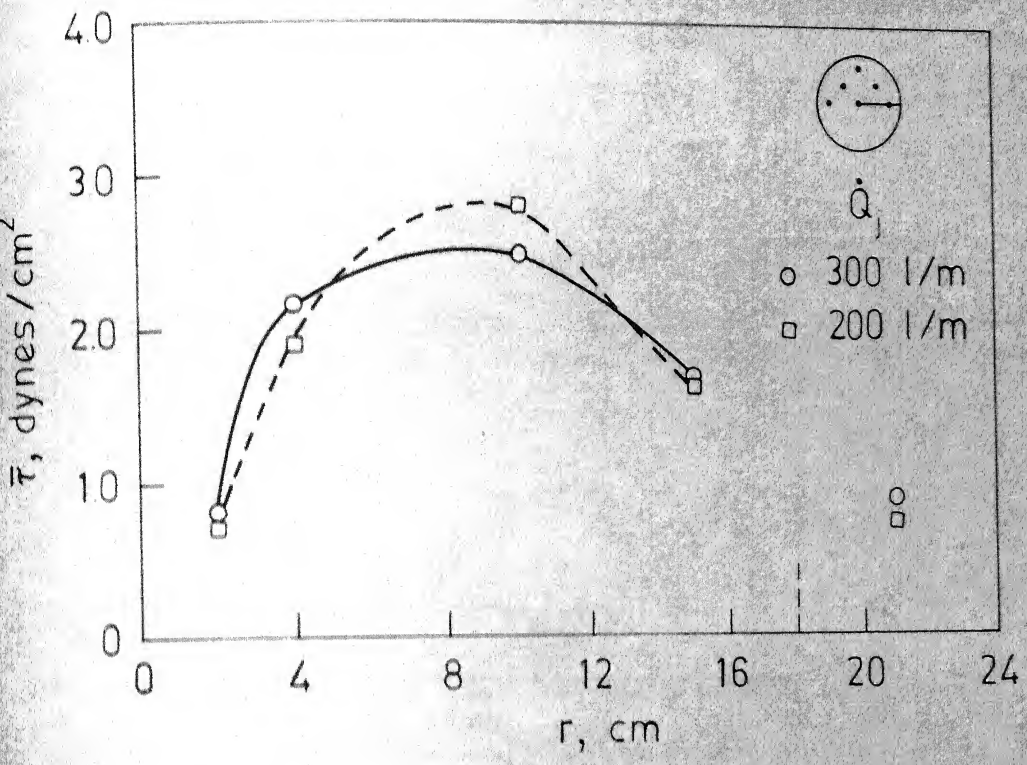

Fig. 3.30 b Variation of the average shear stress $\bar{\tau}$ at the bottom with the radial distance r from the vessel axis when blowing with six asymmetrically placed tuyeres, $l/d_j = 0$. The circle at the top right corner indicates the radius along which the measurements were made.

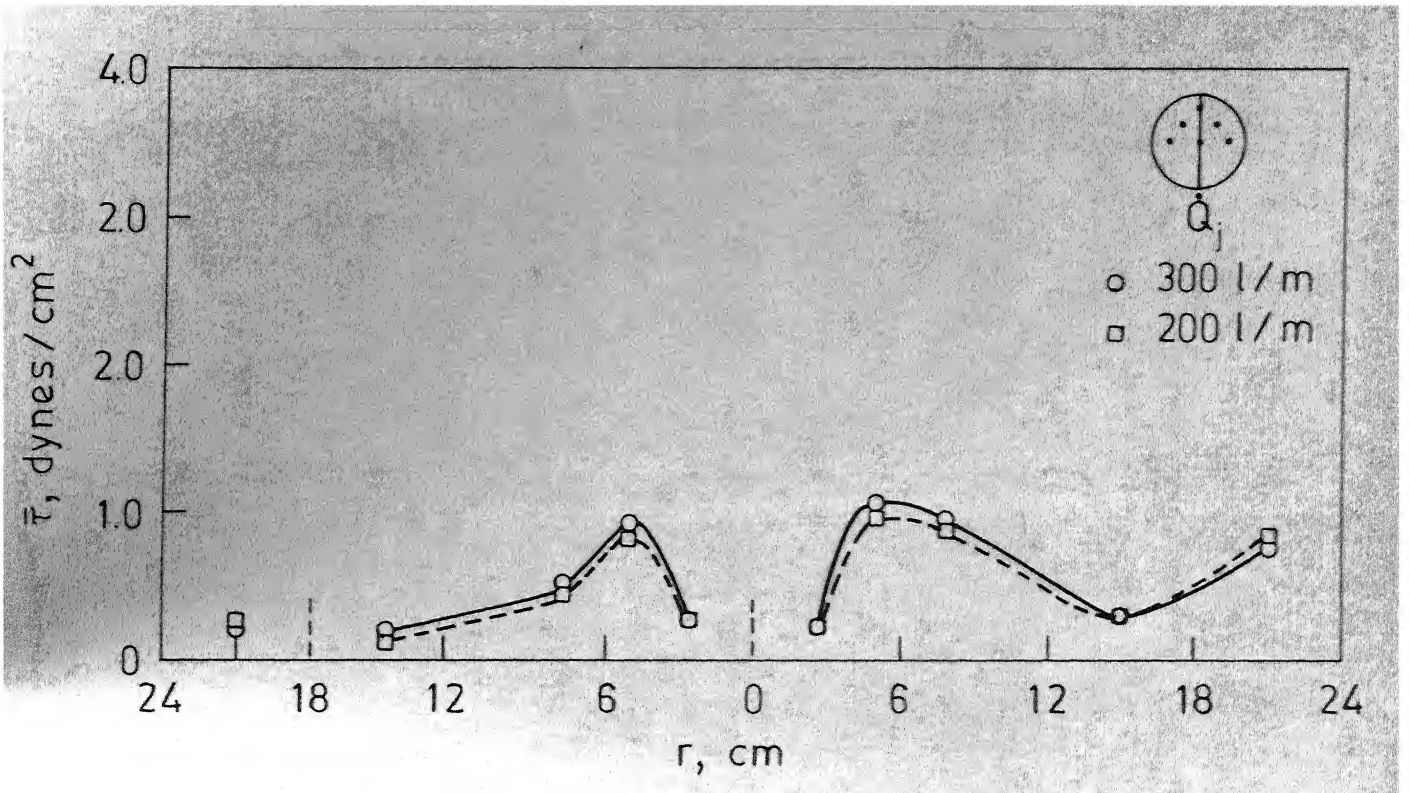

Fig. 3.31a Variation of the average shear stress $\bar{\tau}$ at the bottom with the radial distace r from the vessel axis when blowing with six asymmetrically placed tuyeres; $l/d_j = 4$. The circle at the top right corner indicates the diameter along which the measurements were made.

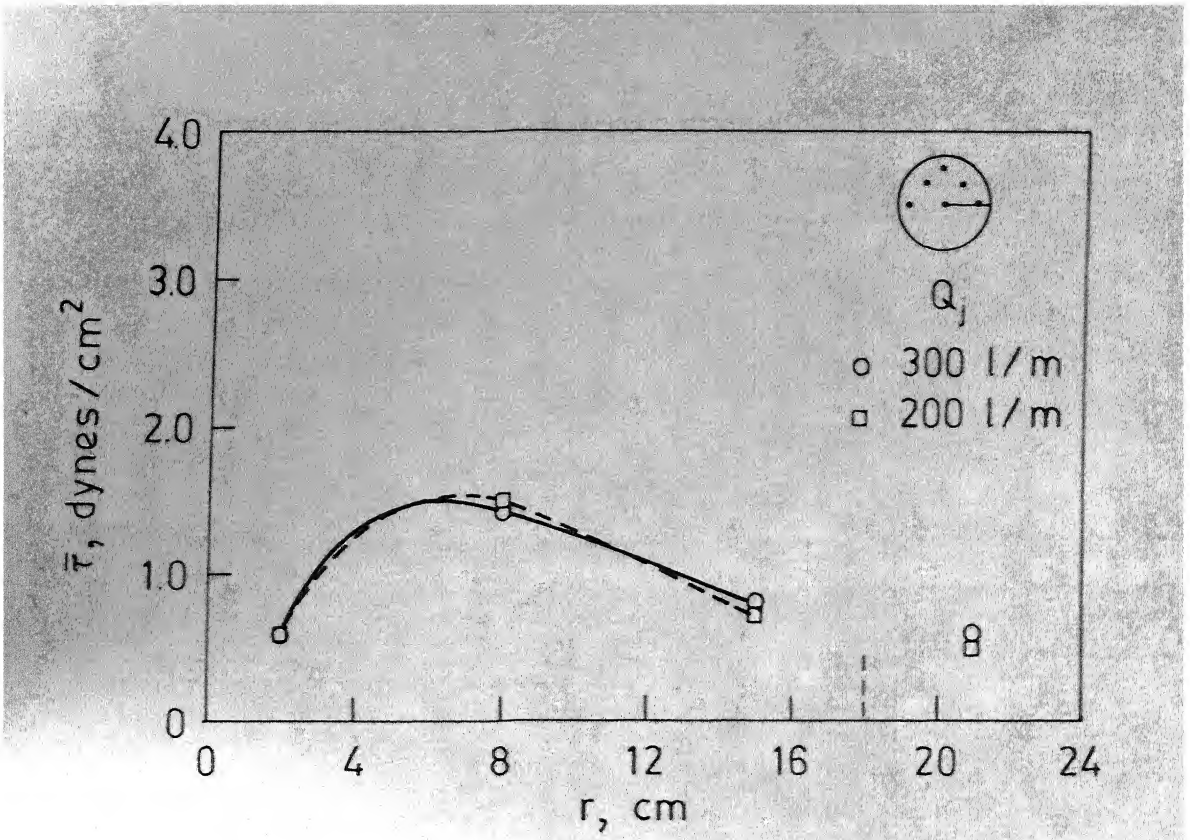

Fig. 3.31b Variation of the average shear stress $\bar{\tau}$ at the bottom with the radial distance r from the vessel axis when blowing with six asymmetrically placed tuyeres, $l/d_j = 4$. The circle at the top right corner indicates the radius along which the measurements were made.

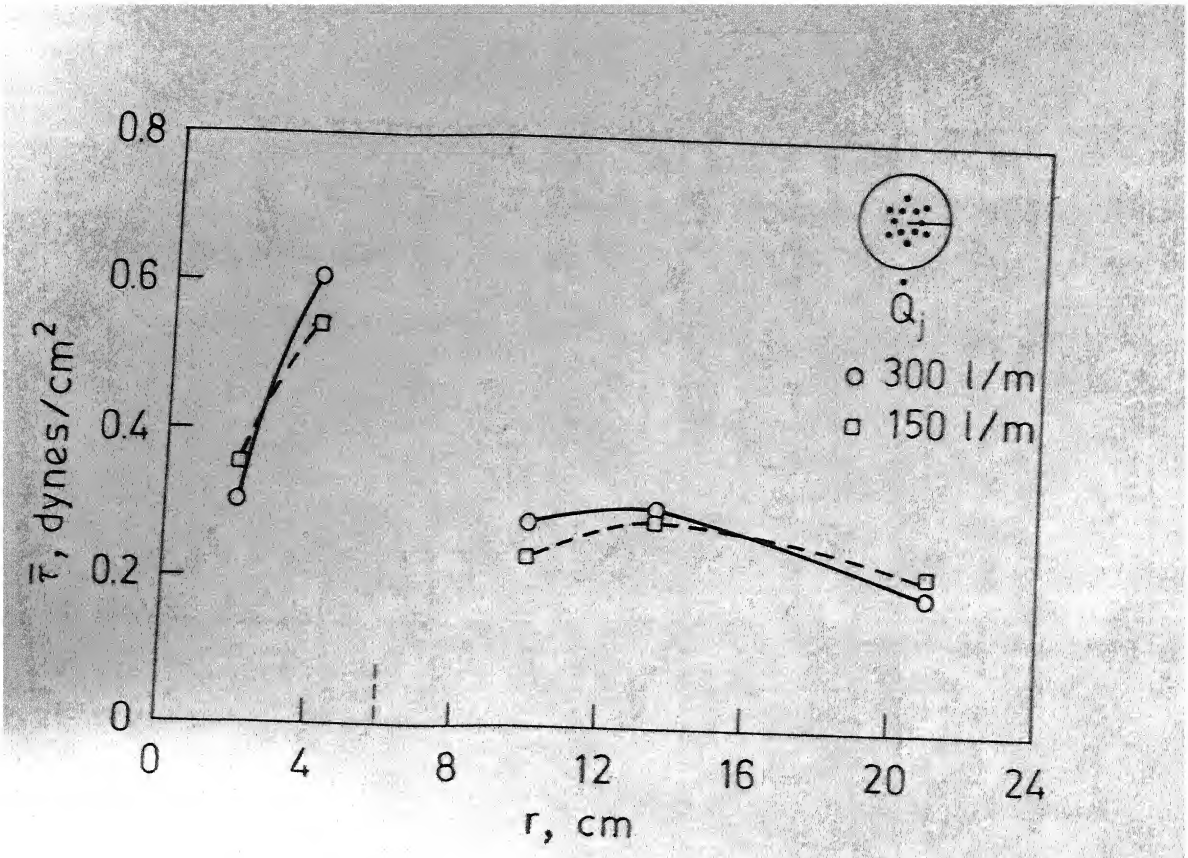

Fig. 3.32 Variation of the average shear stress $\bar{\tau}$ at the bottom with the radial distance r from the vessel axis when blowing with twelve symmetrically placed tuyeres; $l/d_j = 4$. The circle at the top right corner indicates the radius along which the measurements were made.

$$\sqrt{\overline{\tau'^2}} = c\,\bar{\tau} \qquad 3.10$$

The constant of proportionality c, however, was found to be different from that given in Eq. 3.6. The values of c for the various tuyere arrangements are listed in Table 3.7.

Table 3.7

Values of the Constant of Proportionality c in Eq. 3.10 for Various Tuyere Configurations

No. of tuyeres	Configuration	c
3	Symmetric	0.48
3	Asymmetric	0.39
6	Symmetric	0.53
6	Asymmetric	0.42
12	Symmetric	0.33

Some of the characteristics of the flow in experiments with symmetrically placed tuyeres are similar to those in single tuyere experiments. With symmetrically placed tuyeres, the shear stress was large near the axis of the vessel and tapered off towards the sides. However, it should be noted (see Figures 3.16, 3.26, 3.29 and 3.32) that the tapering off was less pronounced as the number of

tuyeres increased. Another common feature that is evident was the increase of shear stress at points far from the axis as the air flow rate was decreased. The reasons for such behaviour are probably similar to those given in connection with experiments with single tuyere based on the visualization of the flow patterns. The system with multiple tuyeres was, however, not amenable to flow visualization.

An important observation to be made with symmetrically placed tuyeres is the remarkable decrease in the level of shear stress all over the bottom as the number of tuyeres increased from one to twelve, as is evident from Figures 3.26, 3.29 and 3.32. With larger number of tuyeres, the fluid flow was, probably, restricted to the upper parts of the bath to a great extent resulting in lower shear stress at the bottom.

In asymmetric arrangements of tuyeres, the shear stress level was higher than that obtained with symmetric configurations. This is evident on comparing Figure 3.27 with Figure 3.28 and Figure 3.29 with Figure 3.31. This is to be expected because of the increased circulation with asymmetrically placed tuyeres.

Shear stress at the bottom, near the axis of the vessel comes down sharply to a low level with both three and six tuyeres, when they are distributed asymmetrically on

one half of the bottom. No explanation for this is being attempted at this time.

Influence of projecting the tuyeres into the vessel to a distance of $4d_j$ on shear stress was not uniform in experiments with symmetrically placed tuyeres. There was a general lowering of shear stress in experiments with six asymmetrically placed tuyeres.

3.6. INFERENCE ON BOTTOM REFRACTORY WEAR FROM THE PRESENT INVESTIGATION

Refractory wear, as discussed in Chapter 1, is a complex phenomenon arising from thermal, chemical and mechanical effects. The present investigation is a model study yielding results on certain mechanical aspects arising out of fluid flow. Therefore, it is not possible to infer about bottom refractory wear in a comprehensive fashion. Predictions and comments made below have to be examined in this light.

3.6.1. Mixing of Gases in Coaxial Jets

(a) According to the results of the present investigation, the shrouding gas in the OBM process is ineffective in physically shielding the liquid metal from the oxygen stream. Hence highly exothermic refining reactions should be taking place right next to the tuyere itself. The effect

of the shrouding gas is therefore mainly thermal. It cools down the tuyere zone on endothermic cracking.

(b) In terms of the dynamics of jet mixing, the ratio of $\dot{Q}_s/\dot{Q}_j$ is the important one. As long as this ratio is kept constant, the flow rate of oxygen can be increased without disturbing the jet mixing patterns, and hence, probably the effectiveness of the shrouding gas.

3.6.2. Measurements of Shear Stress

As discussed in Chapter 1, general refractory wear is a corrosion-erosion phenomenon (apart from spalling due to thermal shocks). The corrosion of the refractory should be enhanced by the increase of the mass transfer coefficient $\bar{k}$. The average shear stress $\bar{\tau}$ and the fluctuations τ' in shear stress should both determine the mechanical erosion. All these three parameters, viz. $\bar{k}$, $\bar{\tau}$ and τ', are related to each other according to Eqs. 2.10 and 3.6. That is,

$$\bar{\tau} \propto \bar{k}^3$$

and

$$\sqrt{\overline{\tau'^2}} \propto \bar{\tau}$$

Therefore, any one of these parameters can be used to characterize general refractory wear by corrosion-erosion mechanism. For example, an increase in $\bar{\tau}$ means increase of $\bar{k}$ and $\sqrt{\overline{\tau'^2}}$. Therefore, erosion as well as corosion would be

enhanced. This does not take into consideration any flow irregularities such as vortex flow or secondary recirculations which may cause localised enhancement of wear.

However, as mentioned earlier, the bottom refractory wear in the bottom-blown oxygen steelmaking processes has been found to be more or less uniform and not localized around the tuyeres as in the Bessemer converters. Therefore, discussion in terms of overall wear of the bottom are not out of place. Certain predictions based on shear stress measurements in the present investigation on multi-tuyere bottom are noted below. As the shear stress did not rise appreciably near the tuyeres, the issue of spatial distribution of shear stress over the bottom vis-a-vis locations of tuyeres is going to be ignored. Discussion would be centered around changes in general shear stress level as process parameters are altered.

(a) Shear stress at the bottom is mainly dependent on the momentum input into the system. It is, therefore, advisable to use as large a diameter of tuyeres as permissible from other considerations, so that the momentum input can be kept as low as possible. By the same argument, increasing the amount of shrouding gas like using coke oven gas in the place of propane, does not increase the shear stress level at the bottom, if the velocity of the shrouding gas at the tuyere exit is kept low.

(b) Asymmetric arrangement of tuyeres increases the shear stress as compared to those with symmetric arrangements. Hence, the refractory wear is expected to be more with an asymmetric arrangement of tuyeres.

(c) It is better to have a greater number of tuyeres for a given amount of gas blown to lower the rate of bottom wear.

(d) Projecting the tuyeres into the bath does not seem to be of significant help in symmetric arrangement of tuyeres. If, however, asymmetric arrangement of tuyeres is chosen, it may be advantageous to project the tuyeres into the bath.

CHAPTER 4

SUMMARY AND CONCLUSIONS

A room temperature model study of bottom-blown oxygen steelmaking processes was undertaken with a view to understand certain aspects of the dynamics of the process with special reference to bottom refractory wear. Water simulated the hot metal in this investigation. The investigation consisted of two parts:

a) Experiments with single tuyere

b) Experiments with multiple tuyeres.

A cylindrical perspex vessel of 48 cm i.d. and 65 cm height was used as the simulation vessel. In the experiments with single tuyeres, the tuyere consisted of two coaxial pipes; the gas blown through the inner pipe simulated oxygen of the bottom-blown processes and the gas introduced through the annular space between the two pipes simulated the shrouding gas. The inner pipe diameter (d_j) was 0.65 cm and the annulus thickness was 0.075 cm. The inner jet pipe could be positioned to any desired extent of projection into the vessel. The tuyeres used in experiments with multiple tuyeres were simple tubes fitted into the bottom.

The study with single tuyere consisted of two sub-sections:

i) Study of mixing of gases in two coaxial jets submerged in water employing air to simulate oxygen and carbon dioxide to simulate the shrouding gas.

ii) Measurement of mass transfer coefficients and shear stresses at the bottom due to the flow of liquid employing air to simulate both oxygen and the shrouding gas.

In the first sub-section profiles of concentration of carbon dioxide at heights of 1 cm, 3 cm and 5 cm from the tuyere exit were obtained by analysing the gas mixture at several points across a cross section using a gas-chromatograph. Three flow rates of air ($\dot{Q}_{air}$) were employed, viz., 50, 100 and 150 liters/min. The ratio of the flow rate of carbon dioxide ($\dot{Q}_{CO_2}$) to that of air ($\dot{Q}_{air}$) was between 0.05 and 0.15.

In the second sub-section of the study with single tuyere, the average value and the rms value of the fluctuations of the mass transfer coefficient and the wall shear stress were measured along the bottom using the electrochemical technique. Total flow rate of air in these experiments was varied between 50 and 200 liters/min. The effect of the shrouding gas was studied by passing 0, 5 and 10 pct. of the total flow through the annulus. The extent

of projection of the inner pipe was 0, d_j and $2d_j$ and the height of the water bath was 20, 30 and 40 cm.

Flow of water when blowing with a single tuyere was visualized using particles of dust and polystyrene beads as tracers. Some photographs of the streak-lines were also taken to obtain the general flow pattern. Time exposure photographs and movie were taken of the jet to understand the jet behaviour.

In the second part of the work, experiments were conducted with 3, 6 and 12 tuyeres of 0.32 cm i.d. with the flow rates of air varying between 150 and 340 liters/minute. Tuyeres were placed in symmetric and asymmetric configurations.

From these measurements, the following conclusions were drawn:

(1) The stream surfaces were torus-shaped with the liquid coming down along the outer region and going up in the axial region in single tuyere experiments. There was some secondary recirculation near the bottom of the sidewalls.

(2) The jet oscillated vigorously as it emerged out of the tuyere. The jet cone angle was found to be $20 \pm 2^\circ$ and compared well with the values reported in literature for the air-water system.

(3) The shrouding gas was ineffective in physically shielding the liquid from the inner jet stream.

(4) The maxima in the profile of the normalized concentration of carbon dioxide at z = 1 cm occurred just above the annulus, indicating that the annular jet is not significantly deflected by the presence of the inner jet. The profile was independent of $\dot{Q}_{air}$ at any fixed $\dot{Q}_{CO_2}/\dot{Q}_{air}$ and varied linearly with $\dot{Q}_{CO_2}/\dot{Q}_{air}$.

(5) The two jets were completely mixed before they reached a distance of 7 to 10 d_j from the tuyere exit. The distance at which complete mixing took place was greater for larger $\dot{Q}_{CO_2}$.

(6) The wall shear stress decreased sharply as the radial distance from the tuyere axis increased in experiments with single tuyere. As the flow rate of air was decreased, the value of the shear stress decreased at points near the tuyere; at larger distances from the tuyere, however, the opposite behaviour was observed.

(7) The rms value of fluctuations in shear stress was found to be proportional to the average shear stress in both single and multiple tuyere experiments. The proportionality constant, however, was different for different numbers of tuyeres and their configurations.

(8) At points along the sidewall and at points far from the tuyere axis in experiments with a single tuyere, the effect of l/d_j and $\dot{Q}_s/(\dot{Q}_s + \dot{Q}_j)$ were not perceptible. At the electrode nearest to the tuyere axis,

the shear stress decreased as $1/d_j$ or $\dot{Q}_s/(\dot{Q}_s + \dot{Q}_j)$ increased at constant $(\dot{Q}_s + \dot{Q}_j)$. As the height of the water bath decreased, the level of shear stress also decreased all along the bottom.

(9) At the point nearest to the tuyere, the following relation was observed between the Euler number, N_{Eu}, and the modified Froude number, N_{Fr},

$$N_{Eu} = a\, N_{Fr}^{b},$$

where 'a' and 'b' were functions of the process parameters. It was observed that the momentum of thejet is of great importance as compared to the total volume of the gas introduced in determining the flow of the liquid in the vessel.

(10) As the number of symmetrically placed tuyeres increased, the level of shear stress along the bottom decreased significantly at any given flow rate of air. Asymmetric arrangement of tuyeres generally resulted in higher shear stress levels as compared to the symmetric arrangements.

(11) Projection of the tuyeres into the bath perceptibly lowered the shear stress along the bottom only when blowing with asymmetrically placed tuyeres. Projections of symmetrically placed tuyeres did not yield any regular trend.

The problem of bottom refractory wear has been discussed in the light of the findings in the present investigation.

CHAPTER 5

SUGGESTIONS FOR FUTURE WORK

The model set-up fabricated in connection with this work may be utilised for further studies as follows:

1. Shear stress measurements may be undertaken with gas lancing from the top as in LD process of steel-making.

2. Mixing in the liquid bath as a function of process parameters may be investigated. However, this may require development of a technique to monitor mixing.

3. The break up of the jet may be studied by movie photography.

4. Slag-metal type reactions may be investigated with water to simulate the metal and, may be, paraffin to simulate the slag.

5. Mass transfer from the jet to the liquid may be investigated.

6. Solid powders may be injected into the jet and their motion studied.

7. Actual rate of corrosion-erosion may be measured by developing a corroding-eroding plate and putting it at the bottom of the model.

LIST OF REFERENCES

1. Shenouda, F., Förster, E. and Richter, H.; Iron and Steel International, 44 (1971) p. 167

2. Hubbard, H.N. and Lankford, W.T.; Iron and Steel Engr., 50 (1973) p. 37

3. Nilles, P.E.; Paper presented at the AISE Annual Convention, (1972)

4 Pearce, J.; Paper presented at the AISE Annual Convention, Philadelphia (1974)

5. Leroy, P.J.; Iron and Steel Engr., 49 (1972) p. 51.

6. Anon.; 33 Magazine, May (1975) p. 36

7. Nilles, P. and Boudin, M.; Ironmaking and Steelmaking, 1 (1974) p. 22

8. Rowe, A.D. and Desai, S.C.; Metals and Materials, May (1975) p. 19

9. Aeron, S.M. and Ramachandran, S.; Paper presented at the seminar on "Iron and Steel Industry – Planning and Commissioning", MECON, Ranchi, India (1974)

10. Brotzman, K.; Paper presented at the Third UNIDO International Symposium on the Iron and Steel Industry, Brazilia, Brazil (1973)

11. Turkdogan, E.T.; Trans. IMM. Section C, 83 (1974) p. C67

12. Brotzman, K., Lankford, W.T. (Jr.) and Brisse, A.H.; Ironmaking and Steelmaking, 3 (1976) p. 259

13. Turkdogan, E.T.; AIME OH Proc., 58 (1975) p. 405

14. Fruehan, R.J. and Martonik, L.J.; Met. Trans., 5 (1974) p. 1027

15. Fruehan, R.J.; Ironmaking and Steelmaking, 3 (1976) p. 33

16. Goto, K.S. and Eketrop. S.; Scand. J. Metallurgy, 3 (1974) p. 1

17. Kor, G.J.W. and Turkdogan, E.T.; Met. Trans., 6B (1975) p. 411

18. Silberman, E.; in 'Proc. 5th Midwestern Conference on Fluid Mechanics', Univ. of Michigan, Ann Abor (1957) p. 263

19. Themelis, N.J., Tarassoff, P. and Szekely, J.; Trans. AIME, 245 (1969) p. 2425

20. Oryall, G.N. and Brimacombe, J.K.; Met. Trans., 7B (1976) p. 391

21. Igwe, B.U.N., Ramachandran, S. and Fulton, J.C.; ibid., 4 (1973) p. 1887

22. Etienne, A.; CRM Rep. No. 43 (1975) p. 15

23. Szekely, J., Wang, H.J. and Kiser, K.M.; Met. Trans., 7B (1976) p. 287

24. Szekely, J. and Asai, S.; Trans. ISIJ., 15 (1975) p. 270

25. Szekely, J. and Asai, S.; ibid., 15 (1975) p. 276

26. Szekely, J., Asai, S. and Chang, C.W.; in 'Mathematical Process Models in Iron- and Steelmaking', The Metals Society, London (1975)

27. Iyengar, R.K., Mazumdar, S., Aeron, S.M. and Iyer, R.S.N.; Paper presented at the National Seminar on Modernization of Existing Steel Plants, Bokaro, India (1978)

28. Chesters, J.H.; "Refractories for Iron and Steelmaking", Metals Society, London (1974)

29. Kappmeyer, K.K. and Hubble, D.H.; in "High Temperature Oxides, Part I", Alper, A.M., Ed., Academic Press (1970)

30. Norton, F.H.; "Refractories", McGraw Hill Book Co., New York (1949)

31. Szekely, J. and Themelis, N.J.; "Rate Phenomena in Process Metallurgy", Wiley-Interscience, New York (1971)

32. Theofanus, T.G., Houze, R.N. and Brumfield, L.K.; Paper presented in "AIAA/ASME Thermodynamics and Heat Transfer Conference", Boston (1974)

33. Anon.; 33 Magazine, Sept. (1972) p. 34

34. Trentini, B. and Allard, M.; Rev. Met., 55 (1958) p. 1195

35. Stearns, R.F.; "Flow Measurement with Orifice Meters", D. Van Nostrand Co. Inc., New Jersey (1951)

36. Anon., "Fluid Meters: Their Theory and Applications", ASME (1959)

37. Davenport, W.G., Wakelin, D.H. and Bradshaw, A.V.; in "Heat and Mass Transfer in Process Metallurgy", Hills, A.W.D., Ed., IMM, London (1967)

38. Schraub, F.A., Kline, S.J., Henry, V., Runstadler, P.W. and Little, A.; J. Basic Engg. (Trans. ASME Ser. D) 87 (1965) p. 429

39. Wolfang, M., "Flow Visualization", Academic Press, New York (1974)

40. Mizushina, T.; Advances in Heat Transfer, 7 (1971) p. 87

41. Reiss, L.P. and Hanratty, T.J.; AIChE J., 9 (1963) p. 154

42. Shaw, P.V. and Hanratty, T.J.; ibid., 10 (1964) p. 475

43. Son, J.S. and Hanratty, T.J.; ibid., 13 (1967) p. 689

44. Shaw, P.V., Reiss, L.P. and Hanratty, T.J.; ibid., 9 (1963) p. 362

45. Ito, S. and Ogawa, K.; J. Chem. Engg. Japan, 6 (1973) p. 507

46. Runchal, A.K.; Int. J. Heat Mass Transfer, 14 (1971) p. 781

47. Berger, F.P. and Hau, K.-F.F.-L.; ibid., 20 (1977) p. 1185

48. Maruyama, T., Fujii, K. and Mizushina, T.; J. Chem. Engg. Japan, 10 (1977) p. 421

49. Son, J.S.; Ph.D. Thesis, Univ. Illinois, Urbana, U.S.A. (1968)

50. Dimopoulos, H.G. and Hanratty, T.J.; J. Fluid Mech., 33 (1968) p. 303

51. Dworak, R. and Wendt, H.; Ber. Bunsen-Gelles. physik. Chemie, 81 (1977) p. 729

52. Dworak, R. and Wendt, H.; ibid., 81 (1977) p. 865

53. Mitchell, J.E. and Hanratty, T.J.; J. Fluid Mech.; 26 (1966) p. 199

54. Sircar, K.K. and Hanratty, T.J.; ibid., 44 (1970) p. 605

55. Fench, E.J. and Tobias, C.W.; Electrochim. Acta, 2 (1960) p. 311

56. Schutz, G.; Int. J. Heat Mass Transfer, 6 (1963) p. 873

57. Postlethwaite, J. and Holdner, D.N.; Can. J. Chem. Engg., 53 (1975) p. 31

58. Postlethwaite, J. and Holdner, D.N.; ibid., 54 (1976) p. 255

59. Lin, C.S., Denton, E.B., Gaskill, H.S. and Putnam, G.L.; Ind. Engg. Chem., 43 (1951) p. 2136

60. Schlichting, H.; "Boundary Layer Theory", McGraw-Hill Book Co., New York (1968) p. 596

APPENDIX I

CALCULATION PROCEDURES

A1.1. CALCULATION OF FLOW RATE OF AIR

The flow rate of air was measured using an orifice meter. Equation 2.3 was used for the calculation of the flow rate and is reproduced below:

$$W = 34.77\, D_2^2\, KY_1 \sqrt{\rho_1 h_w} \qquad \text{A1.1}$$

where W = mass flow rate of air, gm/sec,

D_2 = diameter of the orifice, cm,

K = flow coefficient, dimensionless,

Y_1 = expansion factor, dimensionless,

ρ_1 = density of air at upstream pressure tap conditions, gm/cc

and h_w = differential pressure across the orifice, cm of water.

Following are the steps involved in the calculation[1].

Given: h_w, pressure P_1 in cm of mercury at upstream pressure tap, temperature T, D_2, and height of the water bath h.

1. Calculate.

$$\beta = D_2/D_1 \qquad \text{A1.2}$$

where D_1 = diameter of the pipe of the orifice meter.

2. Calculate the expansion factor Y_1 using the following empirical expression:

$$Y_1 = 1 - (0.41 + 0.35\ \beta^4)\ \frac{\Delta P}{kP_1} \qquad \text{A1.3}$$

where k = ratio of specific heat of air at constant pressure to its specific heat at constant volume = 1.4,

and ΔP = differential pressure across the orifice = $h_w/13.6$, cm of mercury.

3. Calculate ρ_1 at temperature T and pressure P_1. Density of air at STP is to be taken from published data.

4. Calculate W using Eq. A1.1 in terms of K.

5. Calculate the Reynolds number N^o_{Re} (referred to the diameter of the orifice) in terms of K using the following expression

$$N^o_{Re} = \frac{1.273\ W}{D_2\ \mu_{air}} \qquad \text{A1.4}$$

where μ_{air} = viscosity of air at room temperature, poise.

Determine the approximate value N^{o}_{Re}, by substituting K_{∞} for K. The value of K_{∞} as a function D_1 and β is available in the literature[1].

6. Determine the value of K using the following empirical equation

$$K = K_{\infty}\left(1 + \frac{A}{N^{o}_{Re}}\right) \qquad \text{A1.5}$$

The value of A as a function of D_1 and β is available in the literature.[1]

7. Determine W by substituting K in the results of Step 4.

8. Calculate the pressure P_2 at the tuyere exit in cm of mercury from the following expression

$$P_2 = 76 + \frac{h}{13.6} \qquad \text{A1.6}$$

Calculate the density ρ_2 of air at the tuyere exit conditions.

9. Calculate the volumetric flow rate of air from W and ρ_2.

Example:

Given: $h_w = 29.8$ cm

$P_1 = 103.9$ cm of mercury

$T = 20°C$

$D_2 = 0.953$ cm

$h = 40$ cm.

1. $\beta = 0.953/3.81 = 0.25$

2. $\Delta P = \frac{29.8}{13.6} = 2.19$ cm of mercury

Therefore, $Y_1 = 1 - (0.41 + 0.35 \times 0.25^4) \frac{2.19}{1.4 \times 103.9}$

$= 0.9938$

3. Density of air at STP $= 1.293 \times 10^{-3}$ gm/cc.[2]

Therefore, $\rho_1 = 1.293 \times 10^{-3} \times \frac{103.9}{76} \times \frac{273}{293}$

$= 1.647 \times 10^{-3}$ gm/cc

4. $W = 34.77 \times 0.953^2 \times 0.9938 \times \sqrt{1.647 \times 10^{-3}} \times \sqrt{29.8}\ K$

$= 6.952\ K$

5. At room temperatures, viscosity of air is about 1.85×10^{-4} poise.[2] Therefore

$$N_{Re}^{o} = \frac{1.273 \times 6.952\ K}{0.953 \times 1.85 \times 10^{-4}}$$

$$= 5.020 \times 10^4\ K$$

For $\beta = 0.25$ and $D_1 = 3.81$ cm, $K = 0.5978$

Therefore $N^{o}_{Re'} = 5.020 \times 10^4 \times 0.5978$

$= 3.001 \times 10^4$

6. For $\beta = 0.25$ and $D_1 = 3.81$ cm, $A = 200$. Therefore

$$K = 0.5978 \left(1 + \frac{200}{3.001 \times 10^4}\right)$$

$$= 0.5978 \times 1.007 = 0.6020$$

7. $W = 6.952 \times 0.6020 = 4.185$ gm/sec.

8. $P_2 = 76 + \frac{40}{13.6} = 78.94$

Therefore

$$\rho_2 = 1.293 \times 10^{-3} \times \frac{78.94}{76} \times \frac{273}{293}$$

$= 1.251 \times 10^{-3}$ gm/cc

9. Volumetric flow rate of air $= \frac{4.185}{1.251 \times 10^{-3}}$

$= 3.345 \times 10^3$ cc/sec

i.e., $\dot{Q}_{air} = 200.7$ liters/min.

A1.2. CALCULATION OF $\bar{k}$, $\sqrt{\overline{k'^2}}$, $\bar{\tau}$ AND $\sqrt{\overline{\tau'^2}}$

Equations 2.7 and 2.8 have been used to calculate $\bar{k}$ and $\sqrt{\overline{k'^2}}$ and are reproduced below after simplification:

$$\bar{k} = \frac{\bar{i}_d}{96500\ \pi d_e^2\ C_b} \qquad A1.7$$

and $$\sqrt{\overline{k'^2}} = \frac{\sqrt{\overline{i_d'^2}}}{\bar{i}_d} \times \bar{k} \qquad A1.8$$

where

$\bar{i}_d$ = average current, amperes,

d_e = electrode diameter, cm,

C_b = bulk concentration of oxygen, mole/cc,

and i_d' = fluctuating component of current, amperes.

Equations 2.10, 2.13-2.15 have been used to calculate $\bar{\tau}$ and $\sqrt{\overline{\tau'^2}}$ and are simplified as follows:

$$\bar{s} = 1.546\ \bar{k}^3\ d_e/D \qquad A1.9$$

$$\sqrt{\overline{s'^2}} = \frac{3\sqrt{\overline{k'^2}}}{\bar{k}}\ \bar{s} \qquad A1.10$$

$$\bar{\tau} = -\mu_1\ \bar{s} \qquad A1.11$$

$$\sqrt{\overline{\tau'^2}} = -\mu_1 \sqrt{\overline{s'^2}} \qquad A1.12$$

where

D = diffusion coefficient of oxygen in the electrolyte, cm^2/sec

$\bar{s}$ = average velocity gradient at the wall, sec^{-1}

s' = fluctuations in velocity gradient at the wall, sec^{-1}

μ_1 = viscosity of the electrolyte, poise.

The steps involved in the calculation are given below:

Given: the indifferent electrolyte used, d_c, temperature T, $\bar{i}_d$ and $\sqrt{\overline{i_d'^2}}$.

1. Calculate C_b at temperature T using Eq. A2.6, Appendix II.
2. Calculate $\bar{k}$ and $\sqrt{\overline{k'^2}}$ using Eqs. A1.7 and A1.8.
3. Calculate D at temperature T using Eq. A2.2, Appendix II.
4. Calculate $\bar{s}$ and $\sqrt{\overline{s'^2}}$ using Eqs. A1.9 and A1.10.
5. Calculate μ_1 at temperature T using Eq. A2.7, Appendix II.
6. Calculate $\bar{\tau}$ and $\sqrt{\overline{\tau'^2}}$ using Eqs. A1.11 and A1.12.

Example:

Given:

Electrolyte: 0.1 mole/liter KOH,

T = 293°K,

d_c = 0.0213 cm,

$\bar{i}_d$ = 0.626 μA,

and $\sqrt{\overline{i'^2}}$ = 0.091 μA.

1. $\log C_b = -6.5885 - 738.25 \left(\frac{1}{298} - \frac{1}{293}\right) - 0.1 \times 10^{-3} \times 174.6$

$= -6.5638$

$C_b = 2.730 \times 10^{-7}$ mole/cc

2. $\bar{k} = \frac{0.626 \times 10^{-6}}{96500\ \pi \times 0.0213^2 \times 2.730}$

$= 1.67 \times 10^{-2}$ cm/sec

$\sqrt{\overline{k'^2}} = \frac{0.091}{0.626} \times 1.67 \times 10^{-2}$

$= 2.43 \times 10^{-3}$ cm/sec.

3. $\log D = -4.710 + 3.446 \left(\frac{293 - 298}{293}\right)$

$= -4.769$

$D = 1.70 \times 10^{-5}$ cm^2/sec.

4. $\bar{s} = \frac{1.546 \times 1.67^3 \times 10^{-6} \times 0.0213}{1.70^2 \times 10^{-10}}$

$= 529.7$

$\sqrt{\overline{s'^2}} = \frac{3 \times 2.43 \times 10^{-3} \times 527.9}{1.67 \times 10^{-2}}$

$= 230.4$

5. $\log \mu_1 = \log 0.0091 - 2.884 \left(\frac{293 - 298}{293}\right)$

$= 0.0102$ poise.

6. $\bar{\tau} = 529.7 \times 0.0102$

$= 5.38 \text{ dynes/cm}^2$

$\sqrt{\overline{\tau'^2}} = 230.4 \times 0.0102$

$= 2.34 \text{ dynes/cm}^2$

References:

1. Stearns, R.F., Johnson, R.R., Jackson, R.M. and Larson, C.A.; 'Flow Measurement with Orifice Meters', D. Van Nostrand Co. Inc., New York (1951).

2. 'Handbook of Chemistry and Physics', Edited by Hodgman, C.D. et al., Chemical Rubber Pub. Co., Cleveland (1961).

APPENDIX II

PROPERTIES OF THE ELECTROLYTE

The electrolyte employed for the measurement of the mass transfer coefficient and the wall shear stress by the electrochemical technique was a solution of sodium hydroxide or potassium hydroxide in distilled water. The concentration of NaOH or KOH was 0.1 mole/liter. Analytical grade chemicals were always employed in the preparation of the electrolyte. Oxygen dissolved in this solution acted as the electroactive species and was in equilibrium with air at the room temperature. The method of calculation of the diffusion coefficient (D) and the concentration (C_b) of oxygen in the electrolyte and the viscosity of the electrolyte at the temperature of the experiments are described in the following sections.

A2.1. DIFFUSION COEFFICIENT OF OXYGEN

The effect of small concentrations of NaOH or KOH on the diffusion coefficient of oxygen in water has been reported to be quite small.[1-3] Therefore, the values of the diffusion coefficient of oxygen in water as such have been used in the present investigation.

The values of the diffusion coefficient of oxygen in water at 298°K, as reported in the literature, are between 1.90×10^{-5} and 2.00×10^{-5} cm^2/sec.[1-4] Tham et al[3] gave the following formula for the temperature dependdnce of the diffusion coefficient:

$$\ln D = \ln D_{298} + \frac{4700}{R} \left(\frac{1}{298} - \frac{1}{T}\right) \qquad \text{A2.1}$$

where D = diffusion coefficient at T°K,

D_{298} = diffusion coefficient at 298°K,

and R = universal gas constant.

Taking 1.95×10^{-5} cm^2/sec as the average value of D_{298}, the following expression was obtained which was utilised to calculate the diffusion coefficient at the temperature at which the experiments were conducted:

$$\log D = -4.710 + 3.446 \left(\frac{T - 298}{T}\right) \qquad \text{A2.2}$$

The uncertainty in the value of D so calculated is estimated to be about 5 pct.

A2.2. CONCENTRATION OF OXYGEN

The data on the concentration of oxygen in water in equilibrium with air at various temperatures were taken from published literature[5] and the following equation was fitted into them:

$$\log C_b^o = -6.5885 - 738.25 \left(\frac{1}{298} - \frac{1}{T}\right) \qquad \text{A2.3}$$

where C_b^o is the concentration of oxygen in water in moles/cc at T°K.

Davis et al[2] gave an empirical expression for calculating the solubility of oxygen in aqueous solutions of potassium hydroxide which is as follows:

$$\log S = \log S_o - 174.6\, C_{KOH} \qquad \text{A2.4}$$

where S = solubility of oxygen in the electrolyte, moles/cc,

S_o = solubility of oxygen in water, moles/cc,

and C_{KOH} = concentration of potassium hydroxide, moles/cc.

Similarly, for aqueous sodium hydroxide one can obtain[6]:

$$\log S = \log S_o - 182.0\, C_{NaOH} \qquad \text{A2.5}$$

where C_{NaOH} = concentration of sodium hydroxide, moles/cc.

Using Equations A2.3-A2.5, the following expression was obtained for the concentration of oxygen in the electrolyte in equilibrium with air at T°K.

$$\log C_b = -6.5885 - 738.25 \left(\frac{1}{298} - \frac{1}{T}\right) - 0.1\, K' \qquad \text{A2.6}$$

where K' is equal to 174.6 for KOH and 182.0 for NaOH.

The error in the value of C_b so calculated is expected to be within 1 pct.

A2.3. VISCOSITY OF THE ELECTROLYTE

Using the values reported in the literature[6,7] following expressions were obtained for the viscosity μ_l of the electrolyte at temperature T°K:

$$\log \mu_l = \log \mu_l^{298} - 2.884 \left(\frac{T - 298}{T}\right) \qquad \text{A2.7}$$

where μ_l^{298} = viscosity at 298°K, poise.

The reported value of μ_l^{298} is 0.0092 poise for 0.1 mole/liter NaOH solution and 0.0091 poise for 0.1 mole/liter KOH solution.[6] Equation A2.7 is expected to give values of μ_l within 1 pct.

References:

1. Gubbins, E.E. and Walker, R.D. (Jr.); J. Electrochem. Soc., 112 (1965) 469.

2. Davis, R.E., Horwath, G.L. and Tobias, C.W.; Electrochim. Acta, 12 (1967) 287.

3. Tham, M.J., Walker, R.D. (Jr.) and Gubbins, E.E.; J. Phys. Chem., 74 (1970) 1747.

4. Himmelblau, D.M.; in "Diffusion of Gases in Aqueous Solutions", University of Texas, Austin (1963).

5. 'Handbook of Chemistry and Physics', Edited by Hodgman, C.D. et al., Chemical Rubber Pub. Co., Cleveland (1961).

6. 'International Critical Tables', Vol. III, Edited by Washburn, E.W., McGraw Hill Book Co., New York (1928).

7. 'Landolt-Börnstein Zahlenwerte und Functionen Aus Physik, Chemie, Astronomie, Geophysik und Technik', II. Band, 5 Teil, Edited by Eucken, A., Springer Verlag, Berlin (1960).

APPENDIX III

RESULTS OF EXPERIMENTS

Results of the study of gas mixing in coaxial jets are presented in Tables A3.1a-A3.1c. Tables A3.2a to A3.2m present the results of measurement of mass transfer coefficient and wall shear stress in experiments with single tuyere. Table A3.2n presents the values of N_{Eu} and $N_{Fr'}$ calculated from these data. Results of experiments with multiple tuyeres are presented in Tables A3.3a to A3.3g. Diameter of the electrodes for experiments with single tuyere are given in Table A3.2o. For the electrodes used in experiments with multiple tuyeres, the diameters are given in Table A3.3h.

Table A3.1a. Results of Gas Mixing Studies

h = 40 cm. $\dot{Q}_{air}$ = 50 liters/min.

r, mm	pct. CO_2								
	$\dot{Q}_{CO_2}$ = 5 liters/min.			$\dot{Q}_{CO_2}$ = 7.5 liters/min.			$\dot{Q}_{CO_2}$ = 10 liters/min.		
	z=1 cm	z=3 cm	z=5 cm	z=1 cm	z=3 cm	z=5 cm	z=1 cm	z=3 cm	z=5 cm
0	1.9	9.1	9.8	2.7	13.1	15.1	6.2	17.5	17.9
2	-	-	-	-	-	-	12.2	-	-
3	16.3	11.0	10.0	17.0	15.4	15.1	-	21.1	20.0
4	-	-	-	-	-	-	23.8	-	-
6	12.7	11.9	10.5	21.0	16.1	14.8	26.1	22.1	19.7
8	-	-	-	-	-	-	20.3	-	-
9	10.0	11.4	9.3	15.0	15.2	14.9	-	22.1	20.0
10	-	-	-	-	-	-	18.0	-	-
12	8.7	11.6	10.9	14.4	15.0	15.2	-	20.8	20.2

Table A3.1b. Results of Gas Mixing Studies

h = 40 cm. $\dot{Q}_{air}$ = 100 liters/min.

r, mm	pct. CO_2								
	$\dot{Q}_{CO_2}$ = 5 liters/min.			$\dot{Q}_{CO_2}$ = 10 liters/min			$\dot{Q}_{CO_2}$ = 15 liters/min.		
	z=1 cm	z=3 cm	z=5 cm	z=1 cm	z=3 cm	z=5 cm	z=1 cm	z=3 cm	z=5 cm
0	0.58	2.3	4.8	1.2	5.6	8.5	2.6	7.2	14.8
1	1.3	3.2	-	1.3	-	-	2.9	-	-
2	2.3	4.1	-	5.5	-	-	7.9	8.4	-
3	6.4	4.9	4.9	15.5	9.5	9.6	20.1	12.4	15.0
4	7.2	5.7	-	16.9	-	-	29.7	18.4	-
5	6.9	5.1	-	16.9	-	-	28.4	19.3	-
6	5.2	5.1	5.4	12.4	10.6	9.8	22.3	18.6	15.4
9	3.4	5.1	5.0	9.9	9.8	9.6	15.1	16.4	15.3
12	3.3	5.1	5.4	9.1	10.4	9.4	14.4	14.5	14.9

Table A3.1c. Results of Gas Mixing Studies

h = 40 cm. $\dot{Q}_{air}$ = 150 liters/min.

r, mm	pct. CO_2								
	$\dot{Q}_{CO_2}$ = 7.5 liters/min.			$\dot{Q}_{CO_2}$ = 15 liters/min.			$\dot{Q}_{CO_2}$ = 22.5 liters/min.		
	z=1 cm	z=3 cm	z=5 cm	z=1 cm	z=3 cm	z=5 cm	z=1 cm	z=3 cm	z=5 cm
0	0.61	2.0	4.2	1.15	4.7	7.8	2.2	6.8	14.0
1	1.20	-	-	1.30	-	-	2.8	-	-
2	2.20	3.7	-	5.2	-	-	7.6	-	-
3	6.4	-	4.7	15.2	9.5	9.3	22.2	11.8	14.9
4	7.4	5.8	-	16.8	-	-	29.0	18.2	-
5	7.0	-	-	17.0	-	-	28.6	19.6	-
6	5.1	5.2	4.9	12.2	10.3	9.8	22.8	18.7	15.5
9	3.3	5.0	5.1	9.8	9.9	9.7	15.2	16.6	15.3
12	3.3	5.0	5.1	8.9	10.6	9.6	14.5	14.7	15.0

Table A3.2a. Results of Measurement of Mass Transfer Coefficient and Wall Shear Stress in Experiments with Single Tuyere; Indifferent Electrolyte - KOH

h = 40 cm. l = 0 $\dot{Q}_s/(\dot{Q}_s + \dot{Q}_j) = 0$

Electrode No.	Temp., °C	$\dot{Q}_s + \dot{Q}_j$, liters/min.	k, cm/sec		τ, dynes/cm^2	
			Average x 10^3	r.m.s. value x 10^3	Average	r.m.s. value
B_1	20	201	16.7	2.41	5.33	2.31
	20	141	14.8	1.85	3.72	1.40
	21	100	13.3	1.54	2.67	0.95
	21	53	11.5	1.24	1.70	0.60
B_2	18	200	9.61	0.31	1.19	0.117
	18	141	9.74	0.43	1.24	0.165
	18	100	9.22	0.56	1.05	0.190
	18	52	9.98	0.95	1.34	0.38
B_3	18	200	6.91	0.54	0.45	0.105
	18	141	6.76	0.69	0.42	0.126
	18	100	7.68	1.10	0.61	0.262
	18	52	9.47	1.17	1.14	0.43
B_4	18	200	5.38	0.54	0.209	0.063
	18	141	5.71	0.72	0.250	0.095
	18	100	6.22	1.00	0.32	0.156
	18	52	7.53	1.25	0.57	0.286
B_5	16	199	4.72	0.64	0.155	0.063
	16	140	5.27	0.73	0.210	0.088
	16	98	5.59	0.86	0.258	0.118
	16	52	6.71	1.08	0.45	0.213
S_1	17	199	4.31	0.142	0.112	0.011
	17	140	4.35	0.177	0.117	0.014
	17	98	4.35	0.146	0.117	0.011
	17	52	4.54	0.155	0.133	0.014
S_2	17	199	7.19	0.241	0.53	0.053
	17	140	7.38	0.279	0.57	0.064
	17	98	7.66	0.293	0.63	0.072
	17	52	8.23	0.328	0.79	0.094

Continued...

Table A3.2a (Continued)

Electrode No.	Temp., °C	$\dot{Q}_s + \dot{Q}_j$, liters/min.	k, cm/sec		τ, dynes/cm^2	
			Average x 10^3	r.m.s. value x 10^3	Average	r.m.s. value
S_3	17	199	21.19	0.378	13.5	0.72
	17	140	22.14	0.347	15.4	0.72
	17	98	22.52	0.316	16.2	0.68
	17	52	23.65	0.177	18.7	0.42
S_4	17	199	7.14	-	0.52	-
	17	140	7.10	0.227	0.51	0.049
	17	98	6.91	0.184	0.47	0.038
	17	52	6.67	0.259	0.42	0.049

Table A3.2b. Results of Measurement of Wall Shear Stress in Experiments with Single Tuyere; Indifferent Electrolyte - KOH

h = 40 cm. l = 0 $\dot{Q}_s/(\dot{Q}_s + \dot{Q}_j) = 0.05$

Electrode No.	Temp., °C	$(\dot{Q}_s + \dot{Q}_j)$ liters/min.	τ, dynes/cm^2	
			Average	r.m.s. value
B_1	18	201	5.30	2.31
	18	141	3.65	1.39
	18	100	2.73	0.91
	18	53	1.76	0.59
B_2	18	201	1.19	0.117
	18	141	1.24	0.165
	18	100	1.05	0.190
	18	53	1.34	0.38
B_3	18.5	201	0.43	0.102
	18.5	141	0.41	0.125
	18.5	100	0.58	0.252
	18.5	53	1.07	0.40
B_4	Same as in Table A3.2a.			
B_5				

Table A3.2c. Results of Measurement of Wall Shear Stress in Experiments with Single Tuyere; Indifferent Electrolyte - KOH

h = 40 cm l = 0 $\dot{Q}_s/(\dot{Q}_s + \dot{Q}_j) = 0.10$

Electrode No.	Temp., °C	$(\dot{Q}_s + \dot{Q}_j)$, liters/min.	τ, dynes/cm^2	
			Average	r.m.s. value
B_1	20	201	4.84	2.09
	18	141	3.20	1.18
	18	100	2.32	0.72
	18	52	1.51	0.46
B_2	18	201	1.14	0.113
	18	141	1.14	0.149
	18	100	1.05	0.190
	18	52	1.29	0.37
B_3				
B_4				
B_5	Same as in Table A3.2a.			
S_1				
S_3				

Table A3.2d. Results of Measurement of Wall Shear Stress in Experiments with Single Tuyere; Indifferent Electrolyte - KOH

h = 40 cm. l = 0.65 cm. $\dot{Q}_s/(\dot{Q}_s + \dot{Q}_j) = 0$

Electrode No.	Temp., °C	$(\dot{Q}_s + \dot{Q}_j)$, liters/min.	τ, dynes/cm^2	
			Average	r.m.s. value
B_1	19.5	201	4.29	1.96
	19.5	141	3.01	1.19
	19.5	100	2.59	0.90
	19.5	53	1.63	0.57
B_2	18	200	1.10	0.111
	18	141	1.10	0.136
	18	100	1.05	0.190
	18	52	1.29	0.35
B_3				
B_4				
B_5	Same as in Table A3.2a.			
S_1				
S_3				

Table A3.2e. Results of Measurement of Wall Shear Stress in Experiments with Single Tuyere; Indifferent Electrolyte - KOH

h = 40 cm. l = 0.65 cm. $\dot{Q}_s/(\dot{Q}_s + \dot{Q}_j) = 0.05$

Electrode No.	Temp., °C	$(\dot{Q}_s + \dot{Q}_j)$, liters/min.	τ, dynes/cm^2	
			Average	r.m.s. value
B_1	20	201	4.03	1.81
	20	141	2.88	1.15
	20	100	2.48	0.83
	20	52	1.50	0.48
B_2	18	200	1.10	0.111
	18	141	1.10	0.136
	18	100	1.05	0.190
	18	52	1.29	0.35
B_3				
B_4				
B_5	Same as in Table A3.2a.			
S_1				
S_3				

Table A3.2f. Results of Measurement of Wall Shear Stress in Experiments with Single Tuyere; Indifferent Electrolyte - KOH

h = 40 cm. l = 0.65 cm. $\dot{Q}_s/(\dot{Q}_s + \dot{Q}_j) = 0.1$

Electrode No.	Temp., °C	$(\dot{Q}_s + \dot{Q}_j)$, liters/min.	τ, dynes/cm^2	
			Average	r.m.s. value
B_1	19	201	3.78	1.71
	19	141	2.76	1.08
	19	100	2.45	0.74
	19	53	1.52	0.47
B_2	18	200	1.10	0.111
	18	141	1.10	0.136
	18	100	1.05	0.190
	18	52	1.29	0.359
B_3				
B_4				
B_5	Same as in Table A3.2a.			
S_1				
S_3				

Table A3.2g. Results of Measurement of Wall Shear Stress in Experiments with Single Tuyere; Indifferent Electrolyte - KOH

h = 40 cm. l = 1.3 cm. $\dot{Q}_s/(\dot{Q}_s + \dot{Q}_j) = 0$

Electrode No.	Temp., °C	$(\dot{Q}_s + \dot{Q}_j)$, liters/min.	τ, dynes/cm^2	
			Average	r.m.s. value
B_1	19.5	201	3.66	1.92
	19.5	141	2.51	1.02
	19.5	100	2.34	0.82
	19.5	53	1.57	0.54
B_2	18	200	1.10	0.111
	18	141	1.10	0.136
	18	100	1.05	0.190
	18	52	1.29	0.354
B_3				
B_4				
B_5	Same as in Table A3.2a.			
S_1				
S_3				

Table A3.2h. Results of Measurements of Wall Shear Stress in Experiments with Single Tuyere; Indifferent Electrolyte - KOH

h = 40 cm. l = 1.3 cm. $\dot{Q}_s/(\dot{Q}_s + \dot{Q}_j) = 0.10$

Electrode No.	Temp., °C	$(\dot{Q}_s + \dot{Q}_j)$, liters/min.	τ, dynes/cm^2	
			Average	r.m.s. value
B_1	19.5	201	3.37	1.46
	19.5	141	2.36	0.92
	19.5	100	2.21	0.67
	19.5	52	1.52	0.45
B_2	18	200	1.10	0.111
	18	141	1.05	0.149
	18	100	1.05	0.190
	18	52	1.34	0.36
B_3				
B_4				
B_5	Same as in Table A3.2a.			
S_1				
S_3				

Table A3.2i. Results of Measurement of Wall Shear Stress in Experiments with Single Tuyere; Indifferent Electrolyte - KOH

h = 30 cm. l = 0. $\dot{Q}_s/(\dot{Q}_s + \dot{Q}_j) = 0.0$

Electrode No.	Temp., °C	$(\dot{Q}_s + \dot{Q}_j)$, liters/min.	τ, dynes/cm^2	
			Average	r.m.s. value
B_1	26	205	4.03	1.74
	26	146	2.60	0.93
	26	104	1.91	0.63
	26	52	1.26	0.41
B_2	26	205	0.67	0.170
	26	146	0.59	0.113
	26	104	0.41	0.159
B_3	27	205	0.172	0.031
	27	146	0.182	0.058
	27	104	0.204	0.080
B_4	27	205	0.165	0.059
	27	146	0.135	0.052
	27	104	0.190	0.119
B_5	28	202	0.066	0.012
	28	146	0.123	0.049
	28	104	0.182	0.126

Table A3.2j. Results of Measurement of Wall Shear Stress in Experiments with Single Tuyere; Indifferent Electrolyte - KOH

h = 30 cm. l = 0 $\dot{Q}_s/(\dot{Q}_s + \dot{Q}_j) = 0.10$

Electrode No.	Temp., °C	$(\dot{Q}_s + \dot{Q}_j)$, liters/min.	τ, dynes/cm^2	
			Average	r.m.s. value
B_1	26	204	2.97	0.83
	26	146	1.91	0.69
	26	104	1.51	0.49
	26	52	1.03	0.33
B_2				
B_3				
B_4	Same as in Table A3.2i.			
B_5				

Table A3.2k. Results of Measurement of Wall Shear Stress in Experiments with Single Tuyere; Indifferent Electrolyte - KOH

h = 30 cm. l = 1.3 cm. $\dot{Q}_s/(\dot{Q}_s + \dot{Q}_j) = 0$

Electrode No.	Temp., °C	$(\dot{Q}_s + \dot{Q}_j)$, liters/min.	τ, dynes/cm^2	
			Average	r.m.s. value
B_1	26.5	205	2.72	1.04
	26.5	146	1.94	0.64
	26.5	104	1.33	0.41
	26.5	52	1.02	0.291
B_2	26	205	0.64	0.165
	26	146	0.59	0.116
	26	104	0.40	0.156
B_3				
B_5	Same as in Table A3.2i.			
B_5				

Table A3.21. Results of Measurement of Wall Shear Stress in Experiments with Single Tuyere; Indifferent Electrolyte - KOH

h = 20 cm. $l = 0$ $\dot{Q}_s/(\dot{Q}_s + \dot{Q}_j) = 0$

Electrode No.	Temp., °C	$(\dot{Q}_s + \dot{Q}_j)$, liters/min.	τ, dynes/cm^2	
			Average	r.m.s. value
B_1	18	204	3.96	1.64
	18	146	2.13	0.77
	18	104	1.19	0.42
B_2	18	204	0.39	0.139
	18	146	0.26	0.077
	18	104	0.26	0.140
B_3	18.5	204	0.091	0.045
	18.5	146	0.129	0.044
	18.5	104	0.178	0.096
B_4	18.5	204	0.051	0.026
	18.5	146	0.113	0.043
	18.5	104	0.162	0.100
B_5	18.5	203	0.043	0.022
	18.5	146	0.091	0.036
	18.5	104	0.162	0.104

Table A3.2m. Results of Measurement of Wall Shear Stress in Experiments with Single Tuyere; Indifferent Electrolyte - KOH

h = 20 cm. l = 0 $\dot{Q}_s/(\dot{Q}_s + \dot{Q}_j) = 0.10$

Electrode No.	Temp., °C	$(\dot{Q}_s + \dot{Q}_j)$, liters/min.	τ, dynes/cm^2	
			Average	r.m.s. value
B_1	18	204	2.34	0.86
	18	146	1.99	0.71
	18	104	1.67	0.54
	18	52	1.10	-
B_2				
B_3	Same as given in Table A3.21.			
B_4				
B_5				

Table A3.2n. Calculated Values of N_{Eu} at Electrode B_1 and $N_{Fr'}$ in Experiments with Single Tuyere

h, cm	l/d_j	$\frac{\dot{Q}_s}{\dot{Q}_s + \dot{Q}_j}$	$(\dot{Q}_s + \dot{Q}_j)$, liters/min.	N_{Eu}	$N_{Fr'}$
40	0	0	201	4.19	3.25
			141	5.94	1.61
			100	8.47	0.810
			53	19.19	0.228
40	0	0.05	201	4.52	2.95
			141	6.41	1.45
			100	9.53	0.73
			53	20.86	0.215
40	0	0.10	201	4.66	2.63
			141	6.26	1.30
			100	9.02	0.66
			52	20.90	0.193
40	1	0	201	3.37	3.26
			141	4.79	1.60
			100	8.20	0.81
			53	18.38	0.226
40	1	0.05	201	3.50	2.63
			141	5.10	1.30
			100	8.72	0.65
			52	17.88	0.19
40	1	0.10	201	3.65	2.64
			141	5.43	1.30
			100	9.54	0.65
			53	21.16	0.193
40	2	0	201	2.87	3.26
			141	4.00	1.60
			100	7.47	0.81
			52	17.73	0.226
40	2	0.10	201	2.28	2.64
			141	4.64	1.30
			100	8.65	0.65
			52	21.10	0.193
30	0	0	205	3.26	4.38
			146	4.28	2.22
			104	6.24	1.13
			52	14.60	0.282

Continued...

Table A3.2n (Continued)

h, cm	l/d_j	$\frac{\dot{Q}_s}{\dot{Q}_s + \dot{Q}_j}$	$(\dot{Q}_s + \dot{Q}_j)$, liters/min.	N_{Eu}	$N_{Fr'}$
30	0	0.10	204	3.17	3.54
			146	3.88	1.80
			104	6.09	0.92
			52	14.84	0.221
30	2	0	205	2.20	4.38
			146	3.20	2.22
			104	4.36	1.13
			52	11.86	0.282
20	0	0	204	3.03	6.74
			146	3.21	3.41
			104	3.52	1.74
20	0	0.10	204	2.21	5.45
			146	3.70	2.78
			104	6.11	1.41
			52	16.05	0.34

Table A3.2o. Diameters of the Electrodes Employed in Experimen with Single Tuyere

Electrode No.	d_e, cm	Electrode No.	d_e, cm
B_1	0.0213	S_1	0.0219
B_2	0.0213	S_2	0.0219
B_3	0.0213	S_3	0.0219
B_4	0.0213	S_4	0.0219
B_5	0.0213	S_5	0.0219
		S_6	0.0219

Table A3.3a. Results of Measurement of Shear Stress in Experiments with Multiple Tuyeres; Indifferent Electrolyte - NaOH

No. of tuyeres - 3 (symmetric) l = 0

Positions - 1, 2 and 5 (Refer Figure 2.3) h = 40 cm.

Electrode No.	Temp., °C	$\dot{Q}_j$, liters/min.	τ, dynes/cm^2	
			Average	r.m.s. value
3	30.5	303	2.35	1.31
	30.5	235	1.36	0.72
	30.5	197	1.09	0.53
	30.5	104	0.58	0.255
4	30	302	1.76	0.80
	30	235	1.33	0.60
	30	197	1.19	0.52
	30	104	0.80	0.38
5	30.5	303	3.81	2.10
	30.5	197	2.61	1.28
	30.5	104	1.28	0.55
6	32	304	3.08	1.79
	32	251	2.50	1.14
	32	198	1.71	0.76
	32	105	1.01	0.77
8	30	298	0.91	0.38
	30	252	0.79	0.32
	30	198	0.72	0.286
	30	103	0.75	0.34
9	31.5	299	0.43	0.174
	31.5	252	0.41	0.159
	31.5	199	0.39	0.144
	31.5	104	0.51	0.194
10	32	299	0.42	0.174
	32	252	0.41	0.161
	32	199	0.34	0.128
	32	103	0.54	0.240

Continued...

Table A3.3a (Continued)

Electrode No.	Temp., °C	$\dot{Q}_j$, liters/min.	τ, dynes/cm^2	
			Average	r.m.s. value
11	30.5	298	0.251	0.095
	30.5	251	0.222	0.088
	30.5	202	0.208	0.091
	30.5	103	0.299	0.145
12	30.5	298	0.110	0.034
	30.5	256	0.086	0.050
	30.5	198	0.236	0.098
	30.5	103	0.38	0.201
13	32	299	6.44	3.29
	32	252	2.70	1.50
	32	199	1.50	0.84
	32	104	0.75	0.32
15	32	301	0.88	0.34
	32	252	0.78	0.292
	32	201	0.68	0.234
	32	105	0.74	0.304
18	31	301	0.55	0.167
	31	252	0.52	0.158
	31	201	0.52	0.166
	31	104	0.57	0.219
21	31	300	0.47	0.136
	31	252	0.45	0.132
	31	202	0.52	0.163
	31	104	0.66	0.234
24	33	300	1.12	0.54
	33	255	1.21	0.55
	33	202	1.16	0.55
	33	105	1.03	0.297

Table A3.3b. Results of Measurement of Shear Stress in Experiments with Multiple Tuyeres; Indifferent Electrolyte - KOH

No. of tuyeres - 3 (symmetric) l = 1.3 cm

Positions - 1, 2 and 5 (Refer Figure 2.3) h = 40 cm

Electrode No.	Temp., °C	$\dot{Q}_j$, liters/min.	τ, dynes/cm^2	
			Average	r.m.s. value
3	32.5	293	0.77	0.265
	32.5	250	0.55	0.174
	32.5	202	0.38	0.115
	32.5	108	0.28	0.093
4	33	293	1.45	0.53
	33	202	0.86	0.31
	33	108	0.61	0.237
5	32.5	293	4.18	2.12
	32.5	252	3.25	1.60
	32.5	203	2.33	1.11
	32.5	108	1.04	0.40
6	33	293	1.06	0.37
	33	252	0.88	0.322
	33	203	0.83	0.275
	33	108	0.79	0.259
8	35	295	0.82	0.303
	35	252	0.78	0.293
	35	203	0.82	0.293
	35	109	0.75	0.257
10	33.5	294	0.58	0.233
	33.5	244	0.58	0.218
	33.5	203	0.61	0.225
	33.5	108	0.61	0.280
12	33	288	0.271	0.105
	33	252	0.245	0.095
	33	203	0.192	0.080
	33	108	0.278	0.113

Continued...

Table A3.3b (Continued)

Electrode No.	Temp., °C	$\dot{Q}_j$, liters/min.	τ, dynes/cm^2	
			Average	r.m.s. value
13	32.5	292	1.62	0.68
	32.5	252	1.25	0.56
	32.5	203	1.07	0.38
	32.5	108	0.87	0.40
15	32	291	0.82	0.271
	32	252	0.61	0.210
	32	203	0.47	0.166
	32	108	0.51	0.240
18	33	292	0.69	0.304
	33	252	0.59	0.168
	33	203	0.51	0.191
	33	105	0.61	0.230
21	32	291	0.51	0.180
	32	252	0.46	0.175
	32	203	0.46	0.175
	32	105	0.54	0.255
24	32	291	0.69	0.40
	32	252	0.41	0.238
	32	203	0.36	0.166
	32	105	0.37	0.158

Table A3.3c. Results of Measurement of Shear Stress in Experiments with Multiple Tuyeres; Indifferent Electrolyte - KOH

No. of tuyeres - 3 (Asymmetric) l = 1.3 cm

Positions - 1, 2 and 12 (Refer Figure 2.3) h = 40 cm

Electrode No.	Temp., °C	$\dot{Q}_j$, liters/min.	τ, dynes/cm^2	
			Average	r.m.s. value
3	31.5	294	1.96	0.76
	31.5	202	1.43	0.53
	31.5	104	1.01	0.36
4	32.5	292	2.61	0.84
	32.5	252	1.94	0.64
	32.5	203	1.55	0.49
	32.5	104	2.13	0.66
5	32.5	291	2.00	0.80
	32.5	252	2.19	0.87
	32.5	203	2.19	0.86
	32.5	104	1.94	0.71
6	32.5	310	3.63	1.73
	32.5	252	2.99	1.29
	32.5	203	2.10	0.89
	32.5	104	2.02	0.97
7	32.5	303	2.70	1.21
	32.5	252	2.61	1.12
	32.5	203	2.52	1.07
	32.5	104	2.26	1.15
8	32	303	1.62	0.70
	32	252	1.62	0.70
	32	203	1.57	0.65
	32	104	1.57	0.76
9	33	299	1.68	0.72
	33	252	1.62	0.66
	33	203	1.50	0.62
	33	104	1.50	0.76

Continued...

Table A3.3c (Continued)

Electrode No.	Temp., °C	$\dot{Q}_j$, liters/min.	τ, dynes/cm^2	
			Average	r.m.s. value
10	32.5	309	1.12	0.56
	32.5	252	0.93	0.44
	32.5	203	0.74	0.35
	32.5	104	0.83	0.49
12	32.5	295	0.315	0.166
	32.5	252	0.35	0.170
	32.5	203	0.35	0.175
	32.5	104	0.77	0.33
15	32.5	307	1.84	0.60
	32.5	252	1.73	0.55
	32.5	203	1.38	0.60
	32.5	104	1.43	0.46
21	33.5	302	1.46	0.65
	33.5	251	1.37	0.50
	33.5	203	1.14	0.48
	33.5	108	1.02	0.45
23	33	301	0.47	0.199
	33	252	0.45	0.195
	33	203	0.45	0.207
	33	104	0.64	0.259
24	33	301	0.60	0.276
	33	252	0.49	0.237
	33	203	0.51	0.262
	33	104	0.77	0.47
Tuyere positions changed to 1, 5 and 18				
3	29.5	337	0.274	0.135
	29.5	304	0.296	0.139
	29.5	237	0.311	0.148
	29.5	166	0.289	0.137

Continued...

Table A3.3c (Continued)

Electrode No.	Temp., °C	$\dot{Q}_j$, liters/min.	τ, dynes/cm^2	
			Average	r.m.s. value
5	29.5	338	2.04	0.99
	29.5	304	2.11	0.96
	29.5	231	1.98	0.96
	29.5	168	1.80	0.92
7	29	338	1.22	0.68
	29	290	1.43	0.79
	29	226	1.26	0.71
	29	149	1.07	0.58
10	29	338	1.51	0.82
	29	290	1.56	0.86
	29	226	1.23	0.65
	29	149	1.28	0.74
12	29.5	339	0.66	0.32
	29.5	291	0.75	0.43
	29.5	226	0.75	0.41
	29.5	149	0.75	0.45
14	30	339	0.45	0.27
	30	291	0.50	0.29
	30	225	0.52	0.32
	30	149	0.52	0.35
19	30	339	2.11	1.32
	30	291	2.05	1.26
	30	225	2.05	1.15
	30	149	2.11	1.18

Table A3.3d. Results of Measurement of Shear Stress in Experiments with Multiple Tuyeres; Indifferent Electrolyte - NaOH

No. of tuyeres - 6 (symmetric) l = 1.3

Positions - 13, 15, 17, 19, 21, 23 (Refer Figure 2.3) h = 40 cm

Electrode No.	Temp., °C	$\dot{Q}_j$, liters/min.	τ, dynes/cm^2	
			Average	r.m.s. value
3	30	312	0.317	0.164
	30	145	0.242	0.145
6	30	312	0.309	0.113
	30	145	0.258	0.136
10	30	312	0.119	0.059
	30	145	0.102	0.054
12	30	312	0.155	0.100
	30	145	0.171	0.120
14	30.5	313	0.035	0.014
	30.5	145	0.046	0.027
17	31.5	302	0.136	0.062
	31.5	148	0.086	0.056
21	31.5	302	0.121	0.062
	31.5	148	0.116	0.065
23	29.5	300	0.068	0.029
	29.5	165	0.124	0.073
24	29.5	300	0.073	0.031
	29.5	165	0.112	0.078

Table A3.3e. Results of Measurement of Shear Stress in Experiments with Multiple Tuyeres; Indifferent Electrolyte - NaOH

No. of tuyeres - 6 (asymmetric) l = 0

Positions - 1, 14, 16, 24, 27 and 30 h = 40 cm
(Refer to Figure 2.3)

Electrode No.	Temp., °C	$\dot{Q}_j$, liters/min.	τ, dynes/cm^2	
			Average	r.m.s. value
3	30.5	339	0.81	0.185
	30.5	291	0.81	0.177
	30.5	226	0.77	0.159
	30.5	149	0.71	0.129
5	30	339	2.43	0.95
	30	291	2.16	0.84
	30	225	1.91	0.73
	30	149	1.91	0.65
8	30	339	2.66	1.21
	30	291	2.50	1.11
	30	225	2.84	1.28
	30	149	2.75	1.15
10	30	339	1.75	0.93
	30	291	1.70	0.88
	30	226	1.75	0.90
	30	149	1.54	0.73
12	31.5	339	1.01	0.45
	31.5	291	0.87	0.40
	31.5	226	0.77	0.33
	31.5	149	0.71	0.265
14	30.5	339	0.41	0.162
	30.5	290	0.41	0.161
	30.5	226	0.38	0.153
	30.5	149	0.35	0.137
17	30.5	339	1.45	0.69
	30.5	290	1.40	0.63
	30.5	226	1.36	0.57
	30.5	149	1.40	0.54

Continued...

Table A3.3c (Continued)

Electrode No.	Temp., °C	$\dot{Q}_j$, liters/min.	τ, dynes/cm^2	
			Average	r.m.s. value
20	30.5	339	1.28	0.55
	30.5	290	1.19	0.49
	30.5	226	1.10	0.46
	30.5	149	1.06	0.40
23	30.5	339	0.316	0.102
	30.5	290	0.288	0.105
	30.5	226	0.239	0.078
	30.5	149	0.203	0.033
24	31	340	1.22	0.73
	31	291	1.17	0.71
	31	227	1.07	0.64
	31	149	0.94	0.56
Tuyere positions changed to 1, 20, 22, 24, 30 and 33				
14	31	340	0.38	0.121
	31	291	0.328	0.099
	31	149	0.249	0.074
17	31	340	1.73	0.60
	31	291	1.73	0.57
	31	227	1.73	0.53
	31	149	1.49	0.42
20	31	340	1.80	0.61
	31	291	1.68	0.58
	31	227	1.68	0.54
	31	149	1.63	0.56
23	30	349	0.319	0.098
	30	296	0.298	0.088
	30	222	0.285	0.081
	30	163	0.323	0.092
24	30.5	329	1.38	0.77
	30.5	291	1.57	0.87
	30.5	225	1.49	0.83
	30.5	149	1.27	0.74

Table A3.3f. Results of Measurement of Shear Stress in Experiments with Multiple Tuyeres; Indifferent Electrolyte - NaOH

No. of tuyeres - 6 (asymmetric) l = 1.3 cm

Positions - 1, 14, 16, 24, 27 and 30 (Refer Figure 2.3) h = 40 cm

Electrode No.	Temp., °C	$\dot{Q}_j$, liters/min.	τ, dynes/cm^2 Average	τ, dynes/cm^2 r.m.s. value
3	31	349	0.57	0.19
	31	297	0.59	0.19
	31	221	0.58	0.16
	31	163	0.61	0.16
6	30	349	1.37	0.61
	30	296	1.43	0.62
	30	222	1.43	0.59
	30	163	1.50	0.58
10	30	349	0.82	0.43
	30	296	0.82	0.46
	30	222	0.78	0.42
	30	163	0.69	0.35
12	30.5	367	0.63	0.35
	30.5	287	0.63	0.36
	30.5	215	0.53	0.33
	30.5	145	0.49	0.25
14	30.5	367	0.245	0.121
	30.5	287	0.245	0.118
	30.5	215	0.257	0.123
	30.5	145	0.211	0.103
17	30.5	367	0.83	0.39
	30.5	287	0.93	0.41
	30.5	215	0.96	0.39
	30.5	145	0.77	0.28
20	30.5	367	0.61	0.264
	30.5	287	0.48	0.190
	30.5	215	0.48	0.176
	30.5	145	0.45	0.157

Continued...

Table A3.3f (Continued)

Electrode No.	Temp., °C	$\dot{Q}_j$, liters/min.	τ, dynes/cm^2	
			Average	r.m.s. value
23	31	367	0.161	0.078
	31	145	0.128	0.079
24	31	367	0.329	0.172
	31	287	0.218	0.123
	31	215	0.231	0.124
	31	146	0.200	0.112
Tuyere positions changed to 1, 20, 22, 24, 30 and 33				
14	31	302	0.252	-
	31	146	0.252	-
17	31	302	1.05	-
	31	146	0.98	-
20	31	302	0.95	-
	31	146	0.88	-
23	31	302	0.32	-
	31	146	0.33	-
24	31.5	303	0.75	-
	31.5	146	0.80	-

Table A3.3g. Results of Measurement of Shear Stress in Experiments with Multiple Tuyeres; Indifferent Electrolyte - NaOH

No. of tuyeres - 12 (symmetric) l = 1.3 cm

Positions - 2, 3, 4, 5, 6, 7, 13, 15, 17, 19, 21 and 23 (Refer Figure 2.3) h = 40 cm

Electrode No.	Temp., °C	$\dot{Q}_j$, liters/min.	τ, dynes/cm^2	
			Average	r.m.s. value
3	27.5	297	0.30	0.09
	27.5	169	0.35	0.11
5	27	309	0.61	0.20
	27	170	0.54	0.21
8	27	309	0.27	0.06
	27	170	0.23	0.05
9	27	309	0.30	0.04
	27	170	0.28	0.04
12	26	309	0.19	0.06
	26	170	0.21	0.08
14	26	309	0.18	-
	26	170	0.17	-

Table A3.3h. Diameters of the Electrodes Employed in Experiments with Multiple Tuyeres

Electrode No.	d_e, cm	Electrode No.	d_e, cm
1	0.0206	13	0.0206
2	0.0206	14	0.0219
3	0.0206	15	0.0219
4	0.0213	16	0.0219
5	0.0213	17	0.0225
6	0.0188	18	0.0225
7	0.0231	19	0.0225
8	0.0200	20	0.0213
9	0.0200	21	0.0213
10	0.0219	22	0.0219
11	0.0219	23	0.0219
12	0.0219	24	0.0200

VITAE

The author was born in Manipur, Karnataka on the 25th of July, 1950. After completing schooling from Admar Higher Secondary School, Admar, Karnataka, he joined Karnataka Regional Engineering College, Surathkal, and obtained the degree of Bachelor of Engineering in Metallurgy from Mysore University in 1971. He joined Indian Institute of Technology, Kanpur in the same year and obtained his Master's degree in Metallurgical Engineering from there in 1974. Since then he has been at Kanpur working for his doctorate.